UNIVERSITA' DI PISA

Scuola di Dottorato in Ingegneria "Leonardo da Vinci"

XXVII Corso di Dottorato di Ricerca in

INGEGNERIA NUCLEARE

E DELLA SICUREZZA INDUSTRIALE

Tesi di Dottorato di Ricerca

Experimental and Numerical Thermal-hydraulic Analyses in Support of GEN-IV Lead-cooled Fast Reactor Design

Autore:

Daniele Martelli _____

Relatori:

Prof. Ing. *Nicola Forgione* _____

Prof. Ing. *Walter Ambrosini* _____

Dott. Ing. *Mariano Tarantino* _____

Anno 2015

“This page has been intentionally left blank”

Ad Alfio, Donatella & Silvia

“This page has been intentionally left blank”

Acknowledgements

“This page has been intentionally left blank”

ABSTRACT

The aim of this Ph.D. thesis work is the experimental and numerical analysis of thermal-hydraulic phenomena of interest in support of GEN-IV LFR reactor design. The research activity is performed at the Department of Civil and Industrial Engineering of the University of Pisa in collaboration with the Experimental Engineering Technical Unit (UTIS) of ENEA Brasimone R.C..

In the first part of this thesis, the Fluent CFD code is used to simulate the experimental test of Uotani aimed to study heat transfer in a thermal stratified HLM system. The goal is the investigation of capabilities/limitations of the CFD code to simulate heat transfer under thermally stratified conditions and to provide a guideline for the subsequent study of this phenomenon in the CIRculation Eutectic (CIRCE) large pool experimental facility (max LBE Inventory of about 90000 kg).

A simplified 2D axial-symmetric domain of the CIRCE facility is developed and "one-way" off-line coupling simulations between the thermal-hydraulic system code (STH) RELAP5 mod/3.3 and the CFD Ansys Fluent are carried out. The transition from forced to natural circulation condition is investigated together with the thermal stratification phenomena inside the CIRCE pool. The preliminary numerical analysis is followed by the experimental campaign performed in CIRCE facility arranged with the Integral Circulation Experiment (ICE) configuration, aimed at reproducing a Protected Loss Of Heat Sink (PLOHS) with Loss Of Flow (LOF) accidental scenario. Results of two experimental tests (characterized by different boundary conditions) are deeply discussed. A post-test analysis is performed as well setting boundary conditions in agreement with the analysed experiments and introducing thermal losses towards the environment.

In the second part of this work, in order to better reproduce several accidental scenarios and improve the accuracy of numerical simulations, a new "two-way" RELAP5-Fluent coupling tool is developed ("non-overlapping, two-way coupling scheme"). A preliminary application of the developed coupling tool to the Natural Circulation Experiment (NACIE) loop type facility is described. Explicit and implicit numerical schemes are implemented and serial and parallel calculations are carried out (both 2D and 3D CFD domain are used). Obtained results of LBE mass flow rate and pressure differences at inlet and outlet sections of the fuel pin simulator (FPS) are compared with RELAP5 stand-alone calculations and data obtained from the NACIE experimental campaign.

The last part of this work deals with the experimental campaign performed on the Integral Circulation Experiment (ICE) test section installed into the CIRCE pool facility aiming to fully investigate the heat transfer phenomena in grid spaced fuel pin bundles providing experimental data in support of European fast reactor development. A full characterization of the FPS has been experimentally achieved for Peclet numbers in the range of about 500-3000. Obtained experimental data point out a trend of Nusselt number as a function of Peclet in agreement with Mikityuk and Ushakov correlations showing a general tendency to predict values that lie below the mentioned correlations.

INDEX

NOMENCLATURE

Roman letters

a	Temperature gradient in ambient fluid	°C/m
D	Diameter	m
Gr	Grashof number	-
Gr_x^*	Modified Grashof number	-
h_r	Distance	m
$\dot{m}$	Mass flow rate	kg/s
Nu	Nusselt number	-
P	Pressure	Pa
p	Pitch	m
Pr	Prandtl number	-
q''	Heat flux	W/m^2
Ra	Rayleigh number	-
Re	Reynolds number	-
S	Stratification parameter	°C/m
T	Temperature	°C
t	Time	s
x	Coordinate in the axial direction	m
y	Coordinate in the transverse direction	m
z	Coordinate in the vertical direction	m

Greek letters

α	Void fraction	-
β	Thermal expansion coefficient 1/m	1/m
δ	Displacement thickness	mm
ε	Turbulent kinetic energy	m^2/s^2
λ	Thermal conductivity	W/(m K)
η^*	Similarity variable	-
ρ	Density	kg/m^3
π	Pi	-
σ_i	Standard deviation	-
σ_X/X	Percentage error	-
ν	Cinematic viscosity	m^2/s

Abbreviation and acronyms

ALFRED	Advanced Lead Fast Reactor European Demonstrator
API	Application Programming Interface
ATHLET	Analysis of Thermal-Hydraulics of Leaks and Transients
APS-1	Atomic Power Station 1
ASTRID	Advanced Sodium Technological Reactor for Industrial Demonstration
CATHARE	Code for Analysis of Thermal hydraulics during an Accident of Reactor and safety Evaluation
CEA	French Atomic Energy Commission

CFD	Computational Fluid Dynamics
CFL	Courant-Friedrich-Levy
CIRCE	CIRculation Eutectic
CIRTEN	Italian Interuniversity Consortium for Technological Nuclear Research
DAQ	Data Acquisition System
DHR	Decay Heat Removal system
DICI	Dipartimento di Ingegneria Civile e Industriale
EBR-I	European Breeder Reactor I
EFIT	European Facility for Industrial Transmutation
ENEA	Italian National Agency for New Technologies, Energy and Sustainable Economic Development
ESNII	European Nuclear Industrial Initiative
EU	European Union
FALCON	Fostering ALFRED construction
FBR	Fast Breeder Reactor
FC	Forced Circulation
FPS	Fuel pin simulator
GIF	Generation IV International Forum
G_lift	Gas lift mass flow rate
Gen-IV	Generation IV
GFR	Gas-cooled Fast Reactor
GRS	Gesellschaft für Anlagen- und Reaktorsicherheit
HLM	Heavy Liquid Metal
HX	Heat eXchanger
HS	Heat Source
HZDR	Helmholtz-Zentrum Dresden-Rossendorf
IAEA	International Atomic Energy Agency
ICE	Integral Circulation Experiment
ICN	Institutul de Cercetari Nucleare (Institute for Nuclear Research Pitesti)
ICoCo	Interface for Code Coupling
KTH	Royal Institute of Technology
Labview	LABoratory Virtual Instrument Engineering Workbench
LB-LOCA	Large Break Loss of Coolant Accident
LES	Large Eddy Simulation
LOF	LOSS of Flow
MSR	Molten Salt Reactor
MYRRHA	Multipurpose Hybrid Research Reactor for High-tech Application
MYRTHE	MYRRHA Research and Transmutation Endeavour
NACIE	NAtural CIrculation Experiment
NaN	Not a Number
NC	Natural Circulation
NPP	Nuclear Power Plant
NPS	Nominal Pipe Size
PC	Personal Computer
PID	Proportional Integral Derivative
PLOHS	Protected Loss of Heat Sink
PVM	Parallel Virtual Machines
PWR	Pressurized Water Reactor
RANS	Reynolds-Averaged Navier-Stokes equations

RELAP	REactor Loss of coolant Analysis Program
RNG	Renormalized Group
RSM	Reynolds Stress Model
SB-LOCA	Small Break Loss of Coolant Accident
SCWR	Supercritical Water-cooled Reactor
SESAME	Thermal hydraulics Simulations and Experiments for the Safety Assessment of MEtal cooled reactors
SG	Steam Generator
SNEPT	Sustainable Nuclear Energy Technology
SFR	Sodium Fast Reactor
STH	System Thermal Hydraulic
TBMFR	Temperature Balance Mass Flow Rate
TRACE	TRAC/RELAP advanced computational engine
TRASCO	TRAsmutazione SCOrie (Transmutation waste)
THINS	Thermal Hydraulics of Innovative Nuclear System
UDF	User Defined Function
ULOF	Unprotected Loss Of Flow
URANS	Unsteady Reynolds-Averaged Navier-Stokes equations
UTIS	Experimental engineering technical unit
VHTR	Very High Temperature Reactor
XT-ADS	Experimental Accelerator Driven System

LIST OF FIGURES

LIST OF TABLES

1 INTRODUCTION

The international framework of this activity is the Thermal Hydraulics of Innovative Nuclear System (THINS) Seventh Framework Programme of EURATOM for nuclear research and training activities.

The proper understanding of thermal-hydraulic phenomena is a key issue for the design of innovative nuclear power plants, for this reason, intensive experiment-based research activity on Lead-Bismuth Eutectic (LBE) facilities supports the performed numerical analyses. In order to address this task, several experimental facilities are operating or under construction in Europe supported by the European Sustainable Nuclear Industrial Initiative (ESNII).

1.1. International framework

On December 20, 1951, in Arco, Idaho Falls (USA,) the Experimental Breeder Reactor EBR-I (INL, www4vip.inl.gov/ebr/) for the first time, produced electricity by nuclear energy (illuminating four light bulbs). Three years later, at Obninsk, Russia, the Nuclear Power Plant (NPP) Atomic Power Station 1(APS-1) represents the first NPP connected to the grid producing electricity for commercial use (electrical output 5MW). In 1956, close to the village of Seascale England, the first commercial NPP Calder Hall 1 (electrical output 50 MW) was connected to the grid (European Nuclear Society, www.euronuclear.org/info/encyclopedia/n/nuclear-power-plant-world-wide.htm). As of March 16, 2015 in 30 countries, 440 NPP units (279 are PWR) are in operation with a total net electrical capacity of 378027 MW (IAEA, www.iaea.org/PRIS/WorldStatistics/OperationalReactorsByType.aspx).

Moreover, 68 plants with a total net electrical capacity 67125 MW are under construction in 15 countries (25 in China). Thirteen countries depend on nuclear power for more than 20% of their Electricity (France 73.3%, Belgium 52.1% etc., IAEA, www.iaea.org/PRIS/WorldStatistics/NuclearShareofElectricityGeneration.aspx) and among countries which do not have NPPs, Italy and Denmark get almost 10% of their power from nuclear (World nuclear association, www.world-nuclear.org/info/Current-and-Future-Generation/Nuclear-Power-in-the-World-Today/). However, the world demand for energy is set to increase significantly in the next decades, spurred by economic growth, especially in developing countries. Nevertheless, to prevent the most severe impacts of climate change, the international community has agreed to keep the global warming below 2°C compared to temperature in pre-industrial times (European Commission, ec.europa.eu/clima/policies/brief/eu/).

In order to reach this goal, the European Council reconfirmed the European long term policy of reducing greenhouse gas emission by 80-95% by 2050 compared to 1990 (A Roadmap for moving to a competitive low carbon economy in 2050–, European Commission, ec.europa.eu/clima/policies/roadmap/index_en.htm). The EU Research and Innovation programme, Euratom HORIZON 2020, represents the first target of this roadmap (20% reduction greenhouse gas emission compared to 1990, 20% energy saving and 20% of renewable energies in the total energy mix, ec.europa.eu/programmes/horizon2020/). In this international context, as an established source of low-carbon energy, nuclear power plays a key role in achieving the goal of reducing greenhouse gas emission. Actually, further technology development is required to meet future energy demand and the

International and European standards require the design of a new generation of reactors, called Generation IV or GEN-IV systems. In order to define the necessary R&D, in 2000, nine countries have agreed on a framework for international cooperation to support next-generation reactor. From those initial meetings a technology roadmap was begun, leading to the drafting in December 2002 of *"A technological Roadmap for Generation IV Nuclear Energy System"* (Gen-IV International Forum, 2002). In the document, technology goals are defined in four areas of sustainability, economics, safety and reliability, and proliferation resistance and physical protection. Moreover, the GEN-IV roadmap process lead to the selection of six GEN-IV systems from nearly 100 concepts: Gas-cooled Fast Reactor (GFR), Lead-cooled Fast Reactor (LFR), Molten Salt Reactor (MSR), Sodium-Fast Reactor (SFR), Supercritical Water-cooled Rector (SCWR) and Very High Temperature Reactor (VHTR). Actually, the Generation IV International Forum (GIF) has thirteen members including Euratom (2003), People's Republic of China and the Russian Federation (November 2006). The Technology Roadmap has been updated and published in January, 2014 titled "*Technology Roadmap Update for Generation IV Nuclear Energy Systems*" (Gen-IV International Forum, 2014) aiming to assess the current technology status of each system and defining the R&D steps for the next decade.

Europe, through the Sustainable Nuclear Energy Technology Platform (SNETP) has defined its own strategy and priorities for fast neutron reactor (ESNII, www.snetp.eu/esnii/):

- SFR as reference technology (short term). For this type of reactor significant industrial experience feedback is available, Approximately twenty prototypes or demonstrators have been operated with more than 400 reactor-years of operation (100 reactor-years of SFR whit significant power: Superphenix (Vendryes, 1977) BN-600 (Buksha et al., 1997) BN-350 (Leipunskii et al., 1966) Monju (Mochizuki, 2014);
- LFR as a first alternative fast neutron reactor solution (middle term). The feedback for this technology is represented mostly by application started in the Soviet Union in the 1950s, where reactor cooled by Lead-Bismuth Eutectic (LBE) were developed and employed for submarine propulsion. Later, in the 1990s, the Russian Federation and Europe renewed the interest in LFR for civilian fast reactor and for energy amplifier subcritical nuclear system (ADS concept, Knebel et al., 2006);
- GFR as a second alternative technology (long term, alternative option). R&D for GFR in Europe, actually in the "pre-conceptual studies" phase, is primarily carried out by a consortium of European nations ("Visegrád 4" group: Hungary, Czech Republic, Slovakia and Poland while France, dedicates limited effort to supporting the V4G4 ALLEGRO consortium) for the development of ALLEGRO (Poette et al., 2009) as Gas-cooled Fast Reactor Demonstrator.

The ESNII, supports the development of:

- Advanced Sodium Technological Reactor for Industrial Demonstration (ASTRID) as industrial-scale demonstration of GEN-IV SFR;
- Multipurpose Hybrid Research Reactor for High-tech Application (MYRRHA, Abderrahim et al., 2012) as research facility for fast spectrum irradiation tool in support of technology development of the three fast reactor system (SFR, LFR, GFR);

- Advanced Lead Fast Reactor European Demonstrator (ALFRED, Alemberti et al., 2013) as European lead technology demonstrator;
- ALLEGRO as European Gas Fast Reactor Demonstrator Project.

1.2. National framework

Italian R&D activities in Heavy Liquid Metal (HLM) technologies started in the late1990s with the ADS project aimed to transmute the long living radio waste and use them for power production by employment of fast neutrons (TRASCO project approved by ENEA and the National Institute for Nuclear Physics (INFN, trasco.lnl.infn.it/basic.htm) in July, 1997. Nowadays, ANSALDO NUCLEARE, ENEA and CIRTEN (Interuniversity Consortium for Technological Nuclear Research) are deeply involved in researches aimed to support the development of the next-generation nuclear reactors.

Starting in 2010, the Lead-cooled European Advanced DEmonstration Reactor project (LEADER, www.leader-fp7.eu/default.aspx), coordinated by ANSALDO NUCLEARE within the Seventh EU Framework Programme, carried out a series of actions in support of the conceptual design of the European Lead Fast Reactor (ELFR) and of the development of the design of the LFR demonstrator ALFRED considered a key step on the LFR roadmap. ENEA and CIRTEN were consortium partners in the LEADER project. In order to advance both ALFRED design and licensing activities, an international consortium agreement Fostering ALfred CONstruction (FALCON, www.euronuclear.org/e-news/e-news-43/ansaldo.htm) was signed on December, 18th, 2013 by Italian industry (ANSALDO), research organizations coordinated by ENEA and the Romanian Research Institute ICN. Later on, in November 2014 the Rez Research Centre joined the consortium. Main aims of FALCON for AFLRED development are the technical review of projects, the estimate of costs, the execution schedule and the assessments of available funding. Moreover, several technological topics are of common interest for different LFR concepts and LFR, SFR developments as well.

ALFRED and MYRRHA projects, share several design solution, strong synergies are present and a strict collaboration between the two projects is carried out. LFR and SFR systems have several common features, as e.g. the development of MOx fuel manufacturing and reprocessing. Furthermore, they share similar tools for modelling the neutronics and they have several common issues for thermal-hydraulics: mixing and stratification phenomena, fuel bundle behaviour, forced to natural circulation transition, etc.. All these research activities are supported by ENEA, which coordinates the Italian R&D efforts for LFR technology. In particular, the ENEA Brasimone R.C. implemented large competencies and capabilities in the field of HLM thermal-hydraulic, coolant technology, material for high temperature applications, corrosion and materials protection, heat transfer and removal, component development and testing, remote maintenance, procedure definition and coolant handling.

Several experimental activities have been implemented in ENEA Brasimone R.C. concerning integral circulation experiments and pool thermal-hydraulic investigation, heat transfer investigation in fuel rod bundles, corrosion material characterization development of prototypical components and coolant chemistry control.

1.3. Description of the research activity

The cooperation between the DICI of the University of Pisa and the Experimental Engineering Technical Unit (UTIS) of ENEA Brasimone R.C., recently (2014) carried out to the establishment of a framework agreement between the parties. The UTIS unit represents a relevant and innovative experimental laboratory in support of nuclear R&D with seven facilities related to LFR development.

This research activity is devoted to study thermal-hydraulic phenomena of interest in support of LFR R&D. In particular, thermal stratification in LFR pool type reactors was investigated both analytically and experimentally simulating a Protected Loss of Heat Sink with Loss of Flow (PLOHS+LOF). The experimental activity was carried out in the CIRCulation Eutectic (CIRCE) large pool facility aimed at simulating the total loss of the secondary circuit, the consequent reactor scram and activation of Decay Heat Removal (DHR) system. The numerical analyses were performed adopting a one-way coupling methodology between System Thermal Hydraulic (STH) Code (RELAP5/mod3.3) and Computational Fluid Dynamic (CFD, Ansys FLUENT) software.

In order to improve quality and reliability of complex thermal hydraulic studies a "two-ways" coupled (STH-CFD) tool was developed. The geometry or domain to be analysed is divided into regions modelled using the CFD approach and regions that can be reasonably well simulated using a system code. This division identifies the interfaces at which thermo-fluid-dynamics data are transferred from the system-code-portion to the CFD-code-portion of the domain and vice versa ("two-way coupling"). Numerical coupled simulations were executed and supported by experimental activities performed on the LBE loop type facility NAtural CIrculation Experiment (NACIE). Moreover, heat transfer in a rod bundle made of 37 fuel pins (electrically simulated) placed on a hexagonal lattice was experimentally investigated. A set of thirteen experiments were carried out and the data post-processed aiming to obtain Nusselt characterization in the central subchannel of the bundle and for a Peclet range between 400÷3000.

In Figure 1, the flow chart of the performed PhD research activity is reported. Red background highlights CIRCE numerical/experimental activities, while in light blue NACIE numerical/experimental activities are identified.

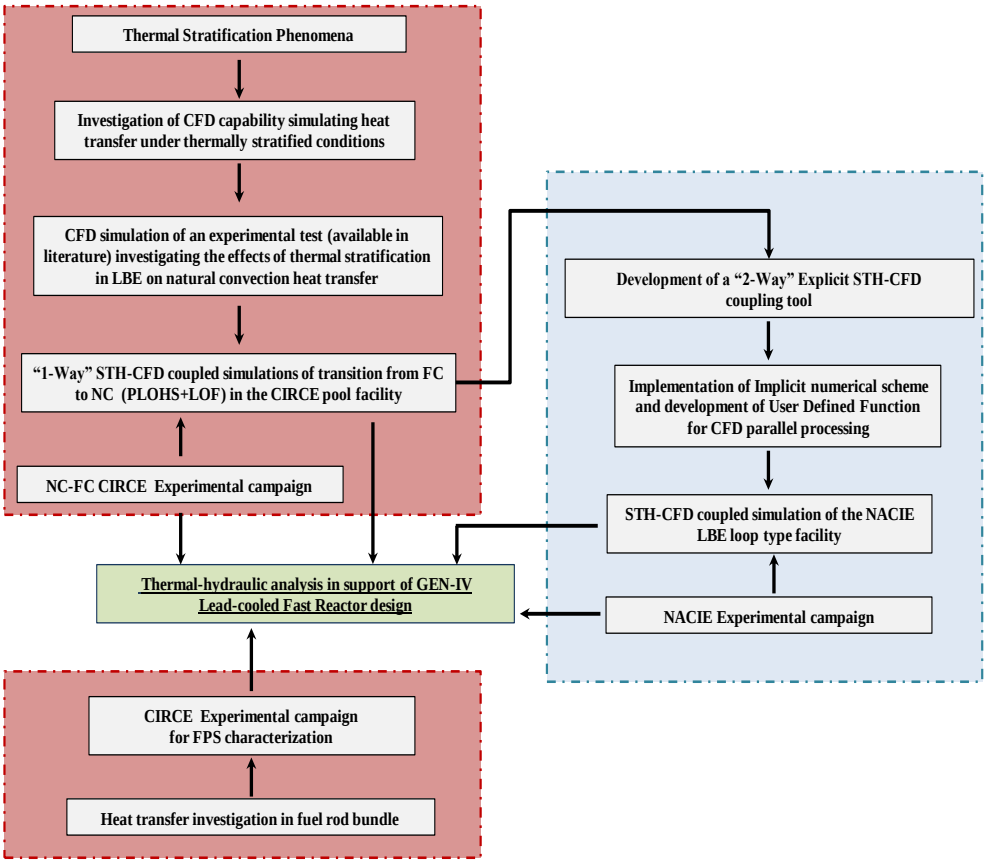

Figure 1: Flow chart of the PhD research activity

1.4. Structure of the thesis

This thesis is structured in five sections and an Appendix. The first section is the introductory chapter describing the background information, the framework of the research activity and its objectives.

From § 2 to § 4 the three main research activities performed in this work are described and finally in § 5 conclusions and future works are reported.

In particular, § 2 deals with the numerical and experimental activities performed in the CIRCE facility and aimed at investigating thermal stratification phenomena in large pool reactor cooled by heavy liquid metal (LBE). The numerical analysis performed in support

of the experimental campaign represents a simplified coupling calculation between the RELAP5 code and the Fluent code.

The coupling tool is then improved and developed in § 3 where an advanced version of the coupling scheme is presented and tested comparing numerical data with experimental data obtained in an experimental campaign performed in the NACIE loop facility. A loop configuration is more suitable for the coupling methodology, allowing focusing on the development of the tool.

Finally, § 4 deals with the experimental campaign performed in the CIRCE facility, both in natural and forced circulation regimes, devoted to investigate heat transfer phenomena in fuel pin bundle. Experimental data are then compared with the Mikityuk and the Ushakov correlations.

In Appendix *A* the error data analysis, concerning the experimental tests analysed in § 4 is described in order to study the effects of the uncertainty in single measurements on the calculated results.

2 THERMAL STRATIFICATION

2.1. Introduction

In the design of next generation Fast Breeder Reactors (FBR), technologies involving passive safe concepts have received attention in order to achieve the goal of safety improvement compared to older generation NPP, in agreement with GEN-IV safety and reliability goals. In this context, natural circulation phenomena that occur in the pool of the reactor play an important role in the decay heat removal. In fact, when the forced flow of liquid metal is lost, heat transfer can be then assured only through natural circulation that strongly affects the temperature distribution in the reactor itself.

In particular, free convection heat transfer under thermally stratified conditions is expected inside the liquid metal pools. Most of the works available in literature, concerning natural circulation phenomena of interest in the nuclear field, deal with results obtained using water or sodium as working fluids (Ishitori et al. 1987 and Watanabe et al., 1994). Furthermore, most of them neglect the thermal stratification that is instead considered one of the most important topics in the study of Generation IV reactors for increasing reactor safety and its structural integrity. Because of an accidental scenario, the reactor is scrammed, and assuming the total loss of the pumping system, the coolant flow rate reduces and large temperature variation takes place causing thermal stratification phenomena inside the pool. A large vertical temperature gradient may induce significant thermal loads on the structure in addiction to existing mechanical loads. Moreover, due to the instability (with respect to the position) of the stratification interface, low frequency oscillations with large amplitude are generated. Since the thermal conductivity of HLM is 10-20 times higher than that of water (for lead at 450°C the thermal conductivity is about 17 W/m K) temperature fluctuations are transmitted with low attenuation to the structures, leading to thermal cycle fatigue on the surface of the structure materials. In order to investigate this phenomenon a preliminary CFD numerical calculation was performed simulating an experimental test available in the scientific literature (Uotani M., 1987).

This step was performed to highlight CFD capability/limitation and to provide a guideline for the next study of heat transfer under thermally stratified conditions in the CIRCE large pool facility, reported in § 2.5.

Then, Fluent CFD code was used to simulate the thermal-hydraulic behaviour of the CIRCE facility. Numerical simulations were supported by experimental activities performed on the CIRCE pool, refurbished with the ICE test section.

2.2. Uotani experiment description

The aim of the experiment conducted by Uotani in 1987 (Uotani M., 1987) was to investigate the effects of thermal stratification in liquid metals on the free convection heat transfer along an immersed vertical metal heated surface. In particular, during the experiment, the temperature field was studied in a cylindrical vessel with a diameter of 400 mm filled with molten Pb-Bi. In Figure 2, the main dimensions of the facility are provided.

The vertical metal surface belongs to a 300 mm high stainless steel plate and the heat flux of the plate surface was maintained constant and uniform during the whole experiment.

Furthermore, an electrical heating wire of 2.3 mm diameter laid uniformly over the plate and fixed with thermal cement heated the vertical plate. This heating surface was backed with thermal insulation ($\lambda \approx 0.6$ W/(m K)) which reduces rearward heat losses below 1%; the front surface was covered with a stainless steel 3 mm thick plate and was plated with Nickel in order to improve wettability. The vessel was filled with 50 *l* of LBE.

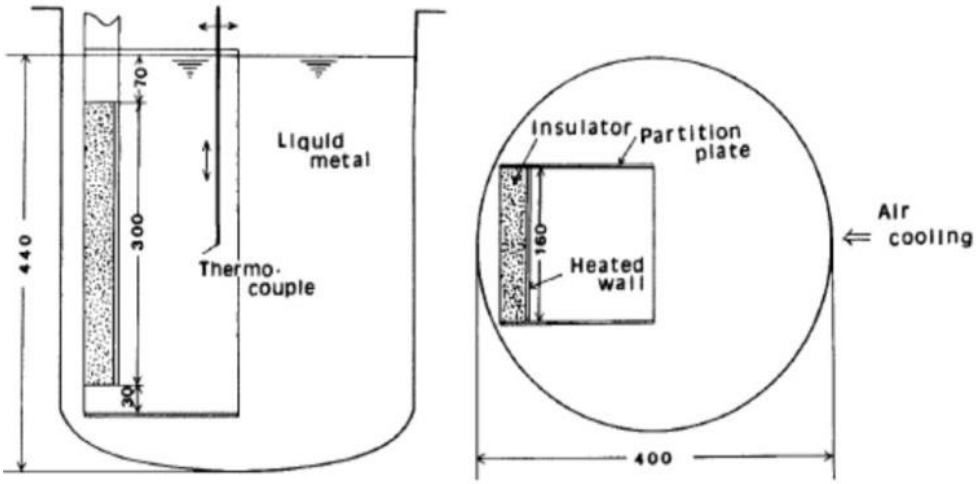

Figure 2: The Uotani facility

The vessel external surface was cooled by airflow supplied by a blower; hence, the degree of stratification was controlled by changing the position of impingement of the cooling air on the external portion of the vessel opposite to the heated plate.

Temperature measurements were carried out by using a series of thermocouples mounted on two hinged rods in order to assume both horizontal and vertical directions. The bulk temperature was obtained by averaging temperature measurements at a fixed height far away the boundary walls. Concerning the test procedure, after the heaters were adjusted to a prescribed power level, the cooling rate of the vessel was regulated to obtain the desired fluid temperature field. Temperature measurements were initiated upon the establishment of steady-state conditions, assumed to be obtained when the rate of change in temperature of the stainless steel plate and the fluid fell below 0.5°C/h. The following relation defines the stratification parameter considered by Uotani for the uniform heat flux:

$$S = \frac{\lambda}{a \cdot q''} \tag{1}$$

Where λ is thermal conductivity, a the temperature vertical gradient in the bulk region and q'' the imposed heat flux.

Figure 3 shows the resulting experimental temperature distributions along the plate wall and in the bulk for two different values of the stratification parameter *S*. The temperatures were reported along the *x*-axis, while the ordinate measures the distance from the leading edge of the heated plate.

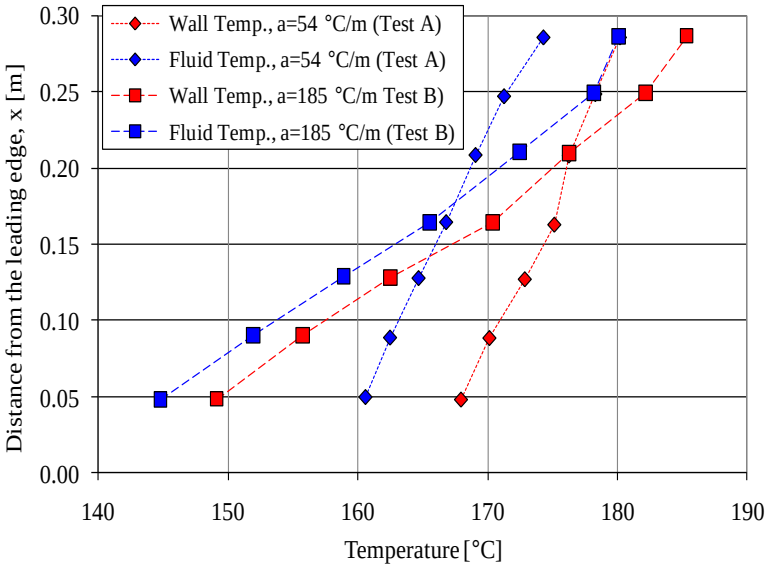

Figure 3: Wall and fluid temperature (q''=18.8 kW/m^2 for a=54°C/m and q''=17.9 kW/m^2 for a = 185°C/m)

The parameter a, was determined from a linear approximation of the axial bulk fluid temperature distribution obtained in the range between x = 0.05 m and x = 0.2 m in order to avoid the two boundaries and the consequent edge effects. For this reason, the discussion of the local heat transfer rates, which will be presented in the next section, is limited to this range of values. Two tests with a=54°C/m (S = 0.028) and a = 185°C/m (S = 0.1), called Test *A* and Test *B* and representative, respectively, of low and high thermal stratification condition are reported.

2.3. CFD simulation of the Uotani's experiment

The calculation domain is selected with a two-dimensional geometry. In particular, the section of the vessel considered most significant for the fluid-dynamic analysis is the one passing through the vertical axis of symmetry of the heated plate. The reference frame is selected with the origin at the leading edge of the heated plate and with the x-axis along the plate and the y-axis normal to it (Figure 4).

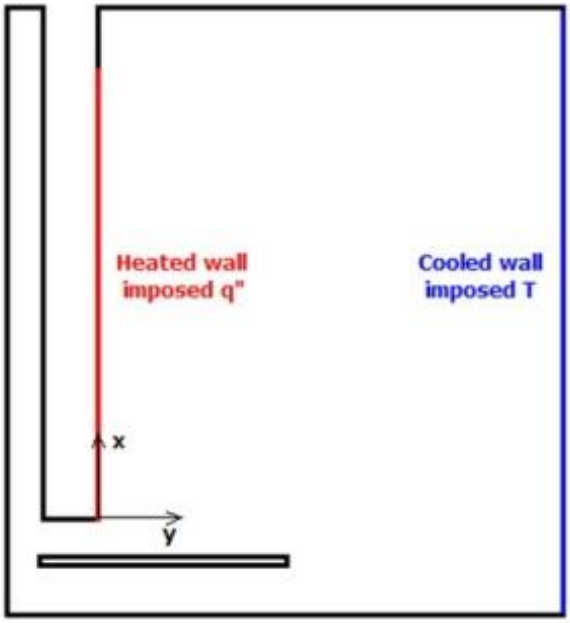

Figure 4: Geometrical simulation domain

2.3.1. Numerical model and spatial discretization

The thermal stratification parameter is set by imposing a linear temperature profile at the cooled boundary. A User Defined Function (UDF) (Ansys Fluent User Guide, 2012) is used to set this particular temperature profile; varying the temperature gradient at the cooled wall, the bulk thermal stratification could be properly changed.

The thermodynamic and thermo-physical properties of the LBE alloy (such as density, molecular viscosity, thermal conductivity and specific heat) are chosen according to the "*Handbook on Lead-bismuth Eutectic alloy and Lead properties, material compatibility, thermal-hydraulics and technologies*", 2007. All the relations giving the thermodynamic properties of the LBE as a function of temperature are implemented in the Fluent code using polynomial functions. The turbulent Prandtl number is set to 4.12 in agreement with what was obtained using the correlation proposed by Cheng and Tak (2005).

The problem is considered unsteady in all the simulations and a time step of 10 ms is adopted. The flow regime evaluation is conducted evaluating both the Grashof number and the product of the Rayleigh number by the Prandtl number (Mohamad and Viskanta, 1993):

$$\mathrm{Gr_x} = \frac{g\beta(T_w - T_\infty)x^3}{\nu^2} \tag{2}$$

Experiments under investigation, envisage temperature in a range between 400÷475 K with T_w-T_∞ being about 10 K. In the definition of the Grashof number, x represents the distance from the leading edge of the heating plate (ranging from 0 to 0.3 m in the present case). The values of the Grashof number for various values of the difference T_w-T_∞ and x are summarized in
Table 1.

Table 1: Gr_x for different values of T_w, T_∞, and x

T [K]		**Values of the local Grashof number**					
T_w	T_∞	*x= 0.05* m	*x= 0.10* m	*x= 0.15*m	*x= 0.20* m	*x= 0.25* m	*x= 0.30* m
410	400	$1.80\ 10^8$	$2.88\ 10^9$	$1.45\ 10^{10}$	$4.61\ 10^{10}$	$1.12\ 10^{11}$	$2.33\ 10^{11}$
475	465	$2.47\ 10^8$	$3.96\ 10^9$	$2.00\ 10^{10}$	$6.33\ 10^{10}$	$1.55\ 10^{11}$	$3.20\ 10^{11}$

Conventionally the transition from laminar to turbulent flow in problems involving natural convection on a vertical plane plate occurs for Grashof number greater than 10^9. In this work for heights greater than $x = 0.05$ m the flow field is therefore expected to be turbulent. In other works with lead-bismuth as working fluid and with conditions similar to those considered here, the product of the Rayleigh number by the Prandtl number is considered in order to investigate the flow transition, considering the value $Ra \cdot Pr = 4.8 \cdot 10^3$ as the lower limit for turbulent flow conditions (Mohamad and Viskanta, 1993).

Table 2, summarizes the values of the product of the Rayleigh number by the Prandtl number as a function of the distance from the leading edge of the heating plates (x).

Table 2: $Ra \cdot Pr$ for different values of T_w, T_∞, and x

T [K]		**Values of the local Ra·Pr number**					
T_w	T_∞	*x= 0.05* m	*x= 0.10* m	*x= 0.15*m	*x= 0.20* m	*x= 0.25* m	*x= 0.30* m
410	400	$4.22\ 10^5$	$6.67\ 10^6$	$3.42\ 10^7$	$1.08\ 10^8$	$2.64\ 10^8$	$5.47\ 10^8$
475	465	$3.14\ 10^5$	$5.03\ 10^6$	$2.55\ 10^7$	$8.05\ 10^7$	$1.96\ 10^8$	$4.07\ 10^8$

This analysis suggests excluding the utilization of a laminar solver for simulating the expected flow field; therefore, the adopted turbulence treatment is the Reynolds-Averaged Navier-Stokes equations (RANS) Reynolds Stress Model (RSM). Two equation turbulent models were also investigated in the present work, but they were found inaccurate for the present purposes. Since an accurate representation of the flow in the near-wall region critically determines the successful predictions in wall-bounded turbulent flows, the "enhanced wall treatment" is adopted in solving the balance equations in the viscous sub-layer near-wall regions (Ansys Fluent User Guide, 2012).

A two-dimensional hexahedral mesh of about 131,000 cells is generated, with special refinements next to the wall boundaries of the domain. Using the values of the wall y^+ as guidance in selecting the appropriate grid configuration, according with the requirement that $y^+ \approx 1$ is desirable for near-wall modelling, the mesh refinements shown in Figure 5 and Figure 6, are adopted.

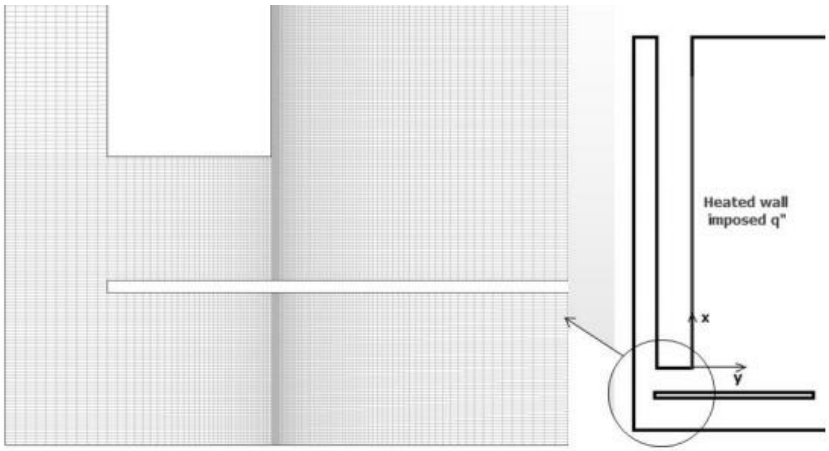

Figure 5: Mesh refinement in the bottom left region of the vessel

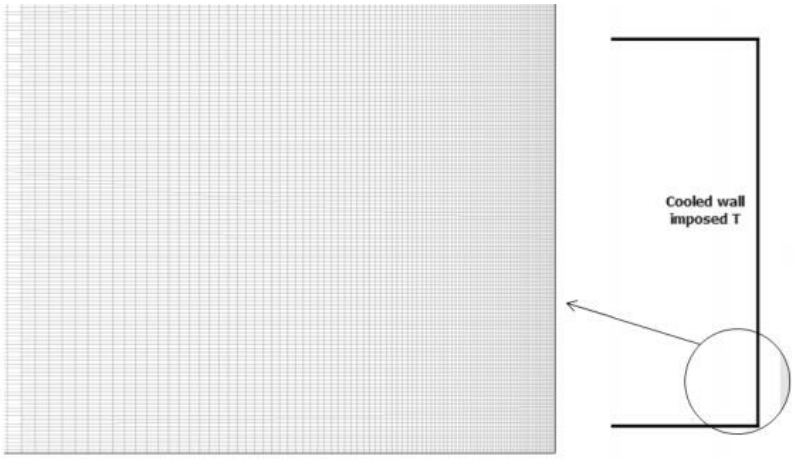

Figure 6: Mesh refinement in the bottom right region of the vessel

Boundary conditions at the cooled wall were not easily predictable because no data were reported about the actual experimental conditions (Uotani M., 1987). In particular, neither temperature measurements on the cooled wall, nor air temperature or air mass flux supplied by the blower were specified. Given this lack of data, it was necessary to perform a number of simulations for each test providing reasonable boundary conditions in order to obtain a good approximation of the bulk temperature field.

The steady-state condition are assumed to be attained when the total thermal power acting on fluid remains, for a sufficient period, less than 10 W. Two sets of simulations are performed with a vertical temperature gradient in the bulk of 54°C/m (Test *A*) and 185°C/m (Test *B*).

2.3.2. Obtained results

Results of the simulations allowed obtaining information in such detail that the experimental study could not provide. Calculated temperature and velocity fields give an

overall view of the phenomena characterizing liquid metal flows in thermal stratification conditions. According to what mentioned in § 2.2, the analysis was focused on the range of coordinates x = 0.05 m and x = 0.2 m. Figure 7 and Figure 8 report the temperature trends on the heating surface and in the bulk flow for simulations of tests *A*, *B*. The imposed uniform heat flux at the heating wall is about 18 kW/m^2. The obtained results show good agreement between the simulated temperature trends and experimental data.

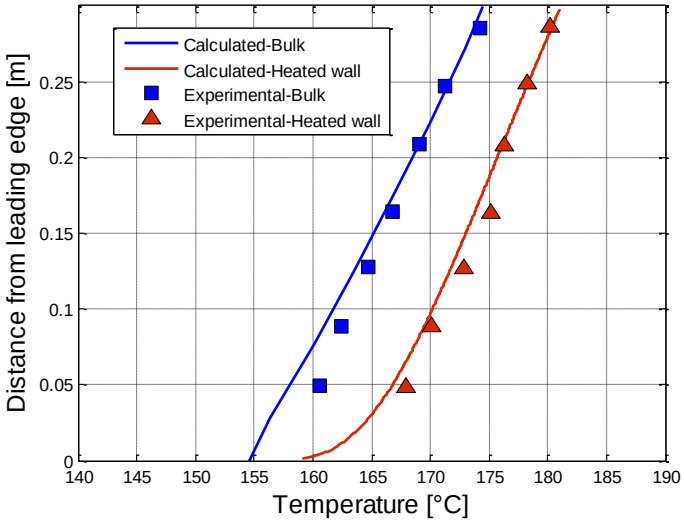

Figure 7: Temperature trends on the heating wall and in the bulk, Test *A* (a = 54°C/m and q'' = 18.8 kW/m^2)

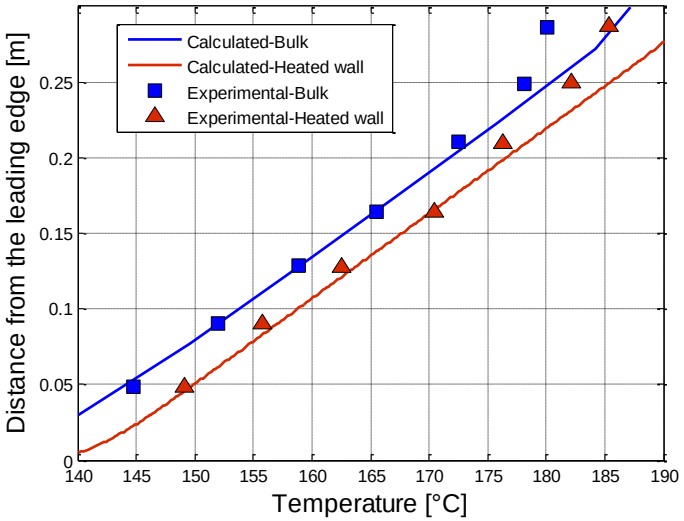

Figure 8: Temperature trends on the heating wall and in the bulk, Test *B* (a = 185°C/m and q'' = 17.9 kW/m^2)

Figure 9 (*a*) and (*b*) show the temperature distribution in the calculation domain highlighting the occurring stratification phenomena. Furthermore, from the analysis of the velocity vector distribution in the calculation domain it can be noted that the thickness of the boundary layer on the two vertical walls is influenced by the fact that few millimetres from the wall there are streams that moves counter flow to the principal flow. In particular, it is possible to see in Figure 10 (*a*) and (*b*) that this stream comes closer to the wall as the thermal stratification degree increases.

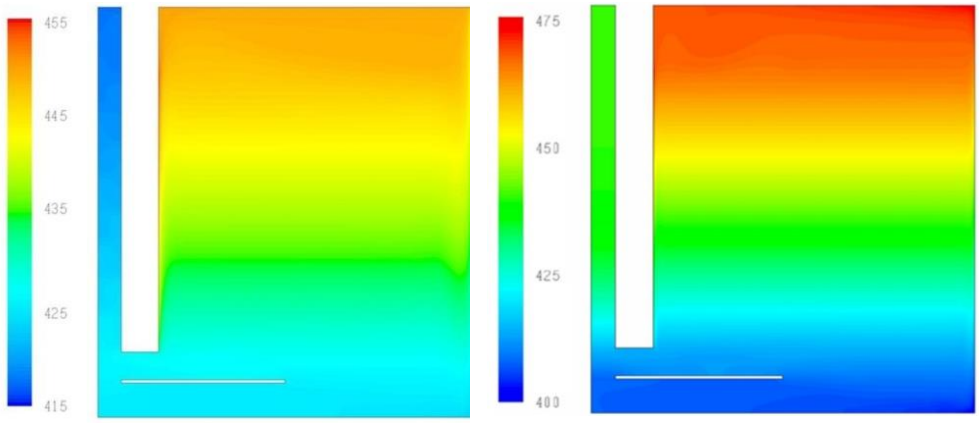

(*a*) (*b*)

Figure 9: Temperature distribution [K], Test *A* (*a* = 54°C/m) (*a*) and Test B (a = 185°C/m) (*b*)

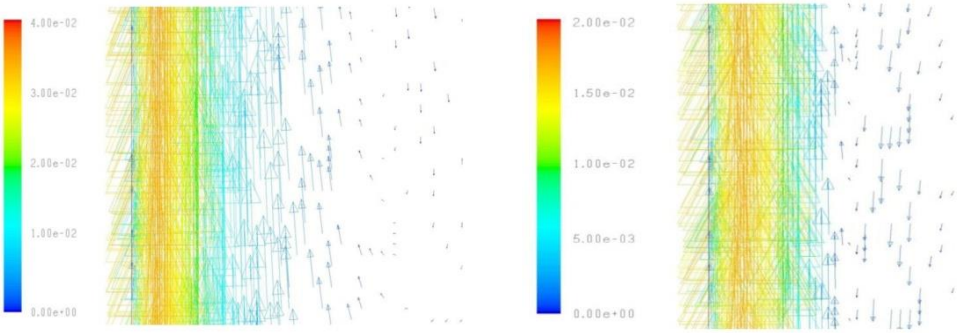

(*a*) (*b*)

Figure 10: Velocity field [m/s] in proximity of the heating wall, Test *A* (*a* = 54°C/m) (*a*) and Test *B* (a = 185°C/m) (*b*)

Natural convection in the boundary layer is induced by the density gradient across it. This gradient is reduced, for stratified bulk fluid, by the fact that moving upwards the fluid encounters higher temperatures zones and, therefore, a lower temperature gradient between the boundary layer and the bulk fluid is established. The resulting reduction of buoyancy force leads to a reduction of thickness in the higher temperature zone close to the heated wall. In liquid metals, the temperature gradient in the boundary layer is very small; hence, the thermal boundary layer thickness is strongly influenced by thermal stratification in the

undisturbed fluid. In the simulation results, in agreement with experimental data, increasing the degree of stratification, and hence *a*, the thermal boundary layer thickness decreases. In Eq. 3, the displacement thickness of the boundary layer (distance by which the external streamlines are shifted owing to the formation of the boundary layer), is evaluated.

$$\delta = \frac{\int_0^{\infty} (T - T_b)\, dy}{(T_W - T_b)} \tag{3}$$

This variable shows a reduction of the thickness of the boundary layer as thermal stratification increases; the obtained results display a similar trends to that obtained experimentally by Uotani. The comparison between the numerical results and those presented in Uotani M. (1987) is pointed out in Figure 11.

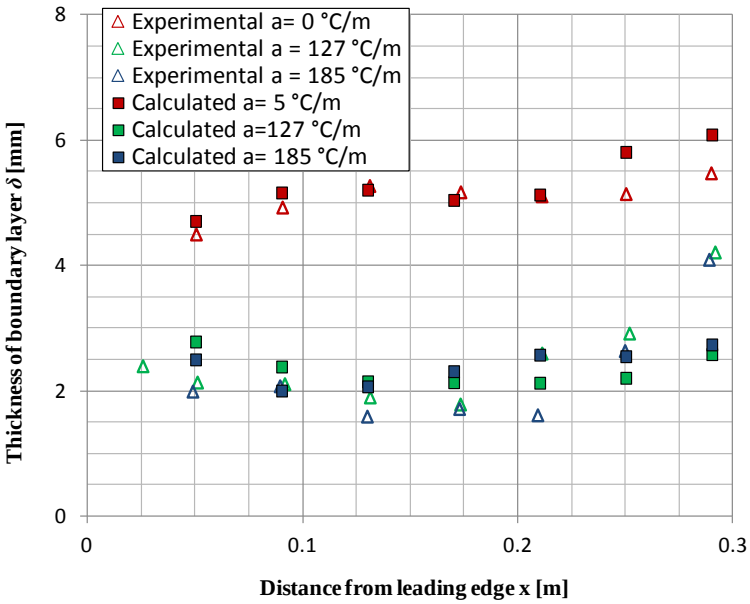

Figure 11: Effect of thermal stratification on thickness of boundary layer

The good agreement found between analytical and experimental results provide confidence in the capability of the Ansys Fluent code in simulating heat transfer under thermally stratified conditions. For this reason, the code was adopted in order to simulate the CIRCE large pool experimental facility.

2.4. CIRCE experimental facility

2.4.1. CIRCE facility and ICE test section

In the frame of the National Program (ENEA–Minister of Economic Development Program Agreement) on Gen. IV Reactors Development and of Thermal Hydraulics of Innovative Nuclear System (THINS) EU project a large scale integral test, named "CIRCE

experiment", was implemented and carried out at the Brasimone-ENEA research Centre using Lead Bismuth Eutectic alloy as working fluid.
The main objective of the CIRCE experiment is to characterize the thermal-hydraulic behaviour in a HLM pool system. In particular, experimental campaigns were designed in order to:

- Investigate the thermal-hydraulics of a LFR primary system both under nominal condition and transient scenarios, e.g. during the transition from forced (nominal) flow conditions to natural circulation typical of Decay Heat Removal (DHR) conditions;
- Support the qualification of CFD codes and models for the simulation of in-pool phenomena;
- Support the assessment of thermal-hydraulic system codes for the simulation of system dynamics in buoyancy influenced flow conditions.

CIRCE is a pool type facility consisting of a cylindrical vessel (Main Vessel S100) filled with about 70 tons of molten LBE with argon cover gas and recirculation system, LBE heating and cooling systems, several test sections welded to and hung from bolted vessel heads for separate-effects and integral testing and auxiliary equipment for eutectic circulation (Turroni et al. 2001, Benamati et al. 2005, Tarantino and Scadozzo 2006, Bandini et al. 2011, Figure 12).

The facility is completed by a LBE storage tank (S200), a small LBE transfer tank (S300) and a data acquisition system. During the loading operations, the LBE is gradually transferred from the storage tank (S200) to the S300 vessel. Then, by pressurization of the S300 cover gas, the liquid metal gradually fills the test vessel (S100) from the bottom (Figure 12).

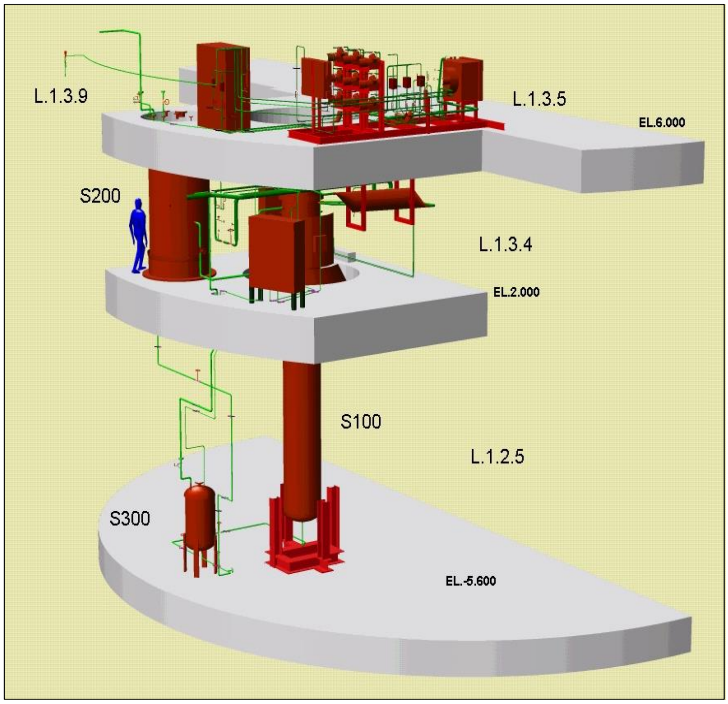

Figure 12: CIRCE isometric view

The main vessel S100 consists of a vertical vessel 8500 mm in height, connected by gates to the other vessels. It is externally equipped with electrical heating cables, installed at the bottom and on the lateral surface. This heating system operates in a temperature range of 200÷400°C. A skimming line and a passive pressure safety system are also present in the main vessel, in order to guarantee the LBE top level and to prevent accidental overpressure. The S100 main parameters are summarized in Table 3.

Table 3: CIRCE S100 main parameters

Parameter	**Value**
Outside Diameter	1200 mm
Wall Thickness	15 mm
Material	AISI 316L
Max LBE Inventory	90000 kg
Electrical Cable Heating	47 kW
Cooling Air Flow Rate	3 Nm^3/s
Temperature Range	200-550°C
Operating Pressure	15 kPa (gauge)
Design Pressure	450 kPa (gauge)
Nominal Argon Flow Rate	8 Nl/s
Argon Injection Pressure	600 kPa (gauge)

The ICE test section (Figure 13) is contained in the S100 main vessel and it was conceived to reproduce thermal-hydraulic behaviour of the Experimental Accelerator Driven System (XT-ADS) and European Facility for Industrial Transmutation (EFIT) primary system (Mansani 2005, Barbensi and Corsini 2006, Giraud 2006, Artioli 2006, Van den Eynde 2007).

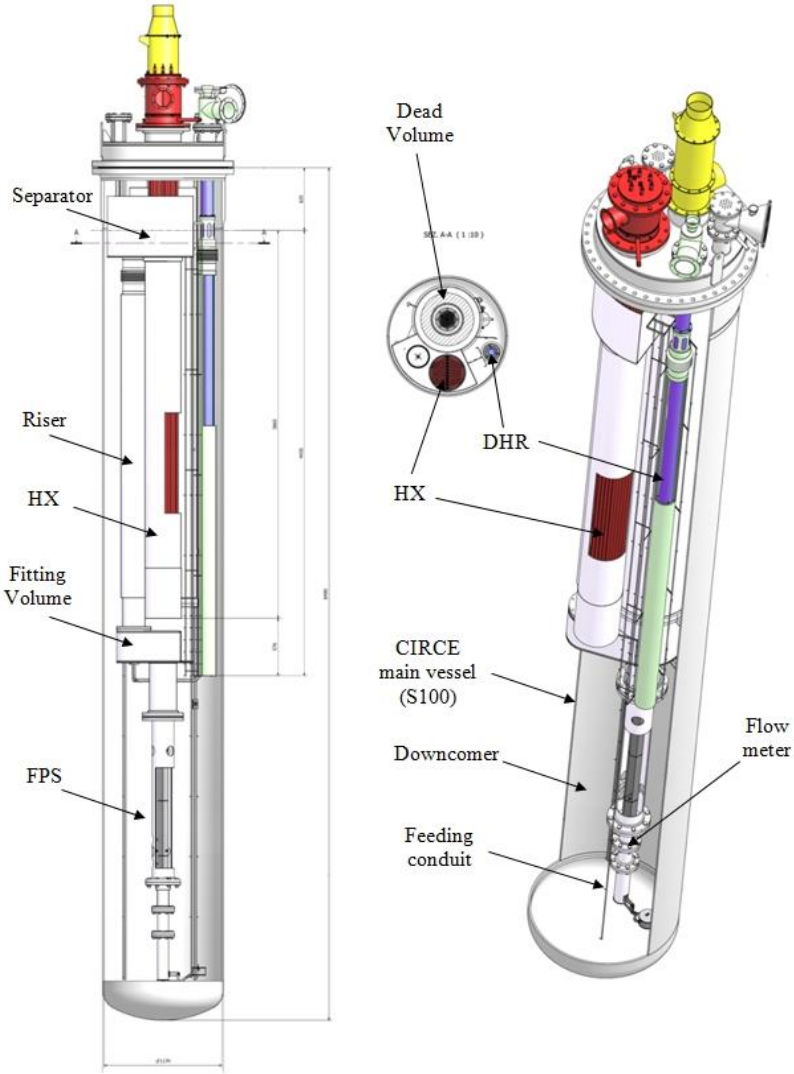

Figure 13: ICE Test section

It is composed of the following main components:

- *Downcomer*: it is the volume between the test section and the main vessel, which allows the hydrodynamic connection between the outlet section of the heat exchanger (HX) and the inlet section of the feeding conduit.
- *Feeding Conduit:* it is the inlet pipe of the test section. It allows the hydrodynamic development of the upward primary flow rate towards the flow meter.
- Flow meter: it is a Venturi-nozzle flow meter. Bubble tubes are adopted to measure the pressure difference through the throat of the nozzle. The flow meter is directly connected to the heat source (HS), without a bypass, thus measuring the primary flow rate through the pin bundle.

- *Fuel Pin Simulator* (FPS): it is a mechanical structure needed to simulate the Heat Source (HS). it is connected in the lower section to the flow meter and in the upper section to the insulation volume by means of the coupling flange. The coupling flange assures the sealing, avoiding the insulation volume flooding by LBE. In the upper section, the FPS is hydraulically linked to the fitting volume, ensuring continuity of the main flow path.
- *Fitting Volume*: it is placed in the middle part of the test section, allowing the hydraulic connection between the HS and the riser.
- *Riser*: it is an insulated pipe (double wall pipe with air in the gap) connecting the fitting volume with the separator. A nozzle is installed in the lower section to allow the argon injection inside this pipe [10-11].
- *Separator*: it is a volume needed to connect the riser with the HX. It allows the separation of the LBE flowing downward into the HX from the Argon flowing in the test section cover gas through the free surface. Moreover, the separator assures that the overall LBE flow rate flows directly into the HX (shell-side) before falling down in the downcomer. In addition, the separator works as an expansion vessel, allowing for fluid expansion during transient operations.
- *Heat Exchanger:* it corresponds to the heat sink of the system. It consists of double-wall bayonet tubes (with helium gap) fed by low pressure boiling water. It has a thermal duty of 800 kW. In order to promote natural circulation along the primary flow path, it is installed in the upper part of the test section.
- *Dead Volume*: it is a component made of two concentric pipes. The inner pipe is connected, by bolted junctions, to the FPS (by the coupling flange) and to the cover head. The volume inside the inner pipe is called Insulation Volume. The outer pipe is welded to the inner pipe in the lower end by a flange, which allows a bolted connection between the dead volume and the fitting volume. It extends to the cover gas, above the free level. The annulus between the inner and outer pipes, kept melt-free by design, is linked to the cover gas and filled by a thermal insulator in order to reduce the radial heat flux towards the insulation volume.
- *Decay Heat Removal System*: it corresponds to the heat sink of the system in the case of DHR scenario, when the HX is unavailable. It is hydraulically de-coupled by the primary system being placed into the downcomer. The DHR heat exchanger was designed to have a thermal duty of 40 kW, which represents 5% of the ICE nominal power (800 kW). It is fed by air at atmospheric pressure.

2.4.2. CIRCE-ICE instrumentation

In order to investigate stratification and mixing phenomena in the pool region and the thermal hydraulic behaviour of the HLM-cooled rod bundles, the facility is instrumented with several *N* type thermocouples with isolated hot junction. Those installed in the Fuel Pin Simulator (FPS) subchannels have a diameter of 0.5 mm the accuracy is ±0.1°C, while the other have a diameter of 3 mm and an accuracy ±1°C. Moreover, a Venturi-nozzle flow meter is installed at the entrance of the test section, after the feeding conduit, in order to evaluate the mass flow rate through the ICE test section. Finally, a hot wire anemometer measures the air mass flow rate flowing through the inner pipe of the Decay Heat Removal system (DHR).

2.4.2.1. FPS instrumentation

The ICE heat source consists of an electrical pin bundle with a nominal thermal power of about 800 kW. It consists of 37 electrical pins arranged in a wrapped hexagonal lattice. Three spacer grids (Figure 14) placed along the axis of the component fix the relative position between the pin bundle and the wrapper. The upper and lower spacer grids are placed at the interface between the active and non-active length of the electrical pins to enclose the mixing zones. The middle spacer grid is placed in the middle section of the bundle's active length. From a hydraulic point of view, the FPS assures that the overall LBE flow rate runs along the HS, without any by-pass. In Table 4, the main data of the HS are summarized.

Table 4: FPS main parameters

Parameter	***Value***
Number of pins n	37
Pin outer diameter ϕ	8.2 mm
Power of a pin	25 kW
Pin wall heat flux	1 MW/m^2
Pitch to diameter p/ϕ	1.8
Active Length	1 m
l' (edge length of the exagonal wrapper)	55.4 mm
H' (Apothem of the exagonal wrapper)	96 mm

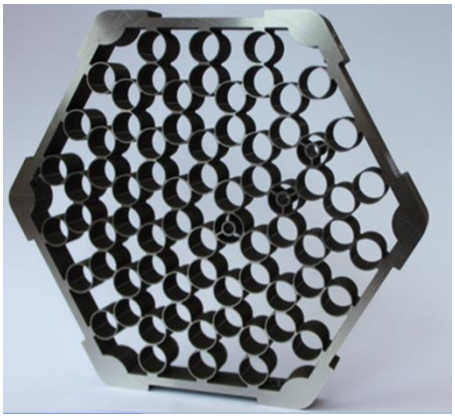

Figure 14: Spacer grid

The LBE temperature at the FPS entrance is measured by three thermocouples with a diameter of 3 mm (TC-FPS-31, 32, 33, see Figure 15). The LBE temperature at the FPS exit section is measured by three thermocouples (TC-FPS-37, 38, 39) of the same type of those at the entrance.

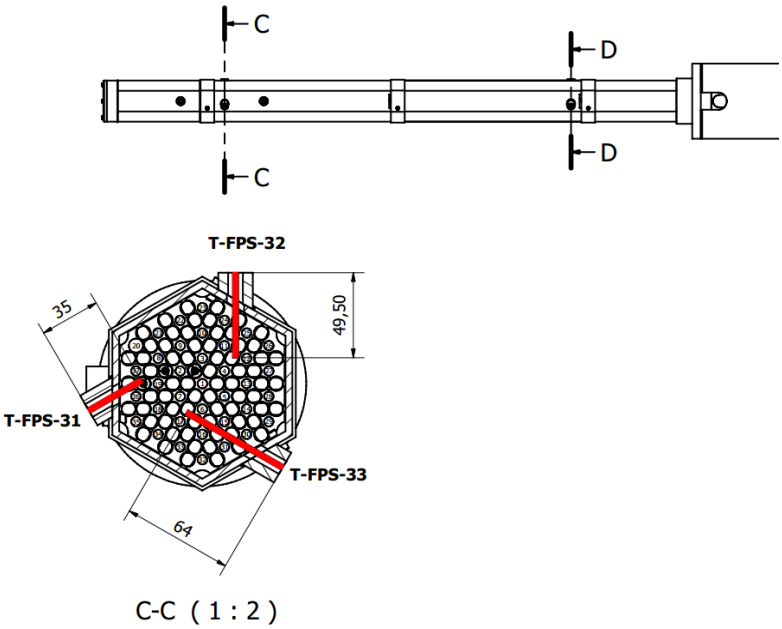

Figure 15: Thermocouples at the FPS Entrance

Regarding the positioning of the thermocouples along the FPS active zone, four different sections are monitored (see Figure 16):

- Section 1 (Figure 17): 20 mm upstream the middle spacer grid. In this section, thre9e different subchannels (external, medium and central or inner subchannels) are instrumented. In each subchannel, both pin clad and LBE bulk temperatures are measured (TC-FPS-01 to 09).
- Section 2 (Figure 18): on the matching surface between the middle spacer grid and the fuel pins. In this section the pin clad temperature for the three subchannels identified at section 1 is monitored (TC-FPS-10 to 14), aiming at the hot spot factor evaluation due to the installation of the spacer grid itself.
- Section 3 (Figure 19): 60 mm upstream of the upper spacer grid. In this section the same subchannels are identified in sections 1 and 2 for temperature measurements at the upper height of the bundle. In each subchannel, both pin clad and LBE bulk temperatures are measured (TC-FPS-16 to 24).
- Section 4 (Figure 20): 60 mm downstream of the lower spacer grid. In this section, the LBE bulk temperature is measured in each subchannel (TC-FPS-28 to 30).

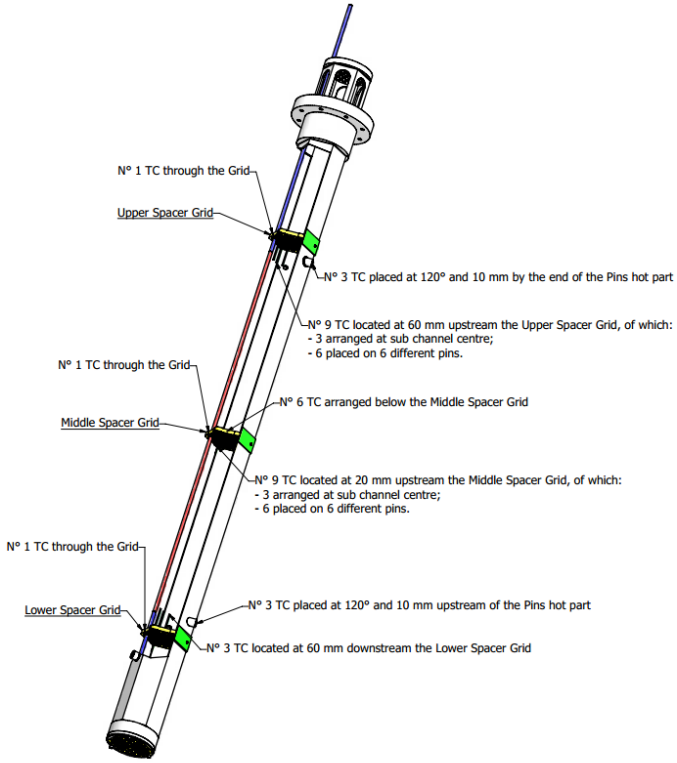

Figure 16: FPS measurement sections

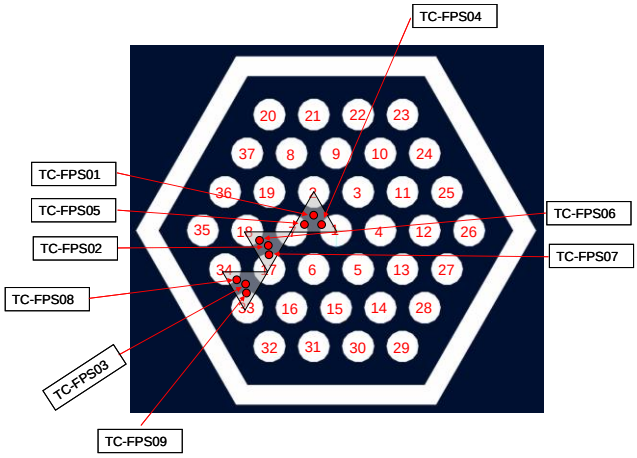

Figure 17: Section 1, subchannels instrumented

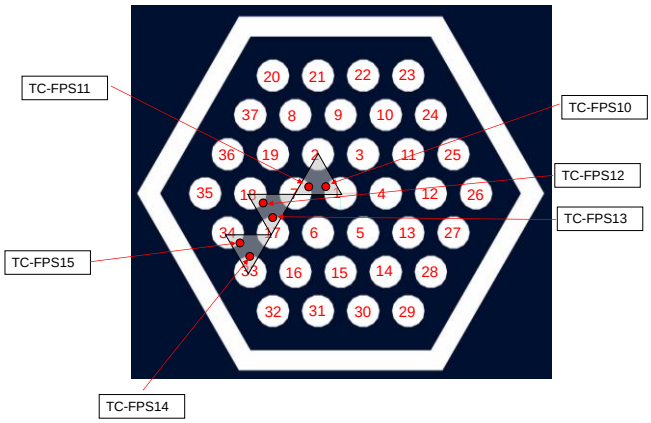

Figure 18: Section 2, subchannels instrumented

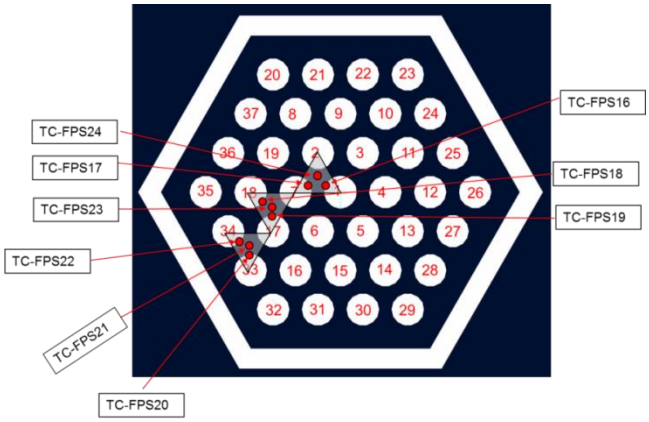

Figure 19: Section 3, subchannels instrumented

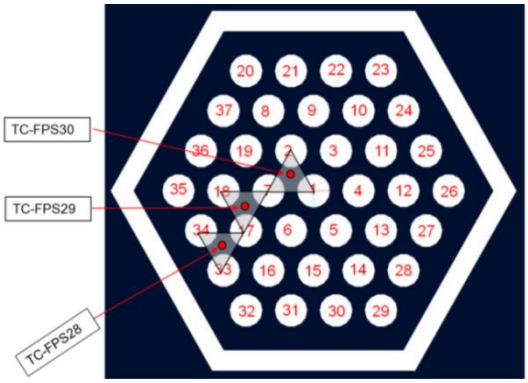

Figure 20: Section 4, subchannels instrumented

Figure 21 shows how thermocouples are fixed on the pin wall and hold in place in the centre of the subchannel.

Figure 21: TCs positioning and fixing

2.4.2.2. Riser and HX instrumentation

The LBE heated by the FPS flows through the fitting volume into the riser; here temperatures are measured using thermocouples (TCs) with a diameter of 3 mm disposed at the entrance section (T-TS-01 to 03) and at the exit section before the separator (T-TS-04 to 06, see Figure 22).

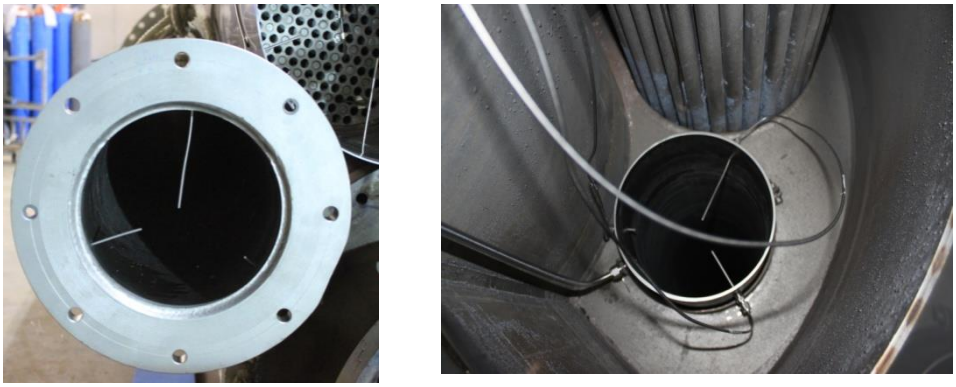

(a) (*b*)

Figure 22: TCs Installed at the riser entrance (*a*) and outlet (*b*) sections

From the riser exit, the LBE flows through the Separator into the HX shell, where the temperatures at the entrance section are measured by three TCs placed at 120°, 30 mm from the bottom of the Separator (T-SG-01 ... 03). Subchannel temperature measurements are taken in a plane placed 30 mm above the lower grid, according to the scheme shown in Figure 23 (T-SG-04 ... 12).

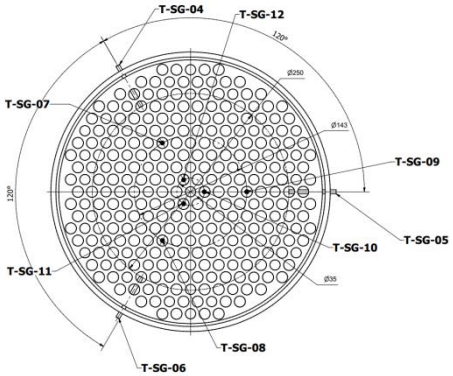

Figure 23: HX Subchannels TCs configuration

Temperatures at the HX exit were measured with six TCs (T-SG-13 ... 18) placed at 60° each and at 100 mm before the HX skirt exit (Figure 24).

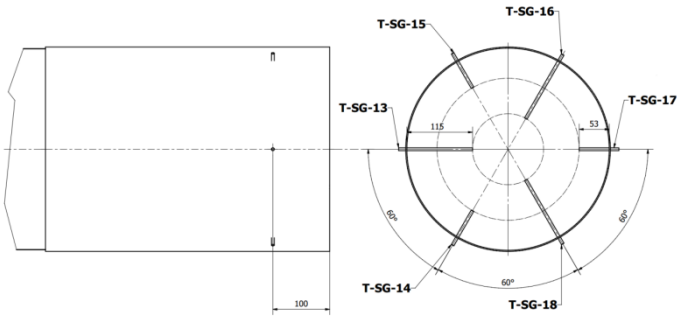

Figure 24: TCs configuration at the HX exit

2.4.2.3. DHR instrumentation

The Decay Heat Removal system is activated to remove heat in the case of an accidental event with total loss of HX heat sink and consequent reactor scram (Bandini et al. 2011). It consists of a bayonet element made of two concentric tubes cooled by low-pressure air. The velocity of the air flowing through the inner tube is measured by a hot wire anemometer placed in the tube at the entrance of the DHR and the mass flow rate is derived using the calibration curve given by the manufacturer. The air temperature is measured at the entrance and at the exit section of the secondary circuit, as shown in Figure 25. Regarding the primary circuit (LBE side), temperatures at the inlet of the DHR are measured by six TCs with a diameter of 3 mm, placed inside the slots at the entrance of the DHR shell according to Figure 26 (T-DHR-07 to 12).

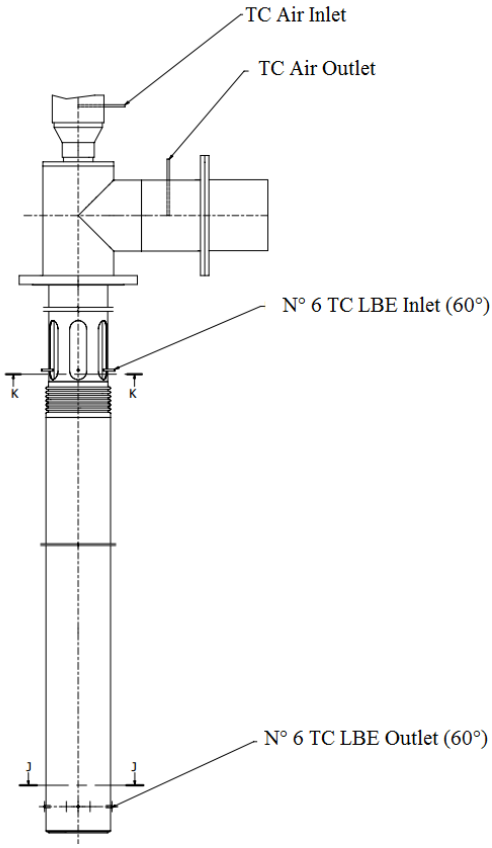

Figure 25: Sketch of TCs placed in the DHR

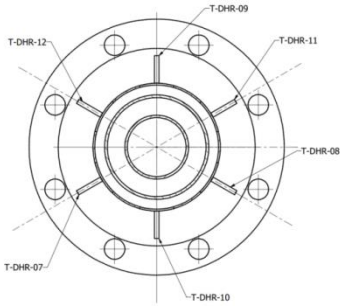

Figure 26: TCs configuration at the DHR inlet

The LBE temperature at the exit of the DHR is measured at 60 mm from DHR skirt outlet section, by six TCs with a diameter of 3 mm (T-DHR-01 to 06) placed at 60° according to the scheme shown in Figure 27 and Figure 28.

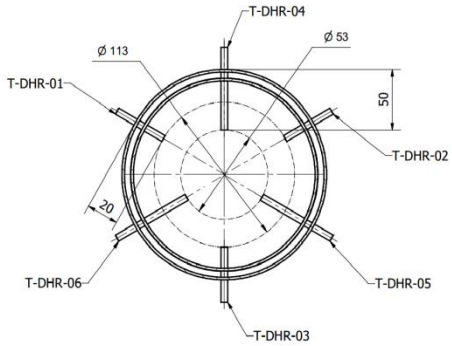

Figure 27: TCs configuration at the DHR outlet

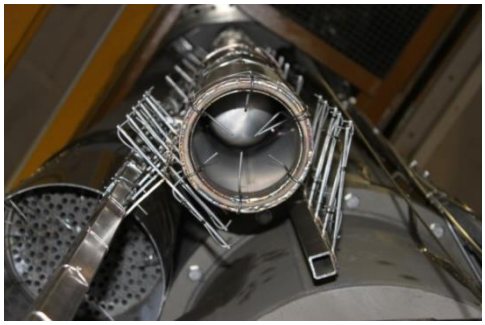

Figure 28: TCs at the DHR outlet

2.4.2.4. LBE pool instrumentation

Several TCs are installed in the LBE pool in order to investigate mixing and stratification phenomena. For that purpose, vertical rods are installed into the pool fixing the TCs at 17 different elevations for a total of 119 TCs with a diameter of 3 mm (T-MS-01 to 119). In particular, according to Figure 29 and Figure 30, TCs on lines *A*, *H* and *I* allow measurements from the bottom side of the test section up to the FPS entrance, while TCs on lines *B, C, D, E, F* and *G* allow measurements up to 600 mm below the exit of the DHR. Finally, In Table 5 all the TCs installed inside the LBE pool are listed specifying their name and vertical position.

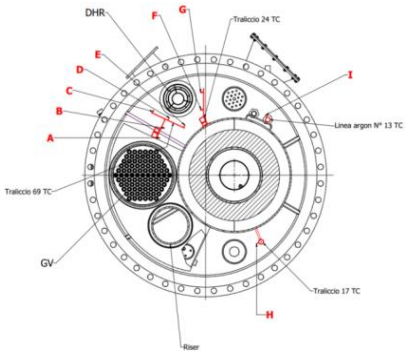

Figure 29: Arrangements of the vertical support for the TCs

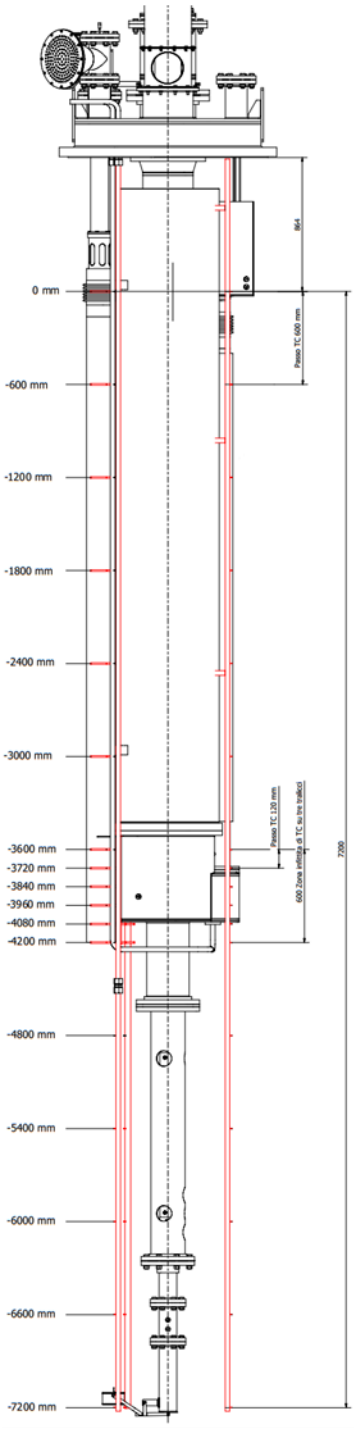

Figure 30: TCs vertical positioning

Table 5: TCs placed inside the LBE pool

TC	Vertical support	Vertical position [mm]
T-MS-01 to T-MS-05	*A, B, C, D, E*	0
T-MS-06 to T-MS-09	*F, G, H, I*	
T-MS-10 to T-MS-14	*A, B, C, D, E*	-600
T-MS-15 to T-MS-18	*F, G, H, I*	
T-MS-19 to T-MS-23	*A, B, C, D, E*	-1200
T-MS-24 to T-MS-27	*F, G, H, I*	
T-MS-28 to T-MS-32	*A, B, C, D, E*	-1800
T-MS-33 to T-MS-36	*F, G, H, I*	
T-MS-38 to T-MS-41	*A, B, C, D, E*	-2400
T-MS-42 to T-MS-45	*F, G, H, I*	
T-MS-46 to T-MS-50	*A, B, C, D, E*	-3000
T-MS-51 to T-MS-54	*F, G, H, I*	
T-MS-55 to T-MS-59	*A, B, C, D, E*	-3600
T-MS-60 to T-MS-63	*F, G, H, I*	
T-MS-64 to T-MS-68	*A, B, C, D, E*	-3720
T-MS-69 to T-MS-71	*F, G, H*	
T-MS-72 to T-MS-76	*A, B, C, D, E*	-3840
T-MS-77 to T-MS-79	*F, G, H*	
T-MS-80 to T-MS-84	*A, B, C, D, E*	-3960
T-MS-85 to T-MS-86	*F, G, H*	
T-MS-88 to T-MS-92	*A, B, C, D, E*	-4080
T-MS-93 to T-MS-95	*F, G, H*	
T-MS-96 to T-MS-100	*A, B, C, D, E*	-4200
T-MS-101 to T-MS-104	*F, G, H, I*	
T-MS-105 to T-MS-107	*A, H, I*	-4800
T-MS-108 to T-MS-110	*A, H, I*	-5400
T-MS-111 to T-MS-113	*A, H, I*	-6000
T-MS-114 to T-MS-116	*A, H, I*	-6600
T-MS-117 to T-MS-119	*A, H, I*	-7200

2.5. *Numerical pre-test simulations of the CIRCE facility behaviour*

CIRCE thermal fluid-dynamic pre-test analyses are performed developing a "one-way" off-line coupling model between the thermal-hydraulic system code (STH) RELAP5 mod/3.3 and the computational fluid dynamic code (CFD) Ansys Fluent. In this coupled methodology, both codes run separately and the variables of interest computed by the STH code (simulating the whole facility) are transferred to the CFD code and set as boundary conditions by means of a UDF (Ansys Fluent User Guide, 2012). No feedback information is exchanged from the CFD to the STH code. Both the primary (LBE side) and the secondary (air-side) domains are reproduced in the model. The transition from forced to natural circulation conditions is investigated together with the thermal stratification inside the CIRCE pool.

2.5.1. *Computational domain and numerical model*

Due to the huge dimensions of the CIRCE facility main vessel (see § 2.4.1) and to the long duration of the envisaged transient, a simplified 2D geometrical domain is developed, aiming at reducing the large computational effort required. More specifically, the calculation domain is modelled as a 2D axial-symmetric geometry, assuming the DHR's axis as an axis of symmetry for the geometrical domain. Only the DHR and the LBE pool regions inside the main vessel are entirely reproduced (Figure 31 and Figure 32). Other components of ICE test section as HS, riser, gas separator and HX are schematically represented whilst maintaining the same transit time of the real geometry and the same heat flux in the HS and in the HX (Figure 32).

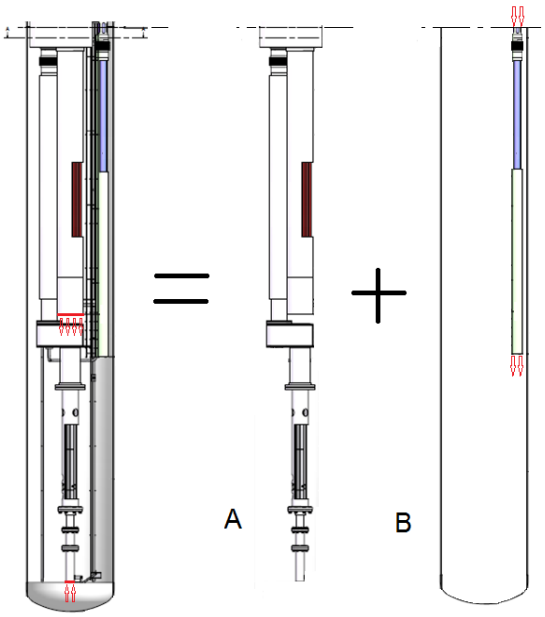

Figure 31: Geometry decomposition of the domain

Gravity acts downward along the *x*-axis (coincident with the symmetry axis). The cross section area of the geometrical domain is equal to that of the CIRCE LBE pool at the same vertical position (the diameter of DHR is included in a cylindrical tank with an inner diameter equal to the equivalent diameter of the cross section of LBE pool). The total mass of LBE considered in the domain is the same contained into the LBE pool.

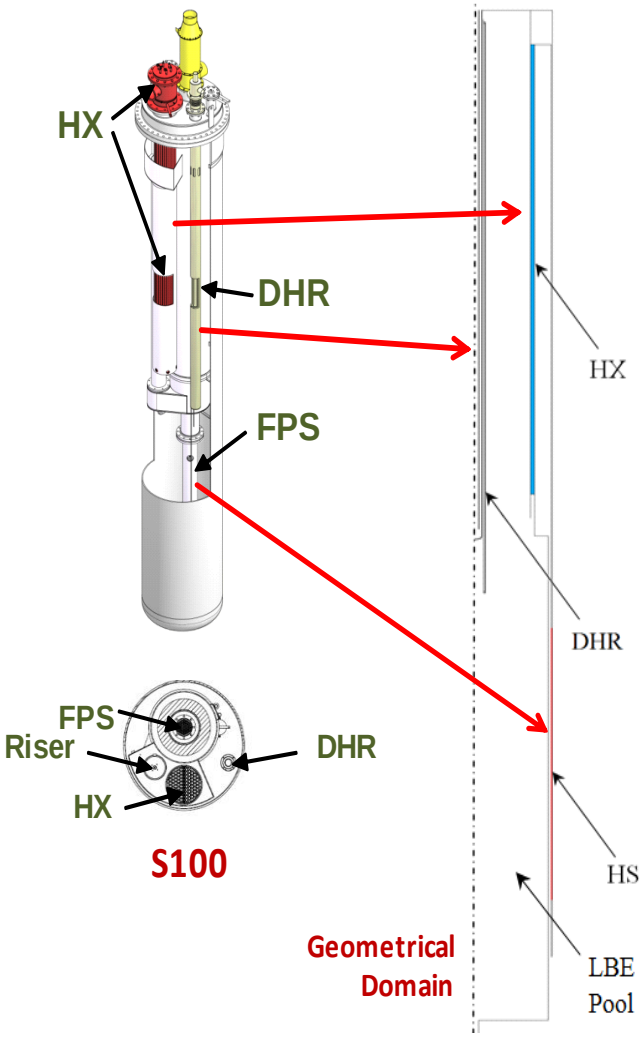

Figure 32: CFD geometrical schematization

The computational domain is discretized using a hexahedral mesh for almost the entire domain. The only exception is represented by the rounded bottom side of the air inner pipe of the DHR heat exchanger. Special refinements near the wall boundaries of the domain are adopted according to requirement $y^+=1$ for enhanced wall treatment model used in the CFD code (Figure 33). The total amount of cells is about 927300. The adopted turbulence model is the *k*-ε Renormalized Group (RNG) with the "enhanced wall treatment" option for near-

wall turbulence modelling. The external walls are set as adiabatic and no slip conditions are assumed.

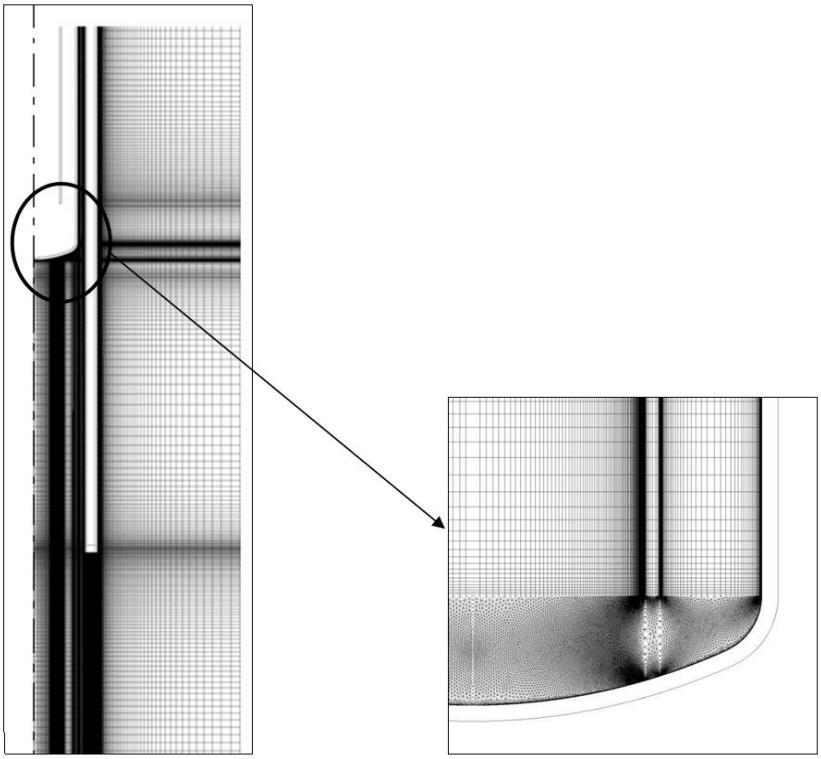

Figure 33: Geometrical discretization

A PLOHS+LOF transient analysis assuming a time step of 1 s is performed and a total of twenty hours of transient is investigated. Temperature, velocity and turbulence kinetic energy fields assigned as initial conditions for the transient simulation are obtained from a preliminary CFD steady state calculation from which the transient from forced to natural circulation is simulated. This steady state calculation is performed assuming nominal operating conditions for the facility (gas enhanced forced circulation regime). The HS thermal power is imposed to a value of 800 kW with an equal power removed by the main HX, the LBE mass flow rate at the entrance of the HS is assumed equal to 54.8 kg/s and a temperature of about 300°C is set in the LBE pool. All the walls separating the facility from the external environment are considered adiabatic (no heat losses were considered).

During the transient, due to the simulated PLOHS+LOF accident, the HS is reduced to a heat power of 40 kW (about 5% of the ICE full power run). The heat flux removed by the HX, during the accidental scenario simulated by RELAP5, decreases from an initial value of about 800 kW to zero in about half an hour. The decrease trend was set at the HX peripheral walls by means of a UDF imposing the heat flux time trends obtained from a previous RELAP5 calculation (Bandini et al., 2011) and reported in Figure 35. The cut-off of the HX results in a decrease in the heat removal trend, mainly due to the heat removed by the evaporation process of the water contained in the HX in the initial phase of the simulated transient. Concerning the boundary conditions for the primary circuit (LBE side),

a mass flow inlet is imposed at the entrance section of the HS in agreement with the results obtained in previous RELAP5 calculation (Bandini et al., 2011). A UDF is implemented in the Fluent code in order to evaluate the LBE average temperature at the exit of the domain and set as LBE temperature at the entrance of the HS (inlet section of the domain). The inlet turbulence intensity of 7% and a proper hydraulic diameter are imposed.

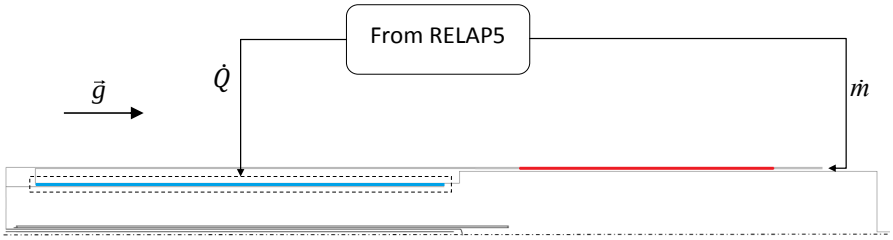

Figure 34: Interfaces between RELAP5 and CFD

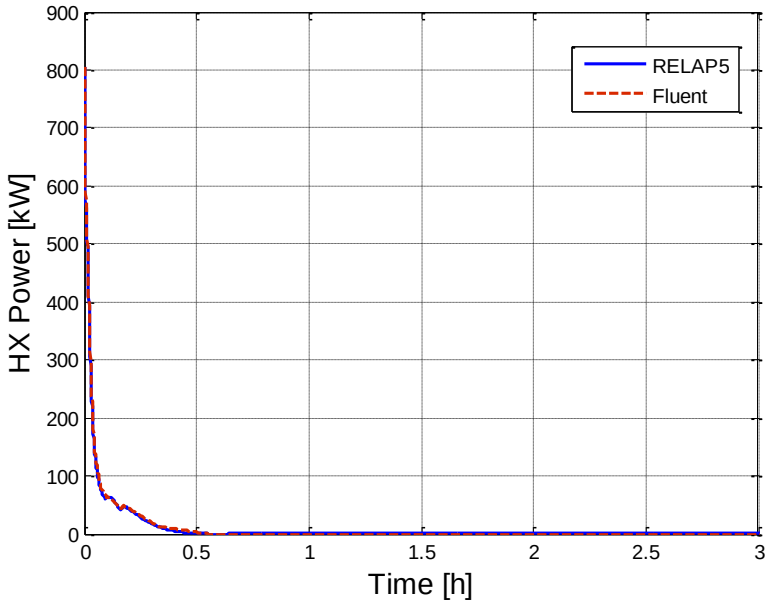

Figure 35: HX thermal power time trend

The PLOHS+LOF transient starts at t = 0 s, the mass flow rate in the primary system quickly decreases (stop of the argon injection) to a value of about 8 kg/s predicted by the RELAP5 code for the stable natural circulation as shown in Figure 36. A "pressure outlet" was assumed at the exit of the geometrical domain (Figure 37 (*a*)). For the secondary circuit (air side), mass flow inlet of 0.3 kg/s at 20°C in the air inlet section and "pressure outlet" at the exit of the air circuit were assumed as boundary conditions according to Figure 37 (*b*).

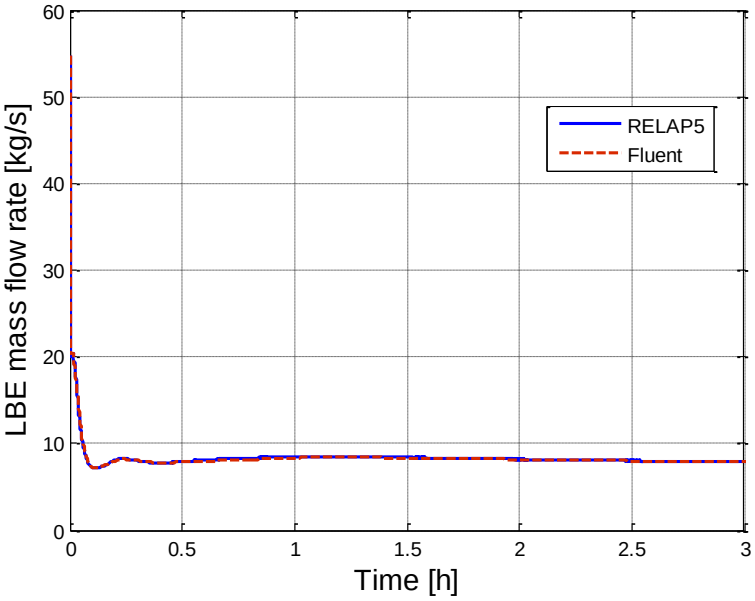

Figure 36: LBE mass flow rate in the primary circuit

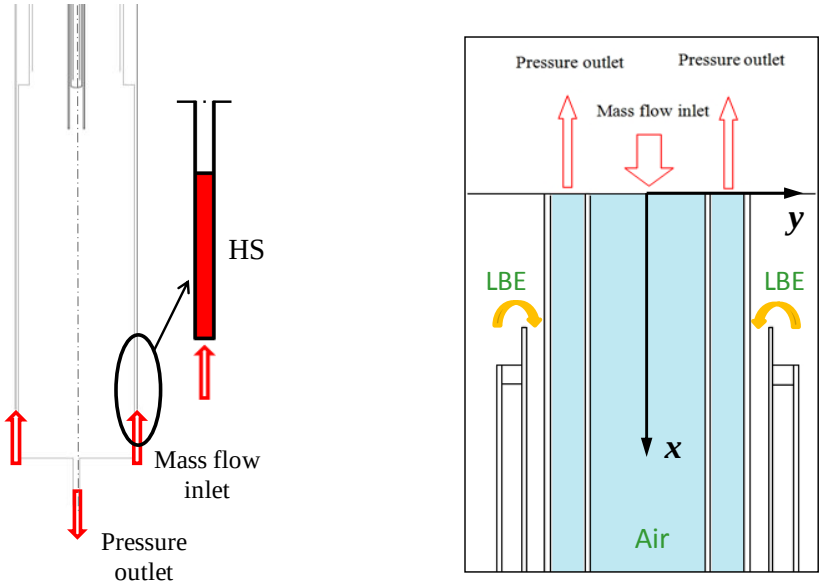

(*a*) (*b*)

Figure 37: Boundary circuit LBE-side (*a*) and air side (*b*)

The thermo-dynamic and thermo-physical properties of the LBE alloy, such as density, molecular viscosity, thermal conductivity and specific heat, were assumed as a function of the temperature (in [K]) in agreement with the "*Handbook on Lead-bismuth Eutectic Alloy*

and Lead Properties, Material Compatibility, Thermal-hydraulics and Technologies", 2007. Air properties were considered as a function of the temperature and implemented into the Fluent code as polynomial functions.

2.5.2. Obtained results

During the transition from forced to natural circulation conditions, the LBE mass flow rate in the DHR annular region are monitored. After 20 h from the start of the accident, the LBE mass flow rate through the primary side of the DHR reaches a steady value of about 7.5 kg/s, which represents 94% of the mass flow rate flowing through the HS. Moreover, as shown in Figure 38, the code calculation predicts a quick start-up of natural circulation in the DHR in agreement with RELAP5 pre-test calculations performed by Bandini et al., 2011.

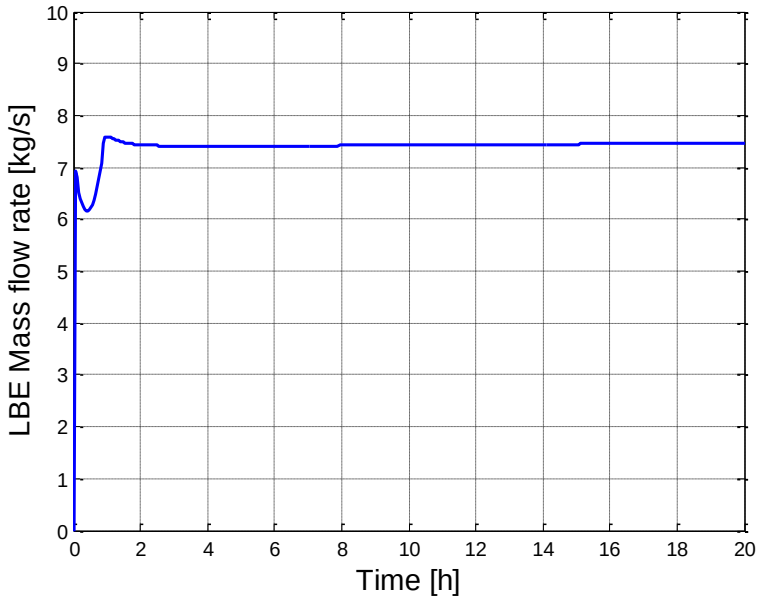

Figure 38: LBE mass flow rate at the inlet section of the DHR cooling annular channel

Furthermore, mixing and stratification phenomena cannot be predicted by STH codes, based on 1D lumped parameter concept. This justifies the motivation for using CFD software. Regarding the temperature trend inside the LBE pool region, at t=0, temperature is uniform at 300°C. After an initial decrease in temperature (in the first hour of transient), due to the sharp reduction in the HS thermal power and to a non-instantaneous reduction in the thermal power removed by the HX, the LBE temperature in the upper vessel zone starts to increase. This is due to the hot LBE mass entering the domain (no longer cooled by the HX), while in the lower part of the vessel region it decreases because of the cooling action of the DHR. After about 8 h, a thermal stratification phenomenon is evident in the entire pool (Figure 39). The LBE temperature in the upper and lower plenum stabilizes at two different levels, respectively of 316°C and 283°C, with a transition zone shown in the region between the elevation of the exit from the HX and of the exit from the DHR.

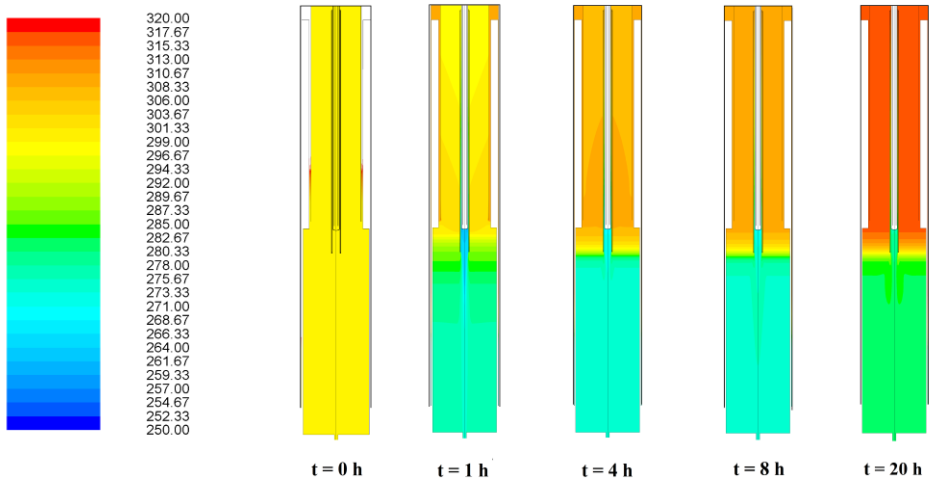

Figure 39: LBE temperature contour plot [°C] for five different times during the transient

A vertical control line placed al y =0.3 m (Figure 40) is used in order to monitor the temperature profile in the LBE pool region, and temperature trends along this line are shown in Figure 41.

Figure 40: Control line at y = 0.3 m in the LBE pool region

The computational analysis predicts a well-defined and restricted thermal stratification region between the HX and the DHR exits. The temperature difference between the upper "hot" region and the lower "cold" region is about 33°C. It can be also noted that after 2 h of transient the stratification region is already well defined, even if, increasing the transient time, the temperature rises.

In the DHR secondary circuit, two control lines are used to monitor the temperature trend along the x direction (vertical) into the internal and the external pipe of the airflow path (Figure 42). The first line matches the axis of the domain, while the second line is placed in the middle of the external annular pipe (at y = 0.04455 m) where the air flows upward. Air temperature increases along the airflow path, especially in the external annular pipe because of heat received from LBE.

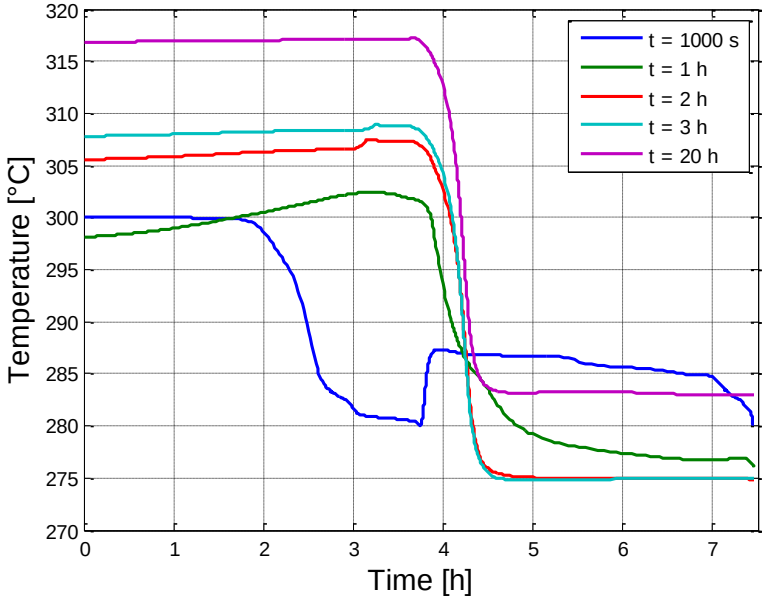

Figure 41: Temperature profile along the vertical control line (y = 0.3 m)

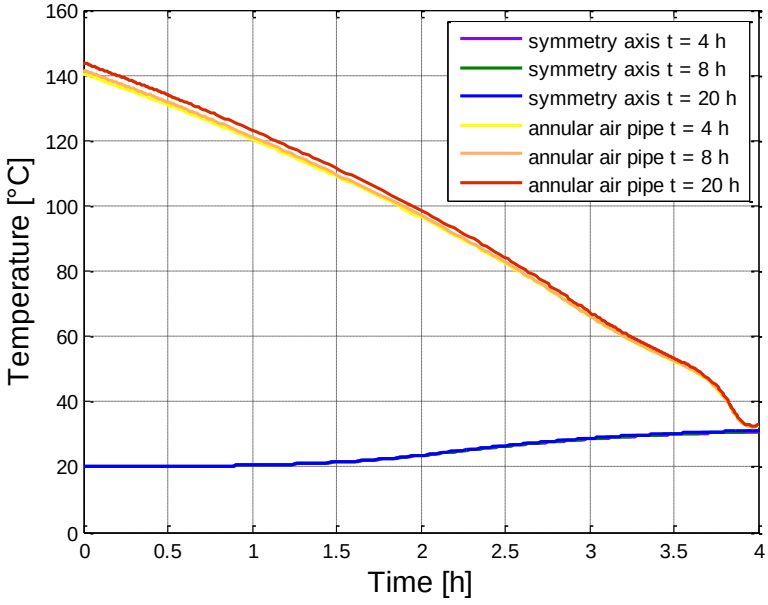

Figure 42: Air temperature distribution along two vertical control lines (y = 0 m and y = 0.04455 m) after 4, 8 and 20 h.

The time trend of the thermal power removed by the DHR is reported in Figure 43. For steady state condition, the DHR must be able to remove the 40 kW produced by the HS and representing the heat decay. Figure 43 shows how suddenly the DHR reacts to its activation and after approximately 2 h it is able to remove about the 92% of the total power supplied

by the HS. At t = 20 h the removed thermal power is about 39 kW, i.e. the 97.5 % of the heating power.

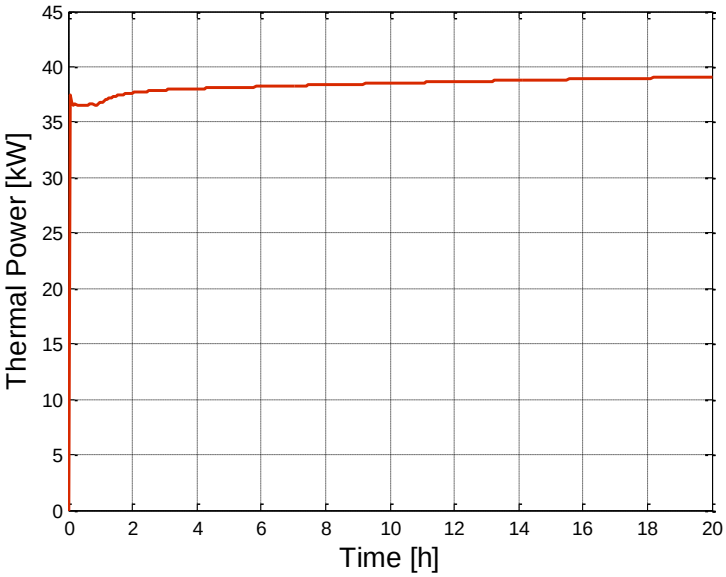

Figure 43: Thermal power removed by the DHR

Figure 44 shows the time trends of the LBE temperature at the inlet section of the HS and at the outlet section of the HX; after 20 h the LBE temperature difference reaches a value of about 34°C because of the heat power imposed at the HS and of the heat removed by the DHR.

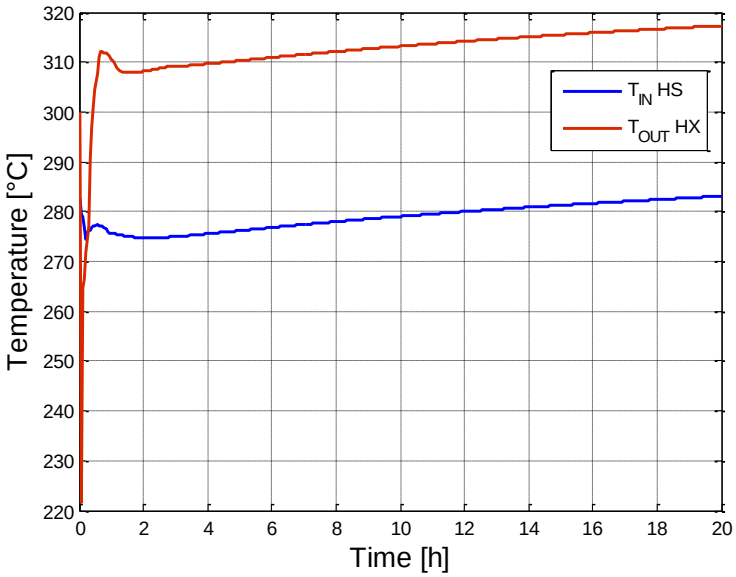

Figure 44: Temperature time trends at the outlet of the HX and at the inlet of the HS

Temperatures at the inlet and outlet section of the DHR are also monitored. In particular, after 20 h the temperature difference is about 30°C (about 4°C lower than what found in Figure 44, because the temperature at the inlet section of the LBE cooling channel is monitored few centimetres below the entrance).

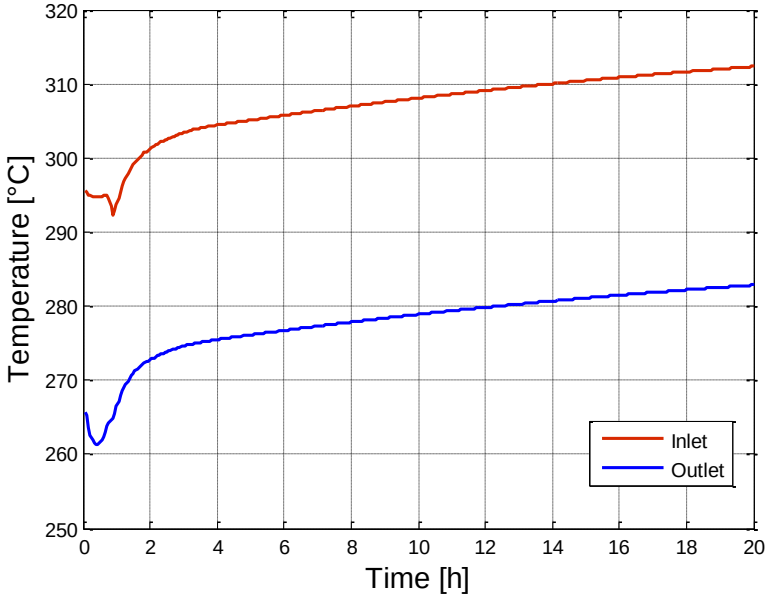

Figure 45: Temperature time trend of points at the LBE cooling channel inlet and outlet

As shown in Figure 39, the temperatures in the upper and lower plenum are uniform with a transition zone shown in the region between the elevation of the exit from the HX and of the exit from the DHR. For this reason in order to investigate temperature evolution during the simulated transient, two points placed respectively in the upper and lower plenum, are chosen as monitor points and the temperature time trends are reported in Figure 46. The hot LBE mass entering the domain influences the temperature trend of the whole pool increasing the average temperature both in the upper and lower zone; it is clear from Figure 46 that steady state conditions have not yet been reached after the simulated 20 h. The experimental campaign should take into account the long-time requested to reach steady state conditions after the transition from forced to natural circulations.

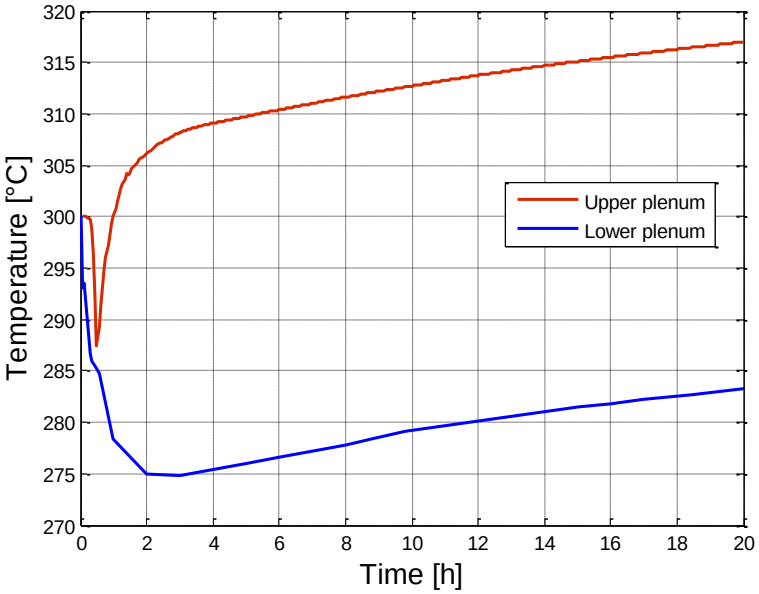

Figure 46: Upper and lower plenum LBE temperatures

In Figure 47, the LBE flow paths at the outlet section of the HX are visualized. At t = 0 when the main heat exchanger is still working and the DHR has not yet been activated, the LBE leaves the HX cooled and flows down due to its higher density. When the HX is stopped, the LBE exits at a temperature higher than the LBE pool temperature and climbs into the upper zone of the vessel reaching the entrance of the DHR lapping the external wall of the HX. After the first hour, the path lines tend to move toward the external wall of the DHR while rising to its entrance (Figure 47).

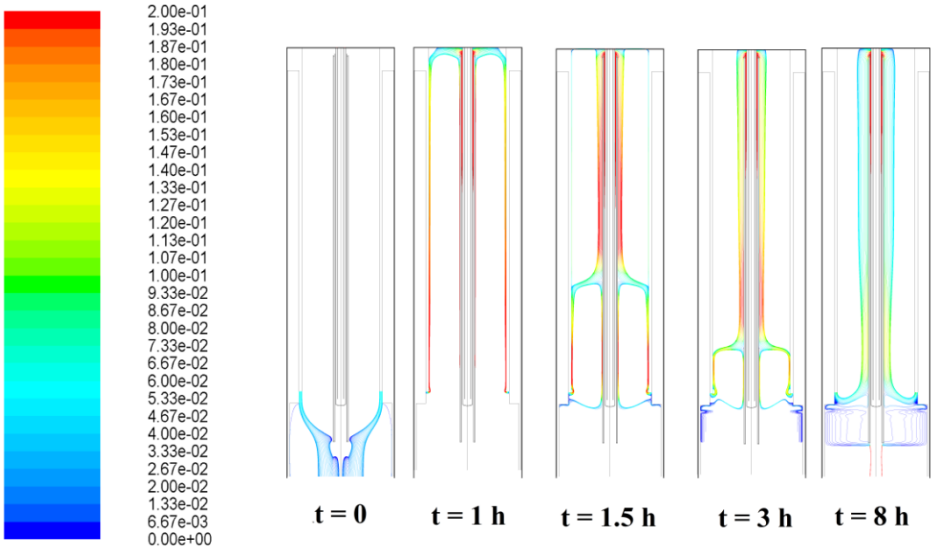

Figure 47: Path lines coloured by velocity magnitude [m/s]

Figure 48 shows an enlarged view of the DHR inlet. At t = 1 h, not all the LBE moved up enters into the DHR cooling annular channel. A certain amount of LBE decreases in temperature due to mixing with the LBE in the upper vessel zone at a lower temperature. It therefore, increases in density and flows downward to the lower vessel zone lapping the outer wall of the DHR. This behaviour seems to move downward as the LBE temperature in the upper vessel zone becomes more homogeneous and when thermal stratification becomes more clearly marked. After 3 h of transient, all the LBE moved up enters in the DHR system. As regarding the LBE domain, the calculated maximum velocity magnitude is about 0.25 m/s in the proximity of the LBE inlet (Figure 48).

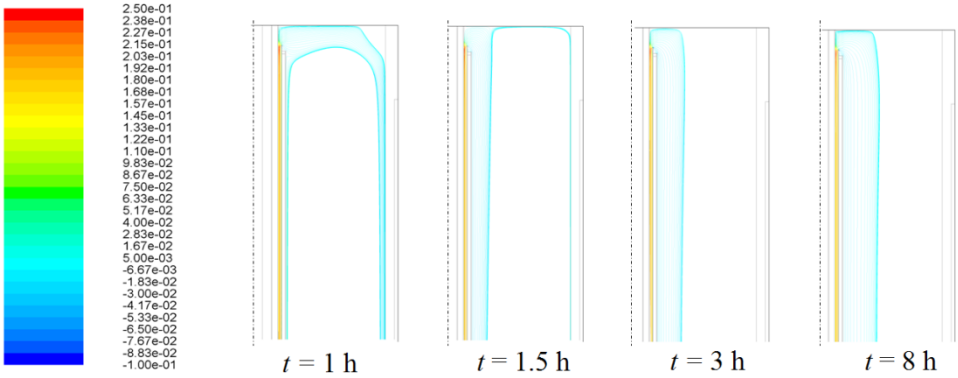

Figure 48: Path lines coloured by axial velocity [m/s] (enlargements at the DHR entrance)

Looking at the HX exit region, not all the LBE that exits the HX moves towards the DHR but a small amount seems to mix with the LBE at a lower temperature near the HX exit and then is dragged downwards and cooled by the LBE plume that exits the DHR (Figure 49).

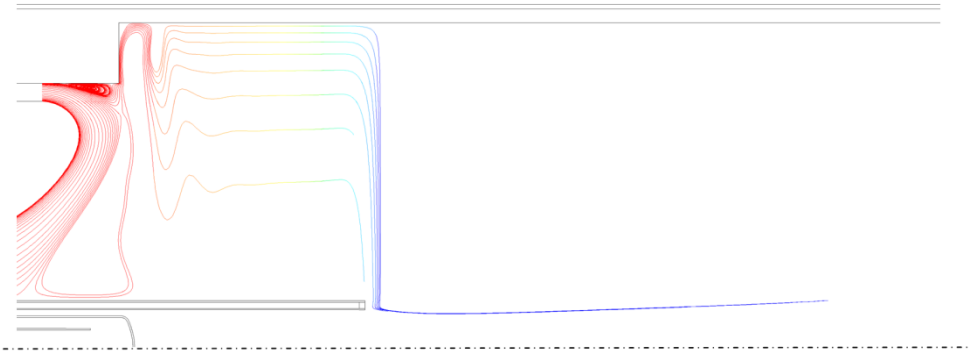

Figure 49: Path lines enlargements at the exit of the HX at t = 20 h

Finally, Figure 50 shows the contour of velocity magnitude in the region between the elevation of the HX exit section and the exit from the DHR. This shows that the two stratified regions with different temperatures (see Figure 39) are separated by a transition zone where the velocity magnitude is almost zero. Inside this transition region, that has a height of about 0.5 m, the heat is exchanged mainly by heat conduction.

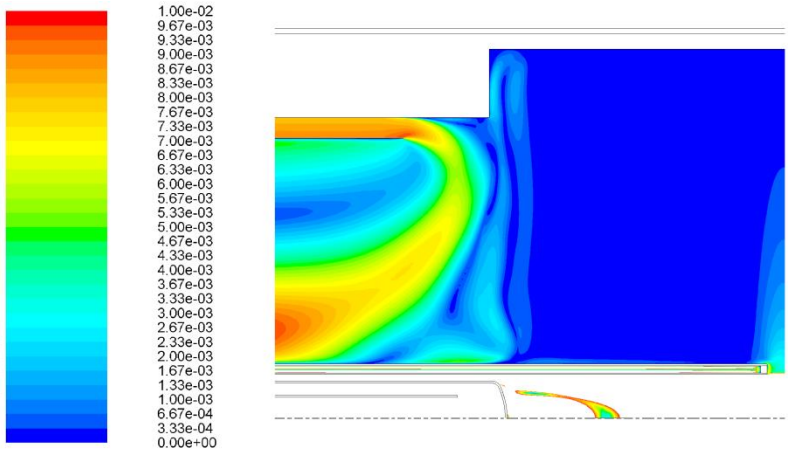

Figure 50: Contour plot of velocity magnitude near the exit section of the HX [m/s]

2.6. CIRCE experimental campaign

2.6.1. Introduction

The aim of this experimental campaign performed in the CIRCE facility, arranged with the ICE configuration, is to characterize the phenomena of mixed convection and stratification in a liquid metal pool in a safety relevant situation. The execution of the experimental campaign was supported by the pre-tests calculations reported in § 2.5 In particular, the accidental scenario numerically simulated is experimentally reproduced, and transition from nominal flow full power conditions to natural circulation decay heat removal conditions is explored. In order to investigate pool thermal-hydraulics and provide experimental data for the validation of CFD models, the on-set and stabilization of the DHR flow path is monitored by means of a suitable instrumentation. Several thermocouples are used in the 3D domain to map the thermal stratification during the transient (§ 2.4.2). Due to the integral nature of the facility, the tests will also be valuable for the verification of the system codes in mixed-convection conditions or to asses coupled STH/CFD methods.

2.6.2. Experiment description

The performed experiments are aimed at reproducing a Protected Loss Of Heat Sink (PLOHS) with Loss Of Flow (LOF) accidental scenario. Practically, the total loss of the secondary circuit is simulated with consequent reactor scram and activation of DHR system to remove the decay heat power (5-7% of the nominal value). In the CIRCE-ICE facility, the transition from nominal condition (forced circulation) to natural circulation is performed reducing the thermal power generated in the HS, stopping the argon injection into the riser, cutting off the main HX and activating the DHR heat exchanger. The main nominal parameters that define the accidental scenario experimentally reproduced are summarized in Table 6.

Table 6: Nominal parameters for the experimental campaign

Nominal Steady State	**PLOH+LOF transient**
HS Thermal Power :700-800 kW HLM flow rate: 55 kg/s (by gas lift) ΔT along the HS: 100°C Average velocity into the HS:1m/s Average temperature along the main flow path: 350°C Vessel heating system: not active HX flow rate: 0.5 kg/s DHR: not active	Isolation of the main HX (isolating the feed water) Core "scram" at 20-50 kW (decay power) Start-up of the DHR-system ($\dot{m} = 0.3$ kg/s) "Main pump" turn-off (the gas injection is interrupted) Vessel heating system: not-active

To drive the data acquisition system (DAQ) boards and the signal conditioning modules, the program LabVIEW® (Laboratory Virtual Instrument Engineering Workbench) is used. Figure 51 shows the synoptic panel for the control of the ICE Test Section, while Figure 52 shows the control panel for displaying the TCs in the FPS and finally, Figure 53 shows the control panel for the loading and unloading of the main vessel S100, the LBE transfer tank (S300) and the LBE storage tank (S200).

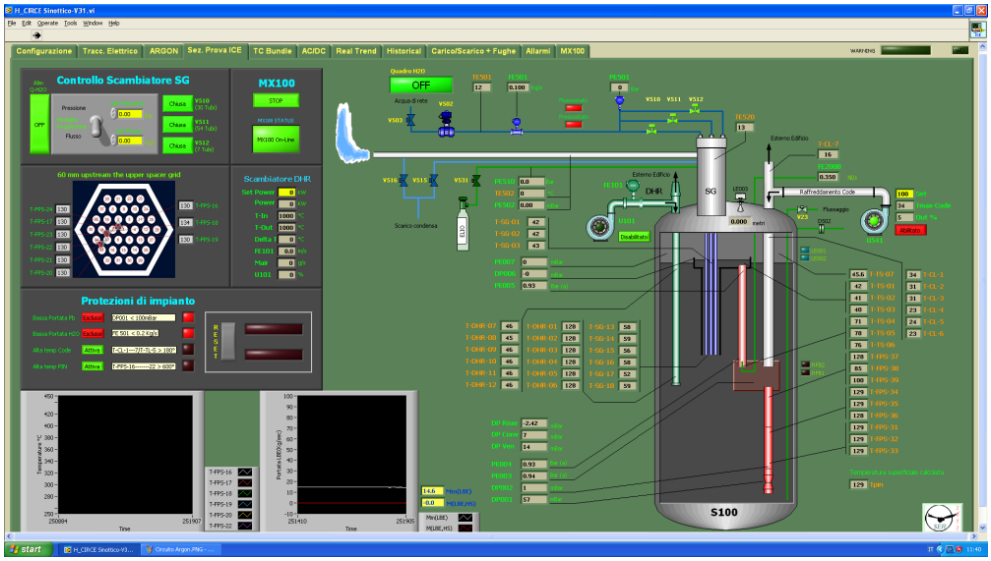

Figure 51: ICE test section control panel

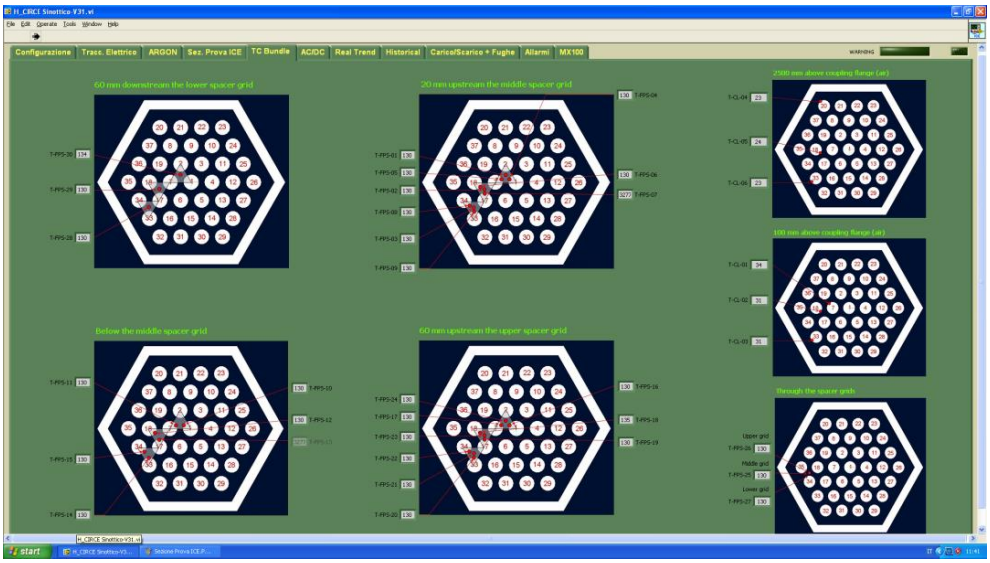

Figure 52: TCs for the FPS control panel

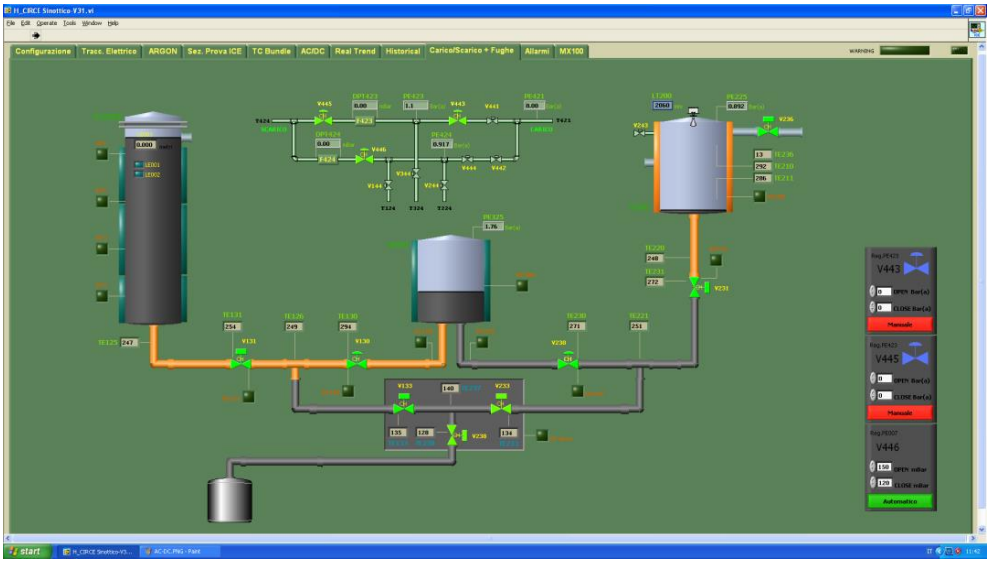

Figure 53: S100 Load-unload control panel

Table 7 shows the test matrix of the performed experimental tests.

Table 7: Test Matrix

Test	*Duration of the test*	*Electrical Power*	
		FC	*NC*
I	48 h	730 kW	50kW
II	97 h	600 kW	23 kW

2.6.3. Experimental results

2.6.3.1. Test I

Figure 54 shows the power transient during the running of Test I. The experiment starts with nominal power of about 730 kW, and after 7 h the transition to 50 kW takes place. The primary LBE flow rate, under forced circulation conditions, quickly reaches its nominal value of about 56-57 kg/s (Figure 55); the strong oscillations in the first phase of the test shown in Figure 55, characterized by argon injection assisted circulation, are related to the specific volumetric blowers used to inject the gas into the riser. After a few hours, a check valve is put in service to dump such oscillations. After the gas injection switches off and the electrical power supply reduces to about 5% of nominal power, natural circulation conditions establish. LBE flow rate tends to about 7.5 kg/s (14% of the nominal flow rate), 0.5 kg/s higher than the results obtained from RELAP5 pre-test calculations and used as b.c. for the RELAP5-Fluent one way coupled pre-test simulation.

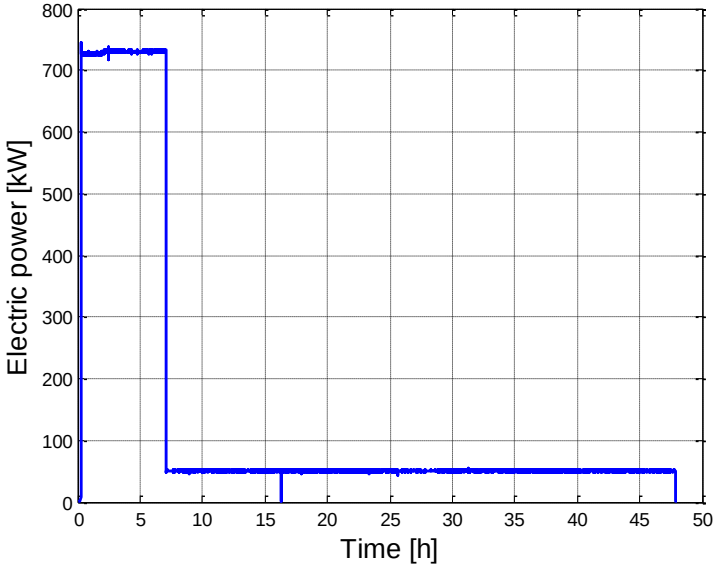

Figure 54: Electrical power supplied to the FPS

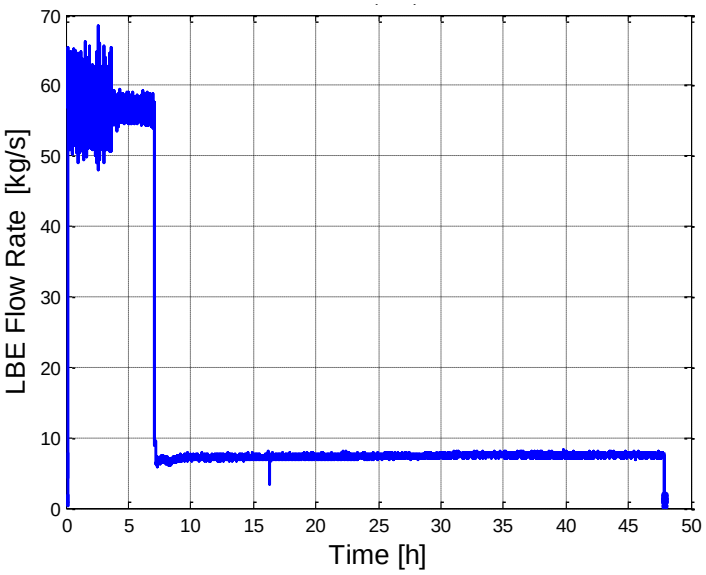

Figure 55: LBE flow rate through the primary system measured by the Venturi flow meter

During the full power run, argon is injected into the riser to promote the main circulation along the primary system (gas-assisted circulation with a gas flow rate of 1.8 Nl/s). After the transition from full power to "decay power", the gas injection is interrupted (Figure 56) to simulate the station blackout, and transition from forced to natural circulation takes place. Argon mass flow rate revealed by the transducer after the injection shutdown shows a value of 0.35 Nl/s, even if the argon line is completely closed due to the signal being at digital full scale (0.35-3.5 Nl/s).

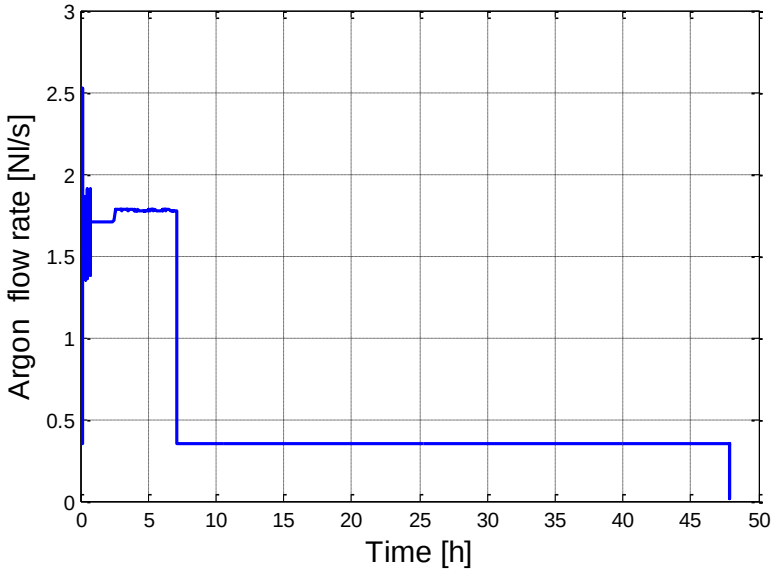

Figure 56: Argon flow rate for the gas-assisted circulation

At full power run the HX is fed by water with a flow rate of 0.65 kg/s and pressure at the inlet of the bayonet tubes (upward the manifold) close to around 2 bar. After the station blackout simulation conditions, the feedwater line is closed and the water flow into the HX falls as shown in Figure 57.

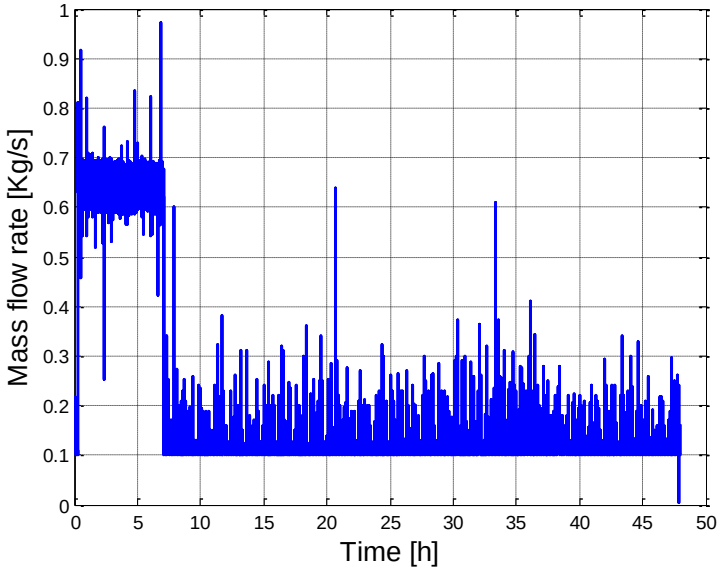

Figure 57: Water mass flow rate in the HX

After the simulated "core scram", in order to remove "decay heat" power, the DHR-system was activated, The air mass flow rate through the DHR is about 0.223 kg/s, as reported in Figure 58.

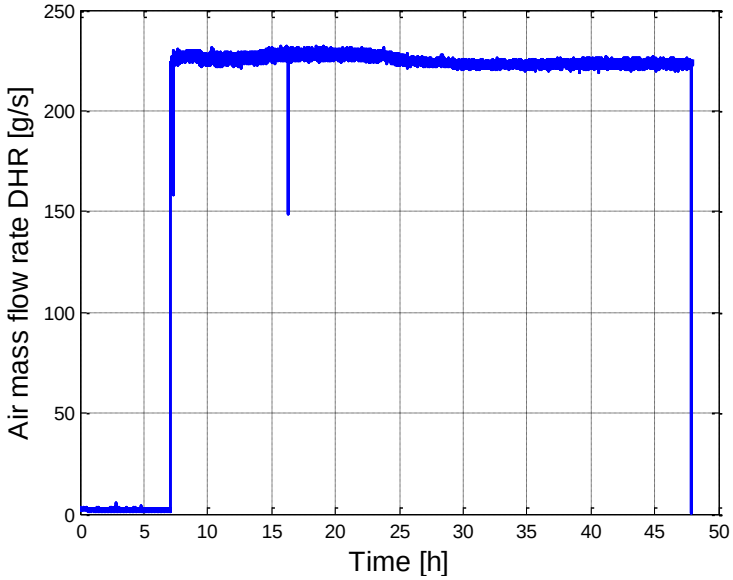

Figure 58: Air mass flow rate through the DHR system

Figure 59 shows the average temperatures at inlet and outlet sections of the FPS. Steady state conditions are achieved at full power after 4-5 h of transients with a temperature difference between the FPS inlet and the outlet sections of about 77°C, the average inlet temperature being 285°C and the outlet average temperature 362°C. At black-out simulation time, the average temperature at the FPS inlet decreases by about 5°C to a value of about 280°C, while the average temperature of the FPS exit decreases by 70°C reaching a value of about 295°C. Under natural circulation flow regime, the temperature difference along the FPS falls to around 24°C, being the average inlet and outlet temperature 349°C and the average outlet temperature of 373°C, at the end of the test. After a natural circulation transient of about 40 h, the average temperature in the FPS still increases, and steady state conditions are not yet reached. This unbalance is essentially due to the fact the air mass flow rate flowing through the DHR system is not sufficient to remove more than 20-23 kW.

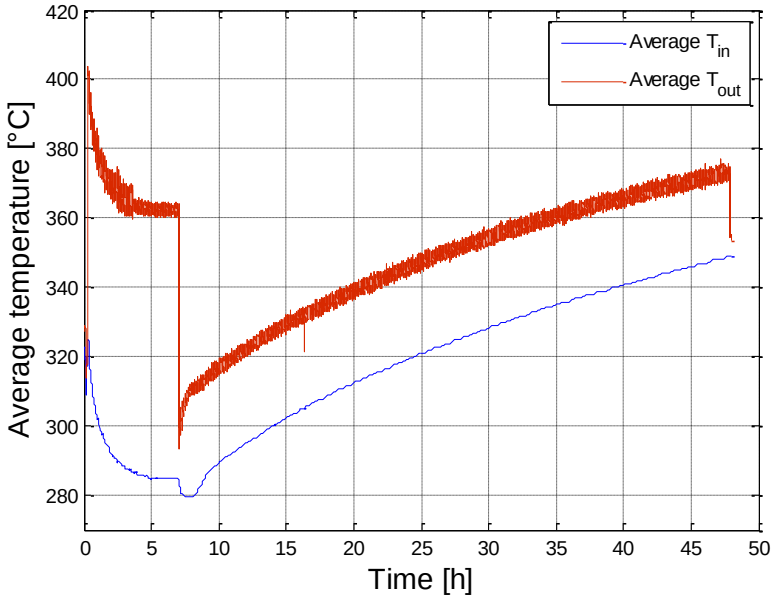

Figure 59: Average temperatures through the FPS

Figure 60 and Figure 61 show the clad temperature of pin 1 and 7 along the active length of the pins associated with central subchannels (for the position of the TCs see from Figure 17 to Figure 20). After about 5 h the temperature at sections 1 and 2 near the middle spacer grid reaches a constant value of about 380-390°C for pin 1 and 7 (T-FPS 4, 5 and 10, 11 respectively). In section 3, the clad temperature for pin 1 (T-FPS 16) is about 20°C higher than the clad temperature of pin 7 (T-FPS 17, 410°C versus 430°C). This difference can be explained by looking at the pin manufacturing as reported in Figure 62. Due to the internal geometry adopted for the Bifilar-type pins, provided by Thermocoax, the thermal flux around the pins is not uniform. From Thermocoax technical documents, pin rods bifilar-type used in the ICE bundle, exhibit an approximate azimuthal variation $\left(q''_{\max} - q''_{\min}\right)/\overline{q''} \approx 0.3$, i.e. of about 30%; therefore, the temperatures measured by the wall-pinched thermocouples can be higher or lower than the average wall temperatures. After the

transition from forced to natural circulation, the clad temperatures increase both for pins 1 and 7, from a value of about 310 to 370°C (section 1), from 320 to 380°C (section 2) and from 330 to 395°C (section 3).

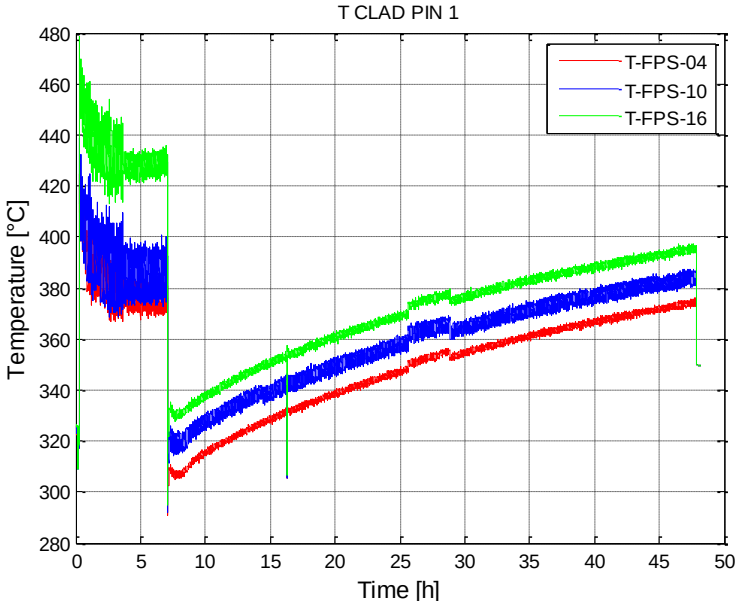

Figure 60: Clad temperature (pin 1) along the active length

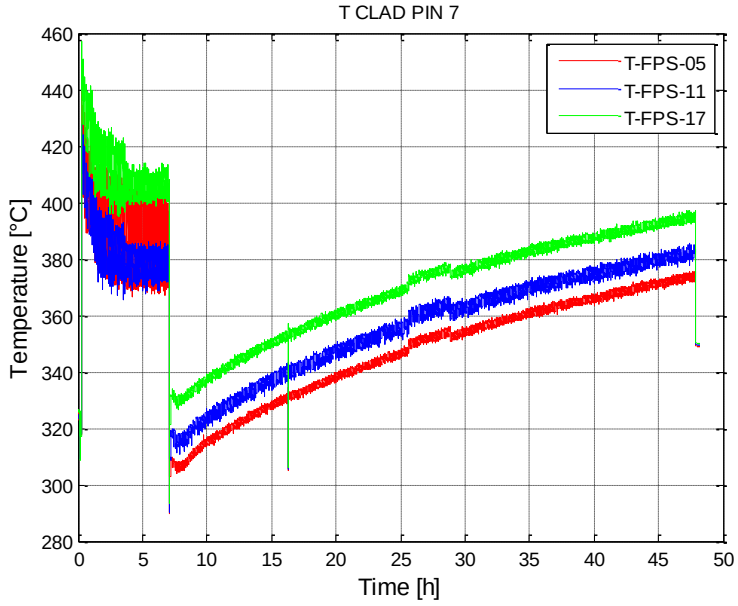

Figure 61: Clad temperature (pin 7) along the active length

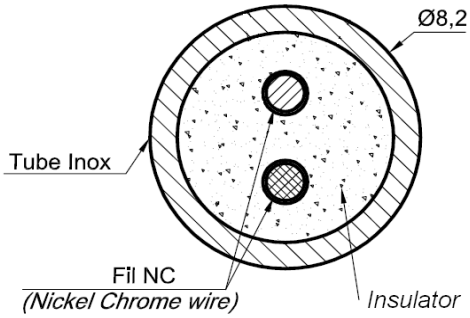

Figure 62: Cross section of the pin Bifilar-type (active zone)

Figure 63 shows the temperature in the centre of the channel for the inner subchannel (Pins 1-2-7). Starting from section 4 (T-FPS 30, 60 mm downstream of the lower spacer grid), temperature, at full power steady state condition, reaches a value of about 280°C. Then it increases along the subchannel reaching a value of about 320°C at section 1 (T-FPS 01) while at section 3 (60 mm upstream the upper spacer grid) the temperature value is about 365°C (T-FPS 24). Hence, the LBE flowing in the inner subchannel, from Section 4 to Section 3, increases its temperature by about 85°C. After the transition, the temperature difference between the lower section 4 and section 3 is in the order of 40-45°C.

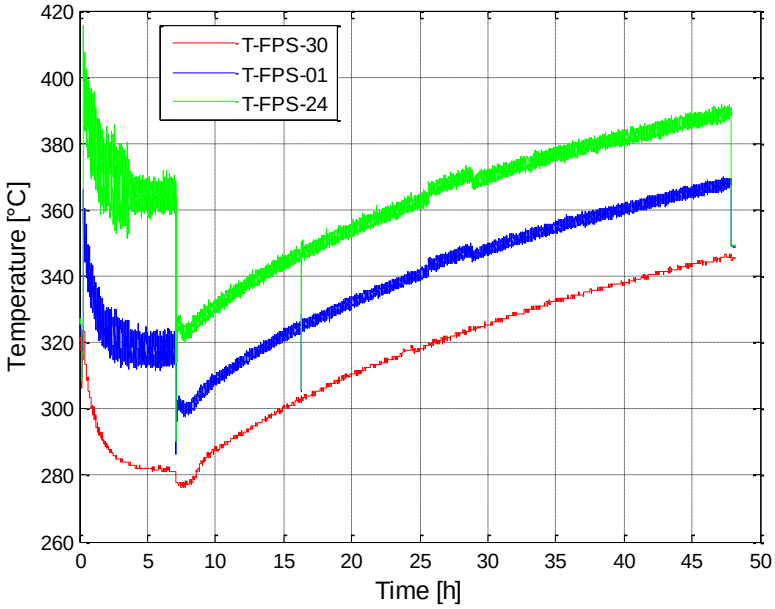

Figure 63: Temperatures in the centre of the central subchannel

Tubes injecting argon below the molten metal level ("bubble tubes") are installed to transfer pressure signals from the LBE alloy to external differential pressure cells operating with gas at room temperature (accuracy ± 1 mm LBE see Ambrosini et al. 2004). During forced circulation conditions, inlet to outlet pressure difference inside the riser is lower than

that measured under natural circulation condition, essentially for the lower value of the two phase flow density compared to the LBE density. In particular, at full power steady state conditions the pressure difference reaches a value of about 3420 mbar while, after the transition, the reached value is in the order of 3670 mbar (Figure 64).

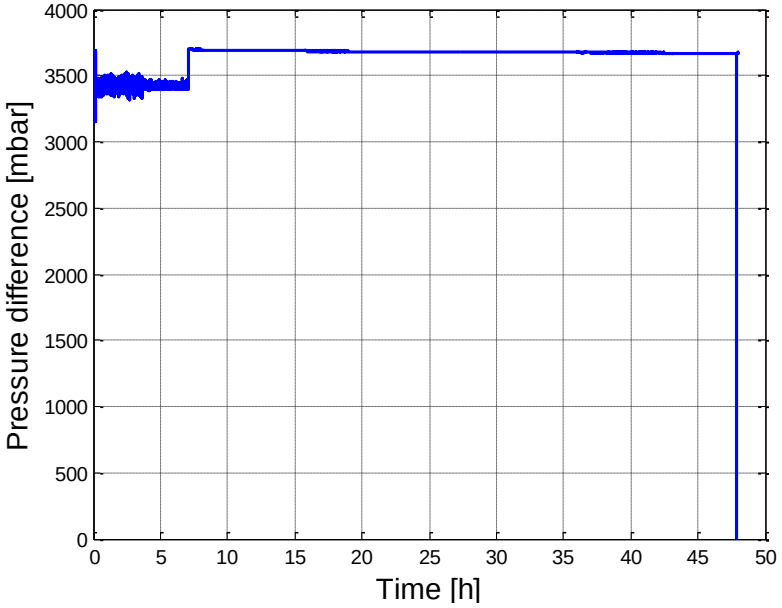

Figure 64: Pressure difference between inlet and outlet section of the riser

The distance between the entrance of the two bubble tubes inside the riser is h_r = 3.6 m computed considering the differential pressure measured before the gas injection and the FPS activation when the LBE is at rest. The pressure drop into the riser can be obtained as the sum of three components, due to acceleration, friction and gravity:

$$\Delta P = \Delta P_{frict} + \Delta P_{acc} + \Delta P_{grav} \tag{4}$$

Considering that, $\Delta P_{grav} >> \Delta P_{frict} + \Delta P_{acc}$ it is possible to approximate the pressure losses in the riser with the pressure losses due to gravity. Then, it is possible to evaluate the void fraction in the Riser by:

$$\bar{\alpha} \cong \frac{\rho_{LBE} - \bar{\rho}_m}{\rho_{LBE} - \bar{\rho}_g} \tag{5}$$

where $\bar{\rho}_m = \frac{\Delta P_m}{g \cdot h_r}$ and $\bar{\rho}_g$ is average gas density in the riser. In such a way, it is possible to evaluate a value of void fraction in the riser of about 11% (Figure 65). Therefore, the maximum available pressure head provided by the gas-lift system in the riser is around 430 mbar as reported in Figure 66.

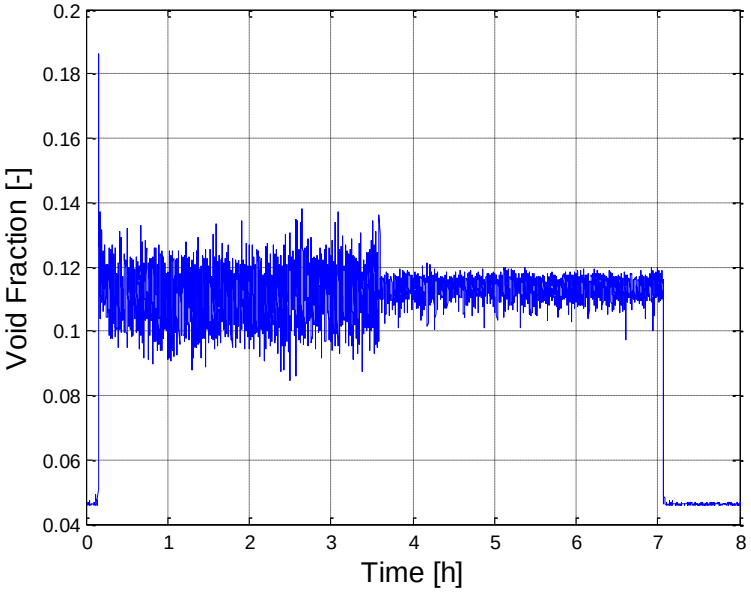

Figure 65: Void fraction in the riser

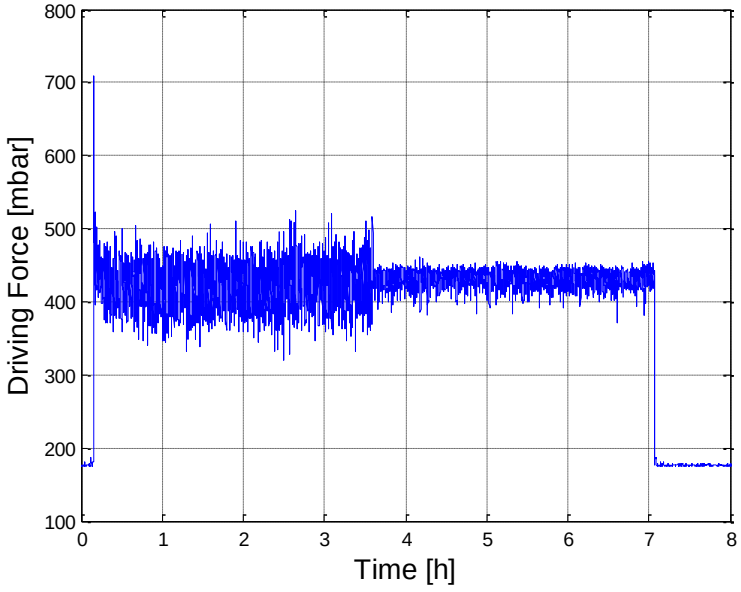

Figure 66: Driving force

Figure 67 shows clad and central channel temperatures in the subchannel associated to the pins 1-2-7 (inner subchannel) at section 1. During full power phase, thermocouples placed on pins 1 and 7 measure temperature values of about 380-390°C, while the thermocouple in the central channel gives a temperature of about 315-320°C. After the transition to natural circulation, the temperature on the clad falls to a value between 305 and 310°C while the

temperature in the centre of the subchannel falls to about 300°C. At the end of the test, the temperatures reached at the pin walls are about 373°C, while that of LBE at the centre of the subchannel is about 367°C.

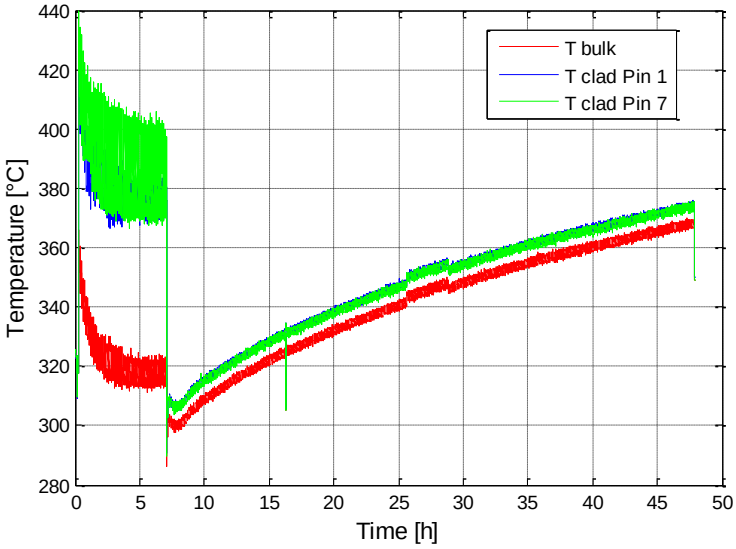

Figure 67: Temperatures in the inner subchannel (section 1)

Although after the transition to natural circulation, the system is globally thermally unbalanced, heat transfer phenomena in the bundle are stationary, and the temperature difference between wall and bulk remains constant as shown in Figure 68.

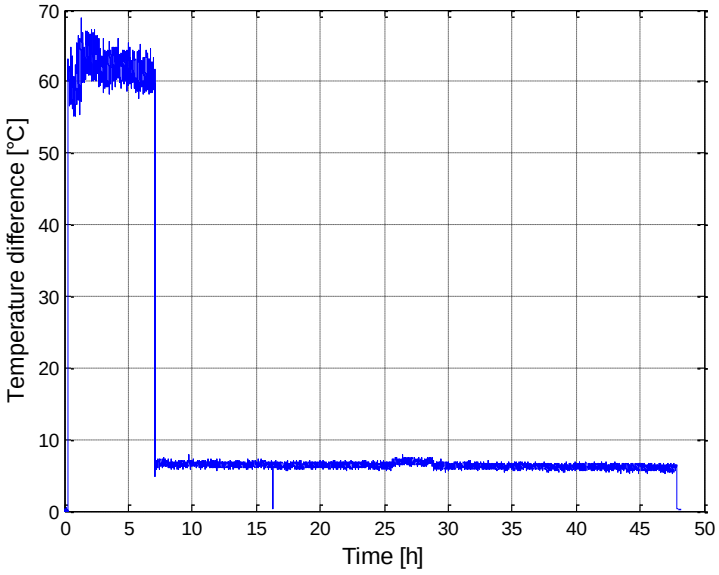

Figure 68: Temperature difference between the clad average temperature and the centre channel temperature (section1)

The difference between the clad average temperature and the LBE subchannel central temperature at full power steady state conditions is about 60°C and after the transition to natural circulation this difference falls to a value of about 6-7°C. Considering the inner subchannel of the FPS at section 3 (placed 60 mm upstream the upper spacer grid) the temperatures at the walls of pins 7 and 1 reach a value respectively of 430 and 410°C (Figure 69). That difference is related to the already mentioned non-uniformity of power generation in the electrical heater rods simulating the fuel pins (Figure 62). At the end of the test, the pins wall temperatures reach a value of about 395°C, while in the bulk fluid the temperature is about 389°C.

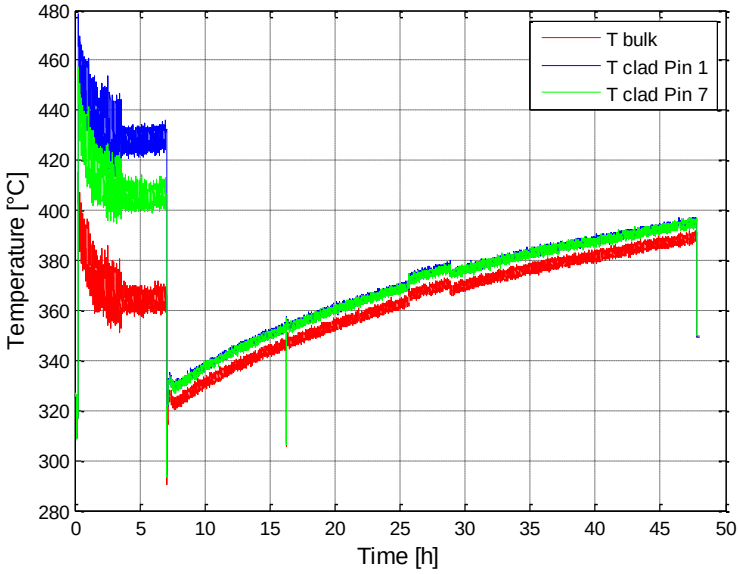

Figure 69: Temperatures in the inner subchannel (section 3)

According to Figure 70, the difference between the clad average temperature and the bulk temperature is about 53°C at full power and about 6°C after thermal power reduction.

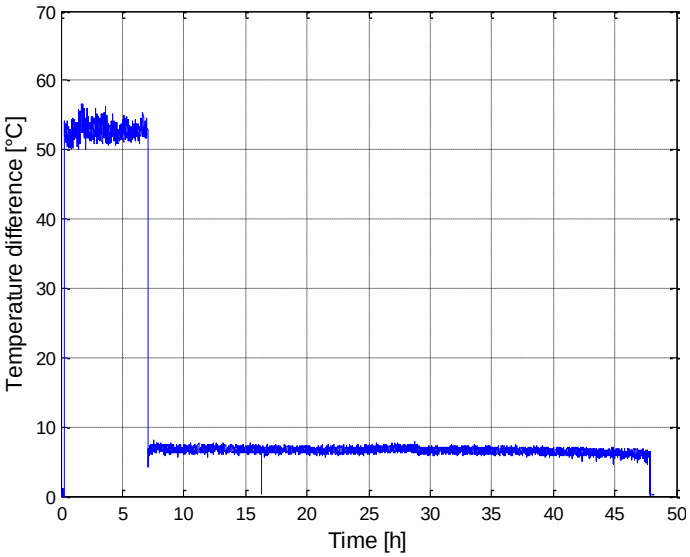

Figure 70: Temperature difference between the clad average temperature and the centre channel temperature (section 3)

The LBE heated by the FPS flows through the fitting volume into the riser; here temperatures are monitored at the entrance of the riser and at the exit (see Figure 22). Due to the absence of heat or sink source in the riser and to its insulation, the temperatures at the entrance and at the exit show the same trend reaching a value of about 357°C at full power steady state condition. After the transition to natural circulation, temperature increases from 308°C to 370°C without reaching a steady state at the end of the test (Figure 71 and Figure 72).

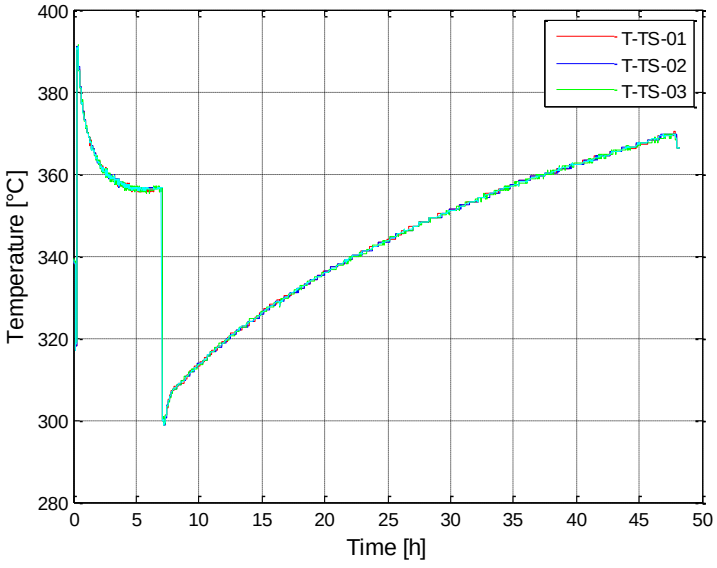

Figure 71: Temperatures at riser inlet section

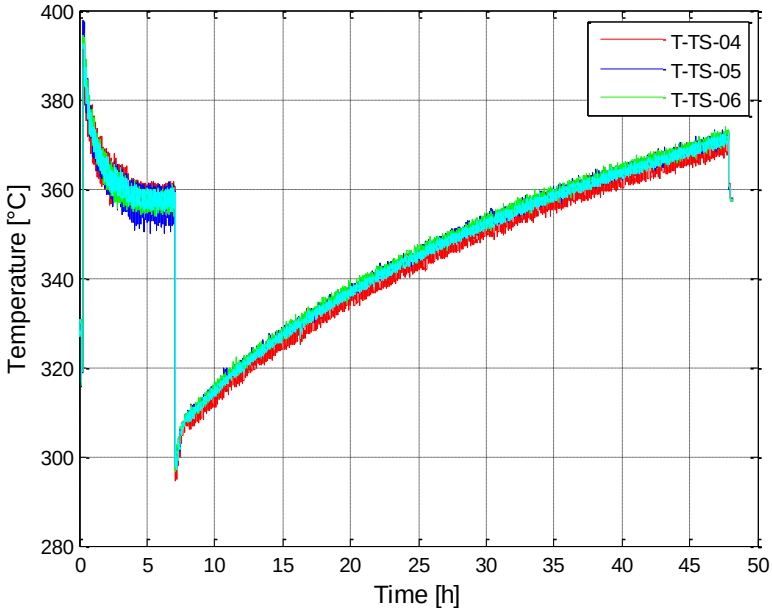

Figure 72: Temperatures at riser outlet section

From the riser exit, LBE flows through the separator into the HX shell. At full power steady state conditions (when the HX is activated) the LBE temperature at the entrance of the HX is about 348°C (Figure 73), then through the HX the LBE exchanges heat with water of the secondary circuit decreasing its temperature by about 78°C, reaching at the exit of the HX the value of about 270°C. Immediately after the transition to natural circulation, the LBE enters the HX with a temperature of 305°C and exits with a temperature of 301°C, while at the end of the experiment the LBE temperature at the HX inlet section is about 366°C. The temperature drop between the HX inlet and outlet section under natural circulation conditions is 4-5°C and it is mainly due to heat losses towards the LBE external pool. Considering energy balance for the steady state at full power run, the difference between the supplied energy and the power removed by the HX is about 90 kW (Figure 75). The difference between electrical power supplied to the FPS and the thermal power removed by the HX in full power steady state condition is essentially due to the following reasons:

- about 5% of the supplied electrical power is converted to heat in the electrical cable for Joule effect and removed by Insulation Volume Cooling System IVCS (Bandini et al. 2011);
- the energy balance does not take into account the power removed by the HX tubes inside the separator before the inlet in the HX pipe where TCs are placed (see Figure 22 (*b*));
- heat losses towards the external environment are indeed present.

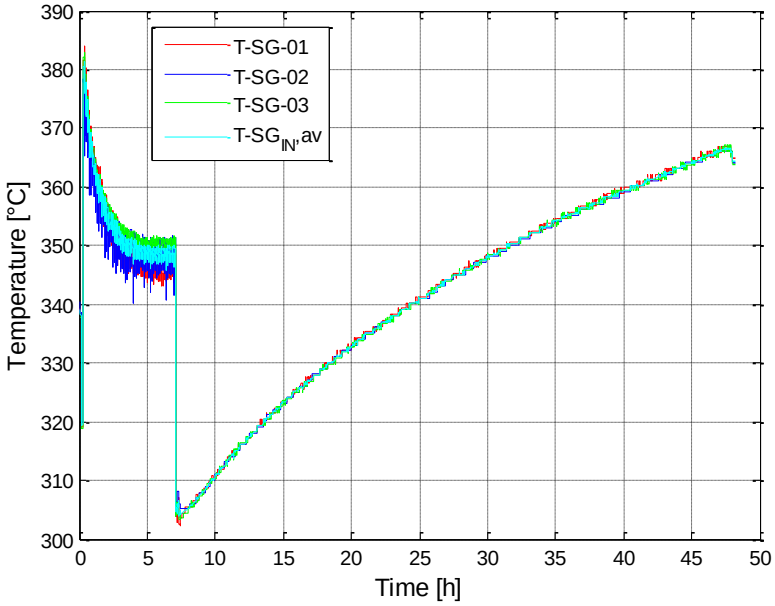

Figure 73: LBE temperatures at HX inlet section

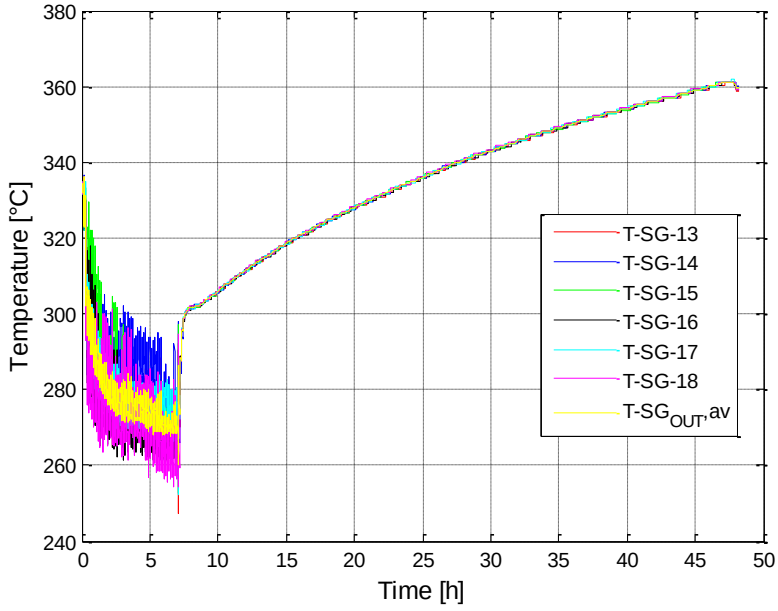

Figure 74: LBE temperatures at HX outlet section

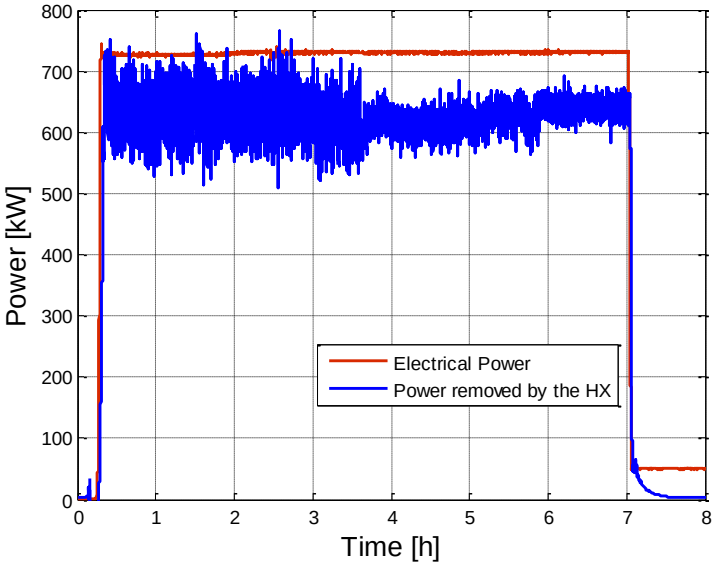

Figure 75: Energy balance at full power run

For the DHR secondary side, the air mass flow rate is approximately 0.223 kg/s (see Figure 58). The temperature difference between the air inlet and outlet section shown in Figure 76, is about 100°C (during the period of its activation).

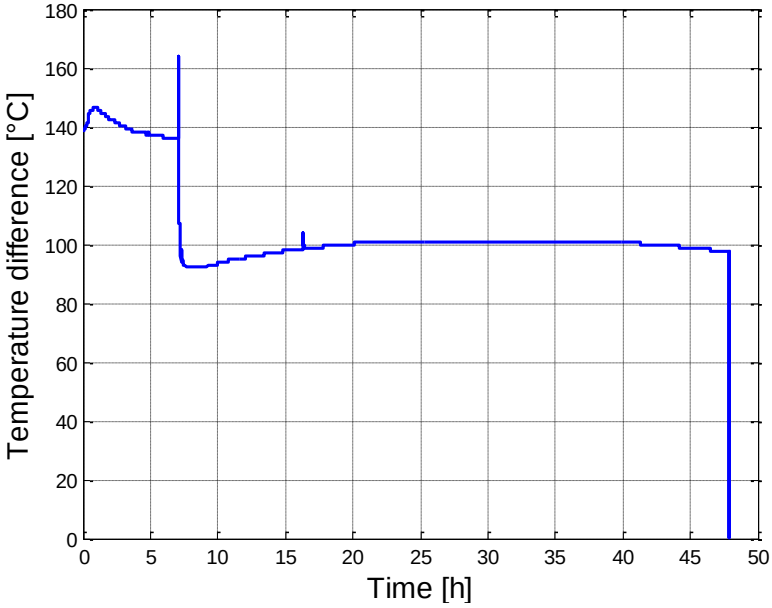

Figure 76: Air temperature difference between entrance and exit sections of the air secondary side

The LBE mass flow rate through the DHR annular channel computed from an energy balance equation (obtained equating the thermal power transferred from the LBE during the

flowing in the LBE annular region, to the thermal power removed by the secondary air-side) quickly reaches 4 kg/s (Figure 77).

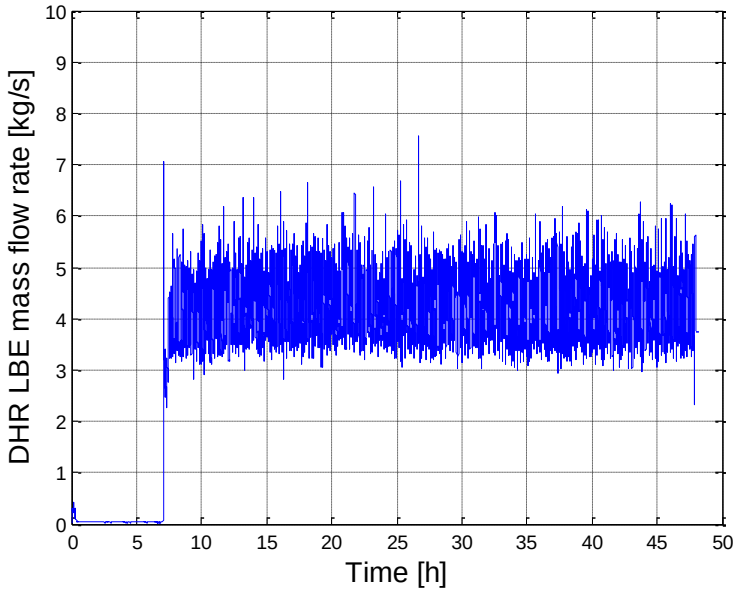

Figure 77: LBE mass flow rate through the DHR.

Assuming a c_p = 1.012 kJ/(kg K) (air at T = 100°C and P = 1 atm) the thermal power removed by the DHR system is around 22-23 kW

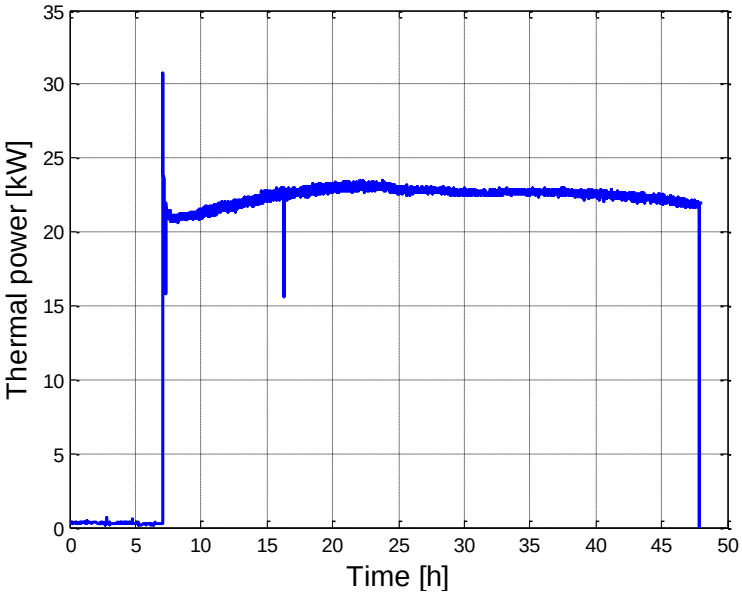

Figure 78: Thermal power removed by the DHR

Inside the LBE pool, several thermocouples are installed in order to investigate mixing and stratification phenomena. From Figure 79 to Figure 82, the LBE pool temperature along eight different vertical lines (see Figure 29) is shown. In particular, TCs on lines *A*, *H*, *I* allow measurement from the upper section (0 mm in Figure 30) to the FPS entrance level (-7200 mm), while TCs on lines *B*, *C*, *D*, *E*, *F*, *G* allow measurement up to 600 mm below the exit of the DHR. Experimental data show that the LBE temperature is homogenous at each horizontal section. The temperature in the pool at the beginning of the experiment (0.3 h, Figure 79), is quite uniform vertically, changing about 10°C from the first upper TC to the bottom one (320-330°C). At this time the electrical power ramp is at one third of its maximum power, the DHR is not activated and the argon mass flow rate is 1.78 Nl/s.

After about 6 h (Figure 80), before transition to natural circulation, with thermal power at steady state condition and at constant Argon mass flow rate, the LBE temperature in the lower region of the pool is at its coldest value assuming a uniform temperature of about 283°C. Between the exits of the DHR and the HX, respectively 4.2 and 3.6 m, a thermal stratification phenomenon with a temperature variation of about 17°C is observed. In the upper part of the plenum then the temperature increases reaching a value of about 340°C. After the transition from forced to natural circulation, the supplied electrical power is reduced to 50 kW, the secondary air system in the DHR is activated and the Argon injection in the riser is stopped. At t = 7.8 h (Figure 81) the LBE temperature in the upper plenum becomes uniform assuming a value of about 300°C.

The region where thermal stratification phenomena are significant moves downwards starting from the DHR outlet section (4.2 m) up to about 4.8 m; the temperature difference between these two sections is about 17-20°C. In the lower plenum of the pool, the LBE temperature is uniform showing a value of about 280°C. From t = 7.8 h to t = 47.8 h (Figure 82), temperatures in the pool gradually rise, reaching, at the end of the experiment, a value of about 360°C in the upper plenum of the pool and of about 350°C in the lower plenum (steady state condition not yet reached).

The temperature difference, in the area where thermal stratification phenomena are relevant, comes down to a value of about 10°C.

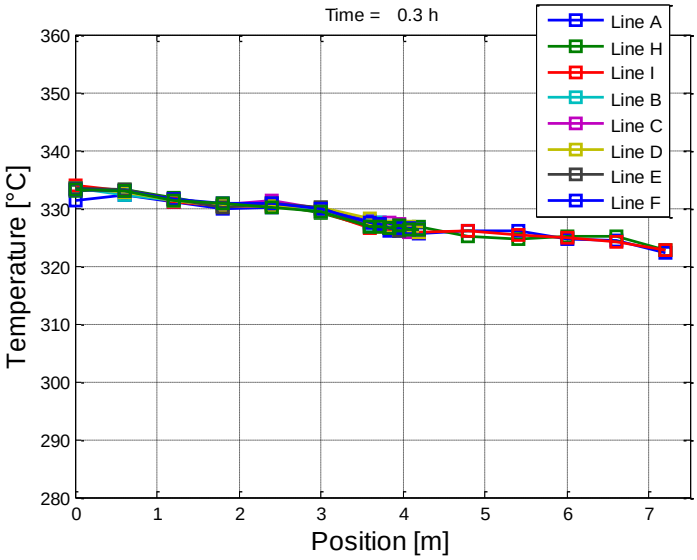

Figure 79: LBE temperature inside the pool at t = 0.3 h

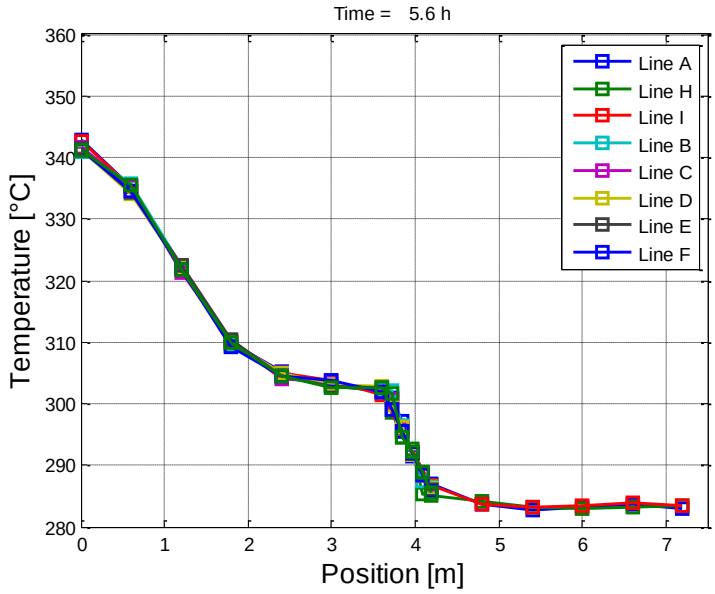

Figure 80: LBE temperature inside the pool at t = 5.6 h

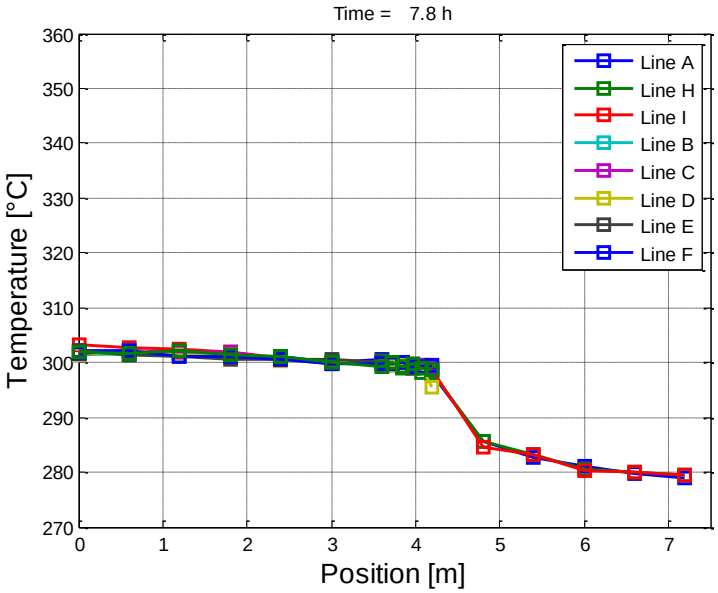

Figure 81: LBE temperature inside the pool at t = 7.8 h

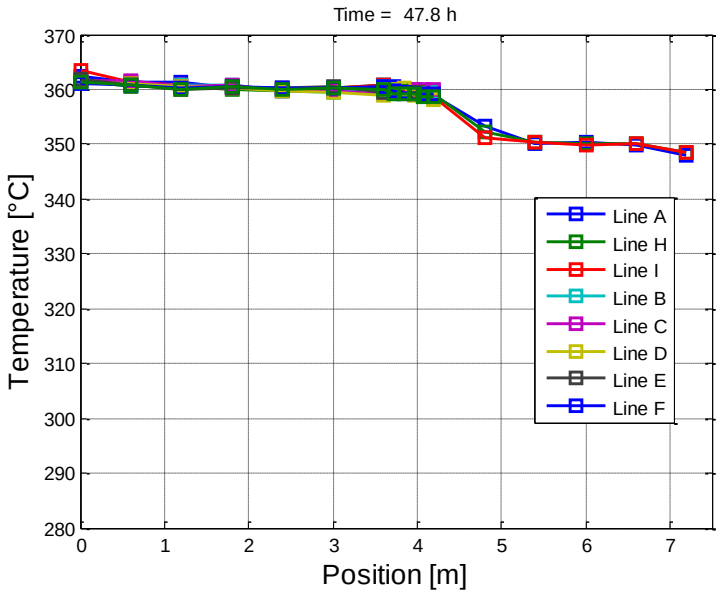

Figure 82: LBE temperature inside the pool at t = 47.8 h

2.6.3.2. Test II

Test II is performed reducing the power supplied to the FPS both during forced and natural circulation conditions, differently from the previous test, with the aim of reaching a steady state temperature trend under natural circulation conditions with decay heat removed by the DHR system. During the full power run of Test II, the electrical power supplied to the FPS is about 600 kW. After the transition, it is reduced to 40 kW (Figure 83). The argon flow rate is set to about 5.2 Nl/s and the obtained LBE mass flow rate in the FPS measured by the Venturi flow meter is in the order of 63-64 kg/s. After the transition to natural circulation, the LBE mass flow rate in the FPS reaches a value of about 8.5 kg/s (Figure 84).

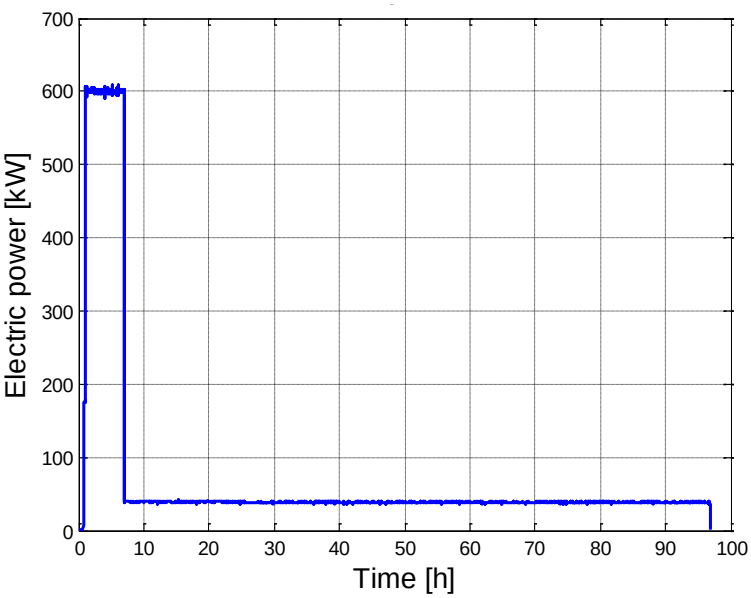

Figure 83: Electrical power supplied to the FPS

For test II the LBE mass flow rate flowing through the FPS under natural circulation conditions is higher than that obtained in the previous step, while in test II the power supplied to the FPS is 20 kW lower than test I. This is essentially due to the fact that in order to avoid uncertainties in the LBE mass flow rate through the DHR system and related to the area of the DHR slot submerged, the free level of the LBE surface is raised so as to ensure that the entrance slot of the DHR are totally below the free surface.

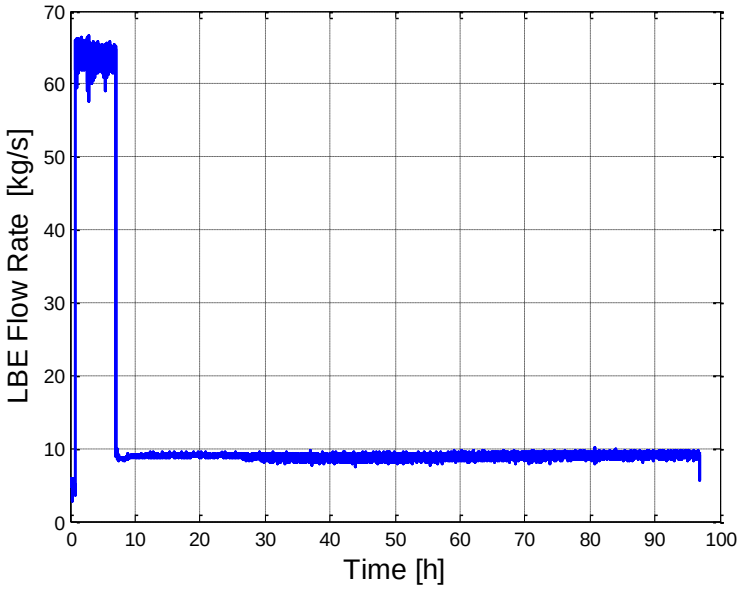

Figure 84: LBE flow rate through the primary system measured by the Venturi flow meter

The secondary water circuit is fed by water with a flow rate of 0.5 kg/s and the thermal power removed by the HX, evaluated from an energy balance on the LBE side, is about 530 kW. The duration of the full power run is about 7 h; after that, the transition to decay heat removal under natural circulation condition take place and the DHR is activated. The power removed by the DHR-system is 20 kW and after about 25 h, it is increased to about 23 kW (Figure 85). In test II, the CIRCE control panel is up-graded introducing a second option for controlling the DHR system. The first option is simply to choose the air mass flow rate injected in the inner pipe of the bayonet element, while the second option is to set the power: in this way the air mass flow rate is adjusted from the PID control to reach the desired power to be removed through the DHR.

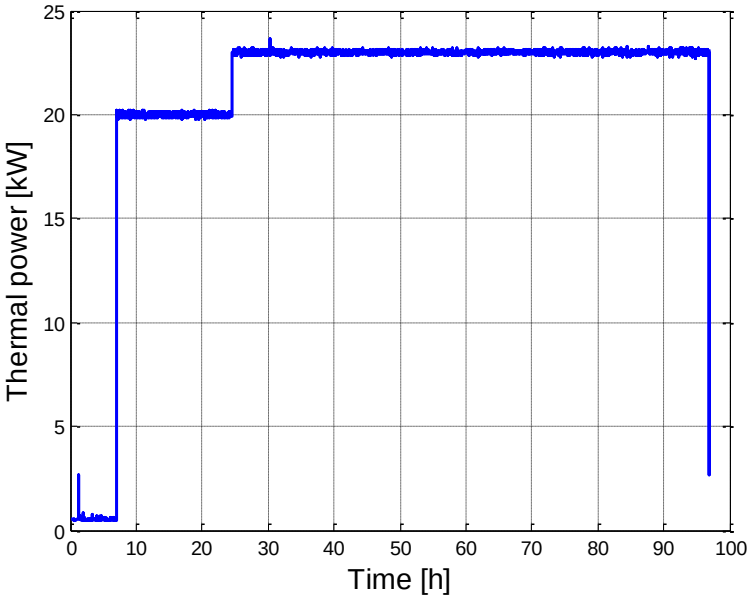

Figure 85: Thermal power removed by the DHR-system

Through the FPS, the LBE increases its temperature of about 60°C at full power run and after the transition, the difference in temperature reduces to about 21°C (Figure 86).

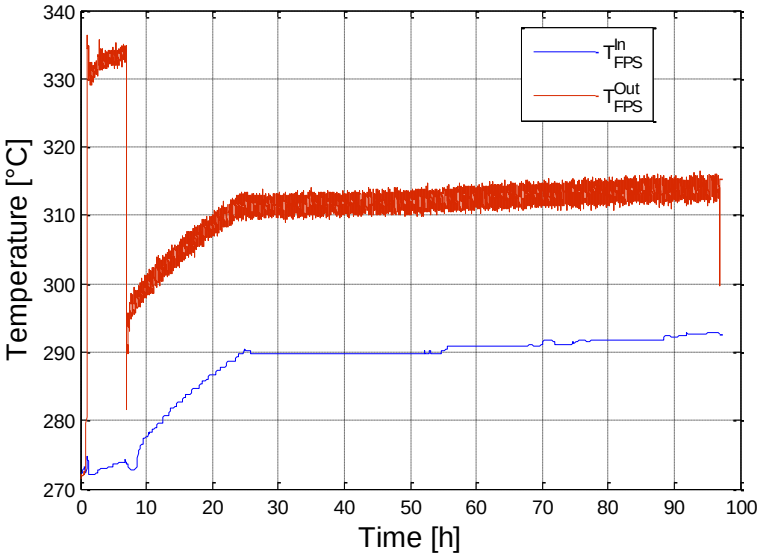

Figure 86: Average temperatures through the FPS

The difference in temperature between the inlet and the outlet sections of the water heat exchanger is about 52°C at the end of the full power run, while the temperature drop in the HX under natural circulation conditions is about 4°C, due to heat losses towards the LBE external pool (Figure 87).

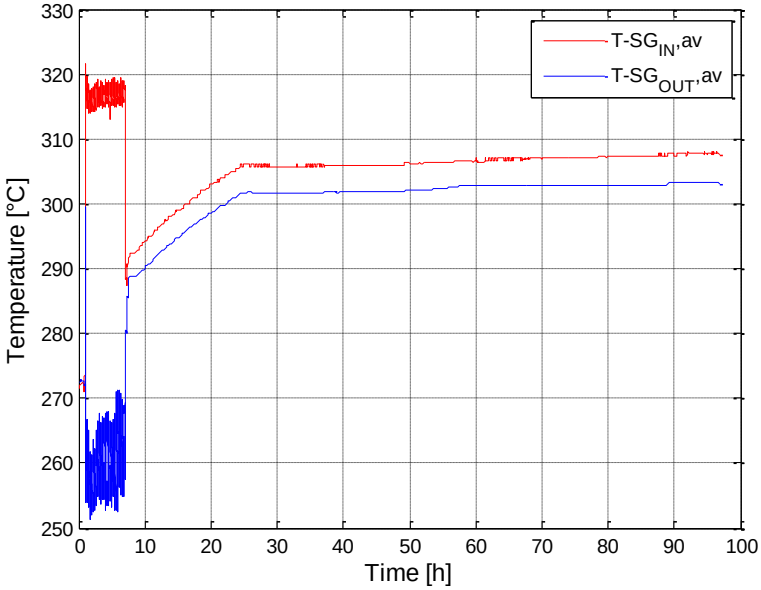

Figure 87: Average temperatures through the HX

The same considerations introduced in Test I (see Figure 75) can be applied to Test II in order to explain the difference between electrical power supplied to the FPS at full power run and the power removed by the HX shown in Figure 88.

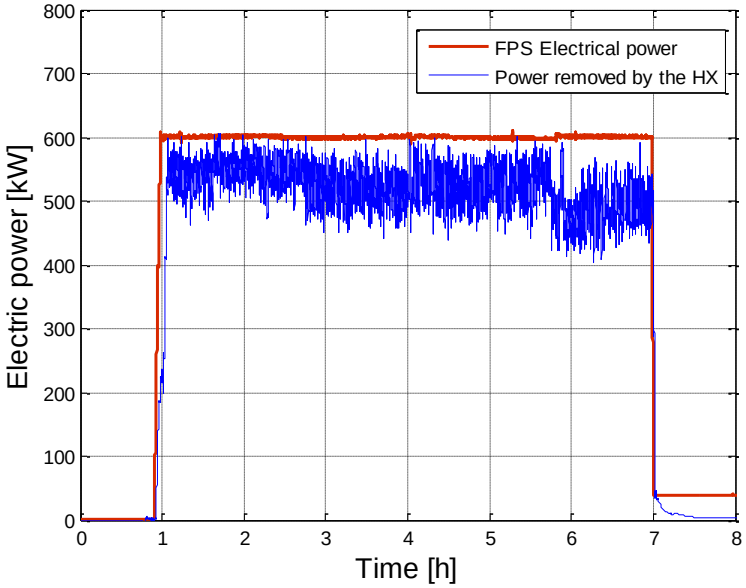

Figure 88: Energy balance at full power run

After transition to natural circulation conditions, the external heat losses at steady state conditions are in the order of about 17 kW. Considering the central (inner) subchannel at section 1 (Figure 89), clad temperature on pins 1 and 7 is about 340°C while in the bulk is about 297°C; hence, the temperature difference between the pins and the LBE in the centre of the channel is 43°C. After the transition to the natural circulation regime, at steady state conditions, the clad temperature is about 312°C and the bulk temperature is 308°C.

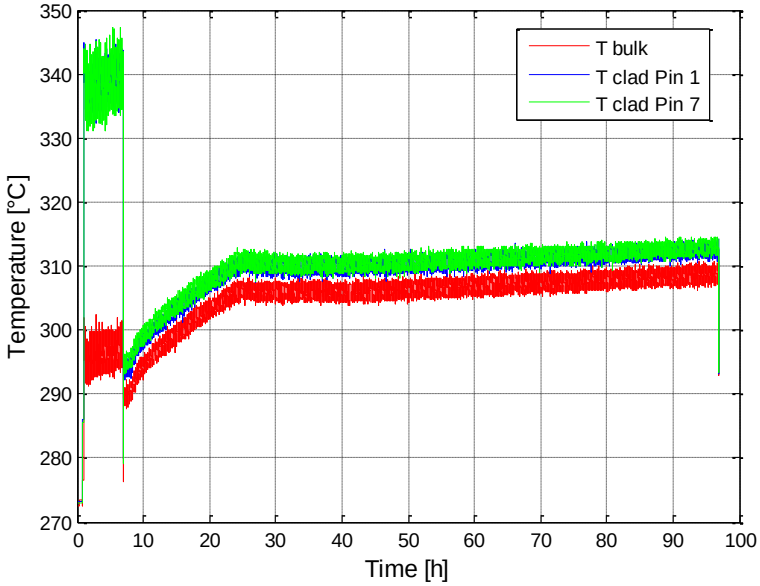

Figure 89: Temperatures in the inner subchannel (section 1)

At section 3, the temperature on pin 7 is lower than that measured on pin 1 due to the internal geometry adopted for the Bifilar-type pins, as already discussed for the previous test I (Figure 62). At steady state full power run, the difference between clad temperature at pin 1 and bulk temperature is about 47°C, while at the steady state of the NC regime it is about 4°C (Figure 90).

Concerning the temperatures inside the CIRCE pool, at the beginning of the test they are uniform, assuming a value of about 272°C (Figure 91). After about 6 h (Figure 92), before transition to natural circulation, the behaviour is analogous to what found for Test I, with a sharp temperature decrease between the outlet sections of HX and DHR (about 15°C in 0.6 m). After transition to natural circulation, the region where thermal stratification phenomena are significant moves downwards starting from the DHR outlet section (4.2 m) up to about 4.8 m. The temperature difference between the upper and lower plenum is about 10-12°C. The stratification in the pool reaches a steady state condition after about 30 h, maintaining the same profile up to the end of the experiment (Figure 93 and Figure 94).

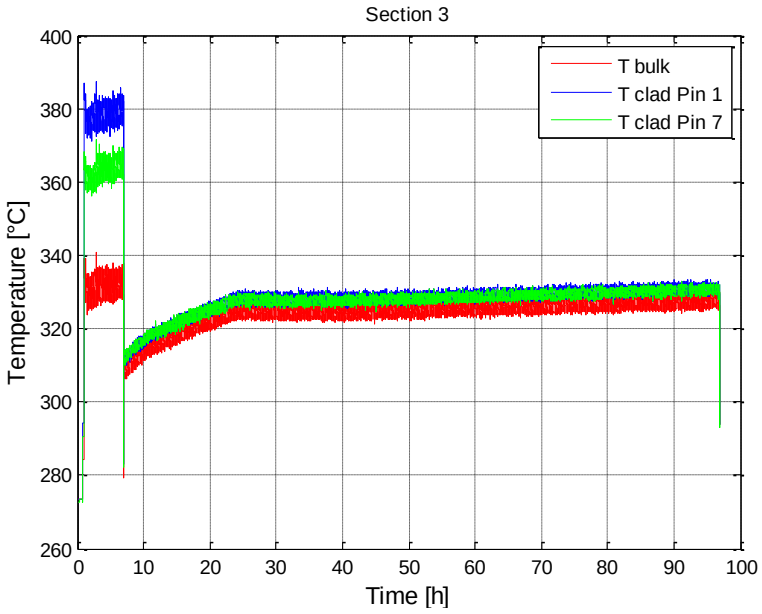

Figure 90: Temperatures in the inner subchannel (section 3)

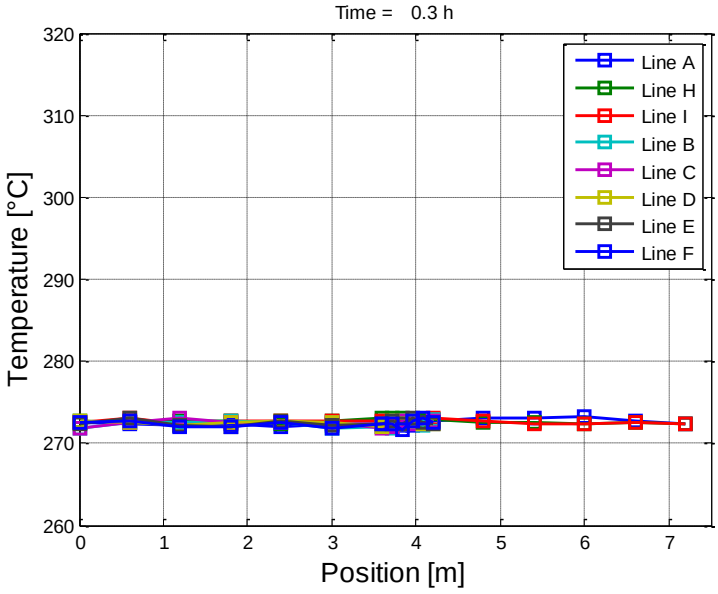

Figure 91: Temperature of the LBE inside the pool at t = 0.3 h

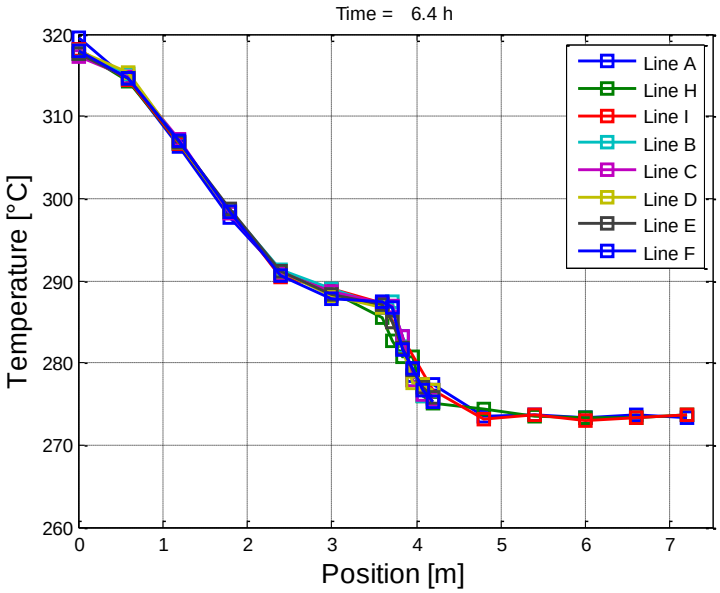

Figure 92: Temperature of the LBE inside the pool t = 6.4 h

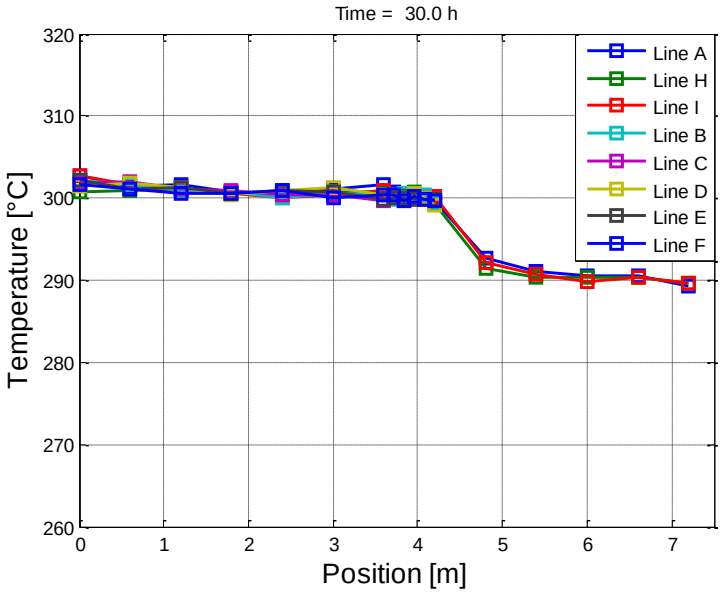

Figure 93: Temperature of the LBE inside the pool at t = 30 h

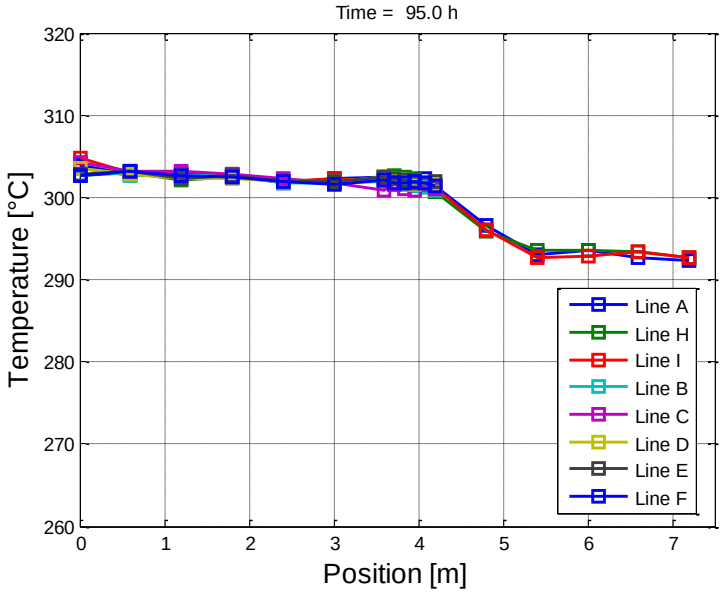

Figure 94: Temperature of the LBE inside the pool at t = 95 h

2.7. Post-test analysis

A steady state post-test CFD analysis is performed in order to obtain the vertical temperature trend in the LBE pool region assuming boundary conditions matching the actual conditions related to the experimental Test I. In particular, the air mass flow rate flowing in the secondary circuit of the DHR heat exchanger is reduced from 0.3 kg/s to 0.22 kg/s according to the experimental data (see Figure 58) and the external walls are considered diabatic with appropriate convective heat transfer. Air temperature at the DHR inlet section is assumed equal to 20°C while, the mass flow rate of the LBE in the primary circuit is imposed using an UDF in agreement with the trend obtained at steady state conditions by RELAP5 as reported in Figure 36.

The temperature profile is investigated along a vertical line inside the LBE pool region placed at y = 0.3 m (see Figure 40) and obtained results are reported in Figure 95. The vertical position where the stratification phenomena are concentrated is well predicted by the simulation. Moreover, the temperature difference between hot and cold plenum obtained from the steady state simulation is about 17°C, improving in this way the agreement between calculated and experimental results, even though it remains slightly greater with respect to what observed experimentally (Figure 96). Furthermore, the post-test analysis confirmed that the heat exchanged with the external environment has an important role and cannot be neglected.

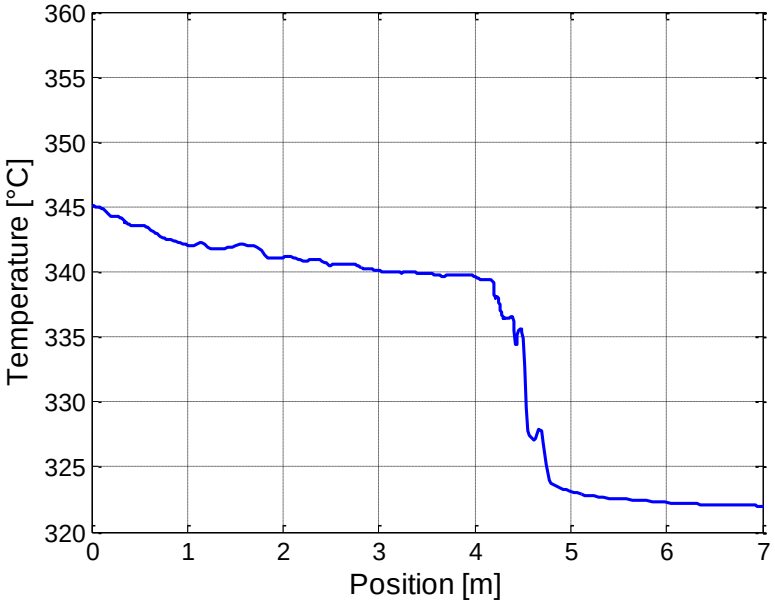

Figure 95: Temperature profile along the vertical control line (y = 0.3 m, post-test analysis)

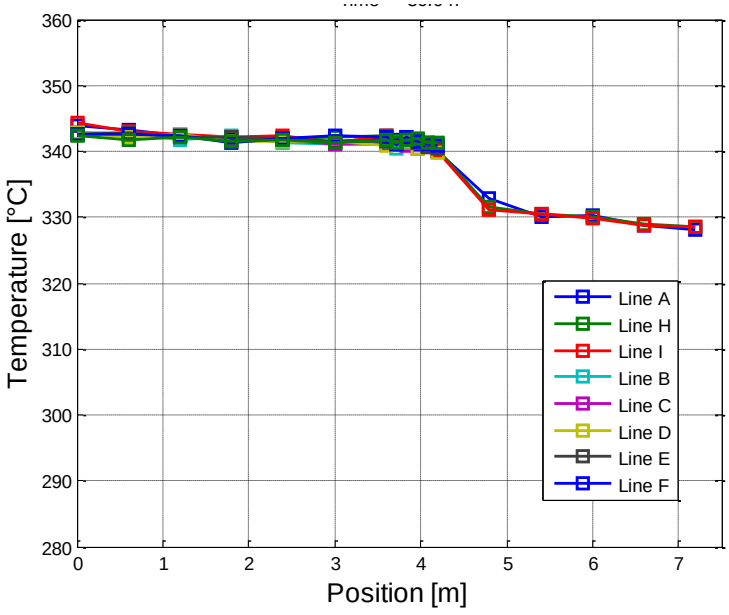

Figure 96: Experimental temperature vertical profile (t = 30h)

3 DEVELOPMENT OF A "TWO-WAY" COUPLING TOOL

3.1. Introduction

In order to better reproduce several accidental scenarios and improve the accuracy of numerical simulations, a new "two-way" RELAP5-Fluent coupling tool needs to be developed.

Simulations will take several benefits from this new methodology. First, a combination of 1D and 3D methods allows running reliable and feasible simulations of the complete system. The need for deeper and more accurate investigation of accidental scenarios and the challenges posed by the design of GEN IV reactors have increased the interest of the nuclear community toward CFD codes during the last years. Due to their relatively high computational costs, the CFD simulations cannot be used to replace system codes in the analysis of an entire thermal hydraulic system; they are rather meant for the analysis of local three-dimensional phenomena. A complex thermal hydraulic analysis generally requires different levels of simulations, from detailed local component-level with CFD simulations to integral system-level simulations.

On the other hand, system codes, based on 1D correlations are not suited to solve problems where complex 3D physics is involved. The coupling tool, moreover, allows to model the interaction of different physical phenomena, in such a way that gas lift forced circulation can be investigated using 1D-STH codes, while mixing and stratification phenomena in large 3D components can be investigated using a CFD approach. In this chapter, details of the developed coupling tool are reported.

One of the main objectives of coupling computer codes is to model the interaction of different physical phenomena. The coupling of codes, referring to nuclear research and development activity, often involves primary system thermal hydraulics codes (STH) and neutronics codes, in order to take into account 3D neutron kinetics and fuel temperature distribution or with structural mechanics codes, in order to take into account vibration induced by the flow or thermal striping (Hannink et all. 2008). Other cases include coupling of STH codes with fission product chemistry or with Computational Fluid Dynamics (CFD) models in order to calculate the system behaviour and the local behaviour simultaneously (IAEA-TECDOC-1539).

In this section, attention is focused on the coupling between STH and CFD codes. System Thermal Hydraulic codes have been widely developed by nuclear R&D and nuclear safety organizations with the aim to improve the reliability of results, while maintaining low computational costs (Davis et Shieh, 2000, Austregesilo et al., 2006, Geffraye et al., 2011, RELAP5-3D code development Team, 2013, RELAP5/Mod.3.3 Code Manual, 2003, etc.). These codes are based on partial differential equations for two-phase flow and heat transfer (mass, momentum and energy) usually solved by finite-difference methods based on one-dimensional approximations. Three-dimensional analyses based on approximate formulation of the momentum balance equations are available in some codes (e.g. RELAP5-3D, CATHARE etc.) with limitations on nodalization, field equations and physical models, including the lack of turbulence modelling and the use of idealized friction tensors in rod bundles.

In the work of Bestion (2010), the Multi-Scale analysis of reactor thermal hydraulics is introduced and four scales corresponding to four categories of simulation software are

illustrated. In particular, the system-scale is dedicated to the overall description of the circuit of the reactor. All accidental scenarios including Large-Break Loss Of Coolant Accidents (LB-LOCA) and Small-Break Loss Of Coolant Accidents (SB-LOCA) can be simulated with reasonable CPU time. The component-scale uses CFD in porous medium. This scale is dedicated to the design and safety of reactor cores and heat exchangers; the minimum spatial resolution is fixed by subchannel size. The meso-scale uses CFD in open medium and the average scale (millimetres or less) allows obtaining a finer description of the flow. This scale includes turbulence models (RANS, URANS, LES etc.). Finally, the micro-scale corresponds to DNS approaches with scales in the order of micrometre or less.

STH codes are generally inadequate when applied to transients investigating mixing and thermal stratification phenomena in large pool systems. On the other hand, the exclusive use of CFD codes still remains prohibitive for the requested computational effort. Coupling between two or more scales thus appears to be a promising technique when the small-scale phenomena taking place in a limited part of the domain, have to be investigated.

For this reason, the leading European research centres give great interest to the R&D of coupled simulation tools that combines system codes and CFD analysis. In particular, at the French Atomic Energy Commission (CEA) a coupled tool between the 3D computational fluid dynamics code TRIO_U with the best estimate thermal hydraulic system code CATHARE, is developed in order to perform single-phase thermal hydraulic analysis for the French SFR Phénix (Bavière et al., 2013). This coupling tool is developed with the aim of supporting the design and addressing safety issues for the SFR ASTRID demonstrator. It is based on a common Application Programming Interface (API), named ICoCo (Interface for Code Coupling). The "overlapping method" was selected. Using this method, the whole geometry is simulated by the STH codes while CFD is simultaneously resolving only a part of the system; variables are exchanged at the interfaces and STH codes use internals models as HTC, artificial heat transfer and local mechanical energy loss coefficients in order to match the CFD solution.

In the coupling application presented in Bavière et al. (2013), the CFD domain was restricted to the core whereas the STH code domain includes the core, the loops and the components (pumps, heat exchanger, etc.). The system code gives at the CFD one boundary conditions as mass flow rates and temperatures, while the CFD domain provides momentum and enthalpy feedback to the system-code.

In Germany, the Gesellschaft für Anlagen- und Reaktorsicherheit (GRS) is deeply involved in the development of a coupling tool between the ATHLET system code (Analysis of THermal-hydraulics of LEaks and Transients) and the Ansys CFX CFD code. In the application presented by Waata and Frank (2008), the working fluid is water and the coupling strategy is based on an explicit coupling scheme. The ATHLET code obtains pressure and temperature from the CFD tool, while it provides at the end of the time step mass flow and enthalpy to the ANSYS CFX Inlet. The calculation of these parameters is inverted when the coupling interface is at the outlet. As a further improvement (Papukchiev and Lerchl, 2009), the interface code was modified to allow the use of "Opening–Opening" boundary conditions in ANSYS CFX (an opening is used at a boundary where the flow direction can change into or out of the CFD domain). With the new strategy, ATHLET provides fluid velocity instead of mass flow rate at the ANSYS CFX inlet "Opening". The CFX-ATHLET coupling strategy is developed in close collaboration between GRS and ANSYS Germany; for this reason, the CFD source is available and the shared library containing the interface and ATHLET code is extended in the CFX code. Recently, at the International COnference on Nuclear Engineering (ICONE22, July 7-11, 2014 Prague)

Ansys Germany, and GRS presented a development of the coupling tool introducing a semi-implicit scheme (Theodoridis et al., 2014).

The division of Nuclear power Safety of the Royal Institute of Technology (KTH) in Sweden is also involved in the development and implementation of a domain overlapping methodology for coupling RELAP5/mod3.3 STH code and Star-CCM+ CFD code. This research activity is dedicated to the GEN IV LFR nuclear reactor and the considered working fluid is LBE. The adopted numerical scheme is an explicit scheme where the STH code provides inlet boundary temperature and mass flow rate to the CFD one that calculates the 3D test section outlet boundary temperature. The STH model is iteratively corrected until its solution match with the CFD solution ("overlapping-domain"). The coupling algorithm is implemented in a Java macro executed by the Star-CCM+ Application Programming Interface (API). The macro controls the time-marching, execution of Star-CCM+, boundary data export from, and import to, RELAP5/Star-CMM+, STH input model correction, execution of RELAP5 and logging of all necessary variables. This tool is applied to the TALL-3D experimental facility, a thermal hydraulic Lead-Bismuth loop designed and built at KTH to provide validation data for both stand-alone and coupled simulations (Jeltsov et al. 2014). Pre-Test simulations are performed but no experimental data are still available.
In Schultz et al. (2005) Fluent and RELAP5-3D©/ATHENA were linked using an Executive Program (PVMEXEC) (Weaver et al., 2002) that monitors the calculation progression in each code, determines when each code has converged, governs the information interchanges between the codes and issues permission to allow each code to progress to the next time step. The Executive Program is interfaced with Fluent and RELAP5-3D©/ATHENA using Fluent User-Defined Functions.

Studies on coupling strategies are also carried out at the Paul Scherrer Institut (PSI) in Switzerland (Bertolotto et al., 2009). In Bertolotto's work, a coupling tool between TRACE and Ansys CFX is presented. In particular, the information exchange is achieved by means of the Parallel Virtual Machines (PVM) software. Both explicit sequential scheme and a semi-implicit scheme are developed for time advancement. Verification of the coupling tool are carried out on a simple test case consisting of a straight pipe filled with water and on an experimental test conducted on a test facility made of two loops connected by a double T-junction.

At the research Institute of Nuclear Engineering of the University of Fukui (Japan) the transient behaviour of flow instability in Steam Generator U tubes is simulated numerically by performing a coupled STH-CFD simulation (Watanabe et al., 2014). The codes involved are the RELAP5/mod3.3 for the simulation of the secondary side and Fluent for the simulation of the primary side. The hot-leg inlet conditions and the secondary-side temperatures are given by RELAP5 as an output file for each time step, and these data are read by FLUENT using an UDF. The cold-leg outlet conditions calculated by FLUENT are averaged and written in another output file using the UDF. This output variables are exchanged with RELAP5 as node and junction variables defined in the restart input file edited by a conversion program. Moreover, a small-scale experiment is conducted with a test facility consisting of the heating loop and the model of the Steam Generator (SG). Obtained numerical results are compared with the obtained experimental data.

At the Department of Nuclear, Plasma and Radiological Engineering of the University of Illinois a coupled CFD system code is developed based on FLUENT and RELAP5-3D and applied to simulate the primary coolant system in Modular Helium Reactor (GT-MHR) GEN IV VHTR (Y. Yan and R. Uddin,2011). The CFD model of the lower plenum is

coupled with the RELAP5-3D model of the reactor core and upper portion of the GT-MHR and set of User Defined Functions (UDFs) are written to perform the interface data exchange during the coupled simulation.

In China, at the Department of Nuclear Science and Technology, State key Laboratory of Multiphase Flow in Power Engineering of Xi'an Jiaotong University, a preliminary study of coupling RELAP5/mod3.1 and Fluent is performed (Li et al., 2014).

In the following section, the in-house developed coupling tool between RELAP5/mod3.3 and ANSYS Fluent is described. In particular, the coupling methodology presented here, represents a first application to a simplified schematization of the NAtural CIrculation Experiment (NACIE) facility developed and hosted at the ENEA Brasimone R.C..

The above shows the great interest for coupling CFD and STH code providing a strong motivation to carry on a similar work for application to cases of our specific interest.

3.2. NACIE experimental facility

NACIE (Tarantino et al., 2010, Coccoluto et al., 2011), is a loop type facility filled with Lead Bismuth Eutectic (LBE). It is conceived to qualify and characterize components, systems and procedures relevant for Heavy Liquid Metal (HLM) nuclear technologies. In particular, the NACIE facility allows performing experiments in the field of thermal hydraulics and fluid dynamics to investigate heat transfer correlations in prototypical fuel bundle simulators. The NACIE experimental campaigns are intended to support GEN IV nuclear power plant design and for the qualification and development of CFD and STH codes.

The facility consists of a rectangular loop made of two vertical stainless steel (AISI 304) pipes (Nominal Pipe Size (NPS) 2½" schedule 40) acting as riser and downcomer connected by means of two horizontal pipes of the same dimension. The heat source is installed in the bottom part of the riser, while the upper part of the downcomer is connected, through appropriate flanges, to a heat exchanger (Figure 97). The overall height, measured between the axes of the upper and lower horizontal pipes, is 7.5 m and the width is 1 m. The maximum inventory of LBE is in the order of 1000 kg and the loop is designed to work with temperatures and pressures up to 550°C and 10 bar respectively. The facility can work both in natural and forced circulation conditions; furthermore, the transition from forced to natural circulation can be investigated.

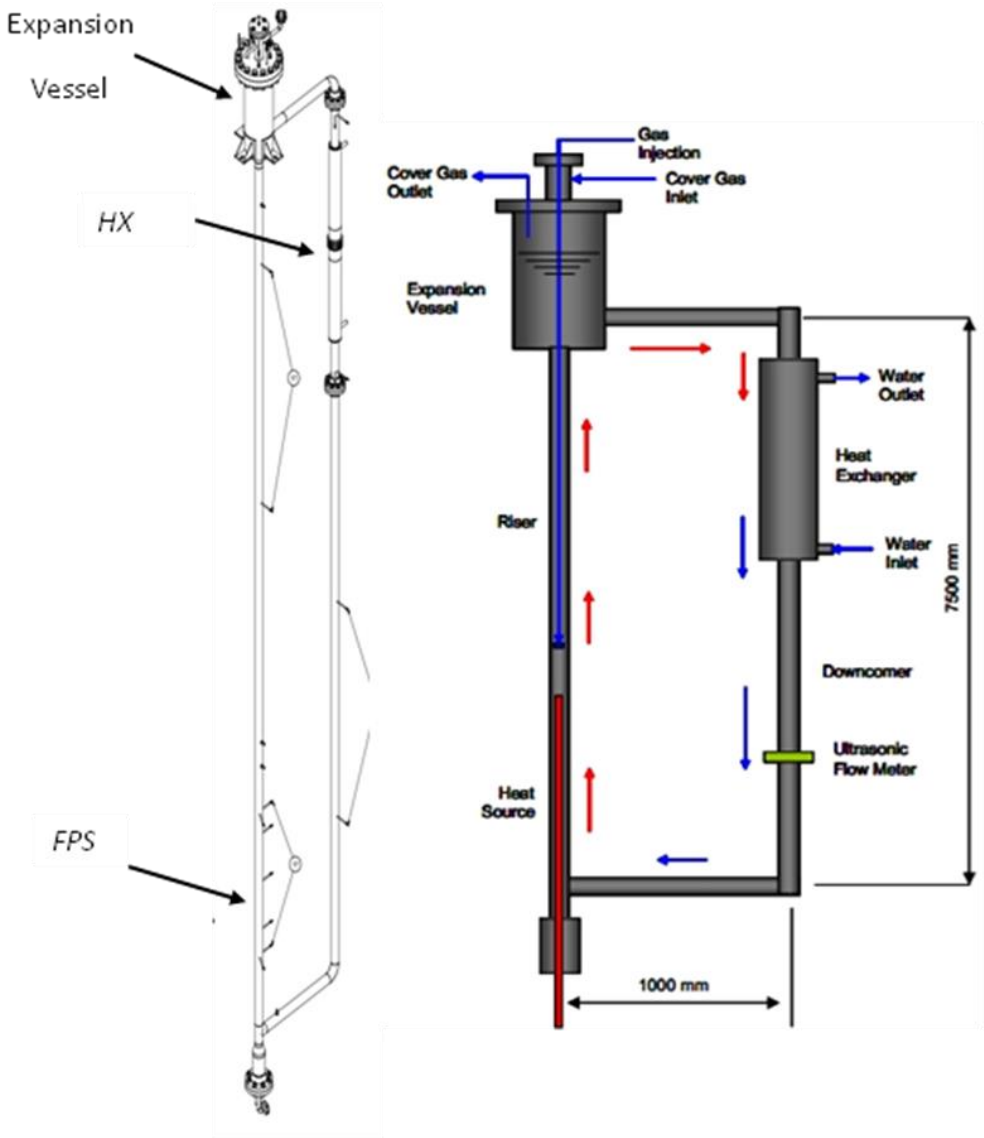

Figure 97: Isometric view and layout of NACIE primary loop

Concerning the operation under natural circulation regime, the thermal centres elevation difference between the heat source (FPS) and the heat sink (Heat Exchanger, HX) of about 5.7 m, provides the pressure head ($\Delta p \sim g\beta\Delta T \cdot H$) required to guarantee a suitable LBE mass flow rate. Under forced circulation conditions, a gas lift technique is adopted to promote LBE mass flow rate along the loop. A pipe with an I.D. of 10 mm is housed inside the riser connected through the expansion gas top flange to the argon feeding circuit, while at the pipe lower section, a nozzle is installed to inject argon into the riser promoting enhanced circulation inside the loop. The Gas injection system is able to supply argon flow rate in the range 1-20 Nl/min with a maximum injection pressure of 5.5 bar. The argon gas flows into

the riser and is finally separated (in the gas expansion vessel) from the two phase mixture, flowing upwards into the cover gas while the LBE flows back into the heat exchanger through the upper horizontal branch. According to the described configuration, the maximum LBE mass flow rate is around 20 kg/s in gas-lift (forced) circulation and 5 kg/s in natural circulation conditions. Figure 98 shows the NACIE loop installed in the HLM experimental-hall laboratory at the ENEA Brasimone R.C..

Figure 98: NACIE facility

The primary LBE side is coupled to the water secondary side by means of a “tube in tube” counter flow type heat exchanger (HX) fed by water at low pressure (about 1.5 bar) and designed assuming a thermal duty of 30 kW. The HX essentially consists of three coaxial tubes with different thicknesses (Table 8 and Figure 99).

Table 8: NACIE heat exchanger geometrical & material data

	Inner Pipe	**Middle pipe**	**External pipe**
I.D.	62.68 mm	84.9 mm	102.3 mm
O.D.	73 mm	88.9 mm	114.3 mm
Thickness	5.16 mm	2.0 mm	6.02 mm
L	1500 mm	1500 mm	1500 mm
Material	AISI 304	AISI 304	AISI 304

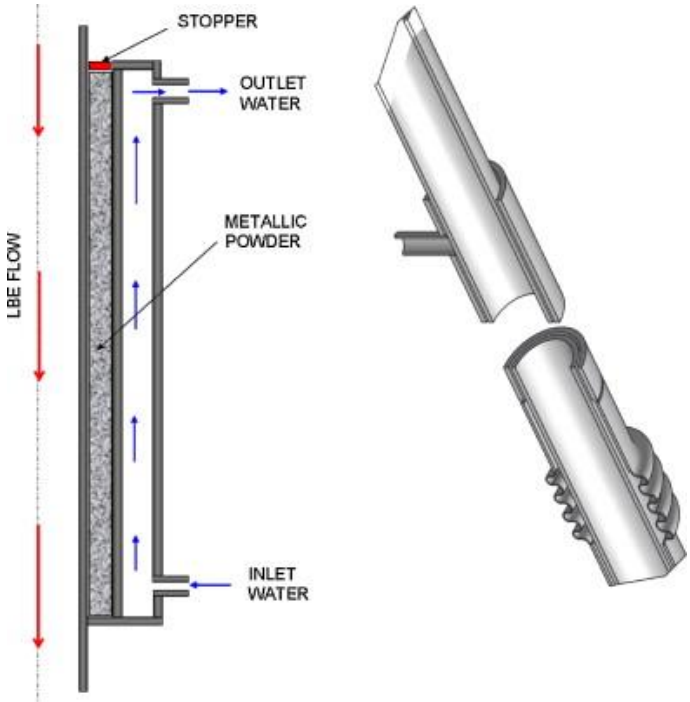

Figure 99: NACIE heat exchanger

LBE flows downwards into the HX inner pipe (Figure 99), while water flows upwards in the annular region between the middle and the outer pipe allowing a counter current flow heat transfer. The annular region between the inner and middle pipe is filled with a stainless steel powder. The aim of this powder gap is to ensure the thermal coupling between LBE and water and to reduce the thermal stress across the tube walls (the thermal gradient between LBE and water is localized across the powder layer). In fact, the three pipes are welded together in the lower section, while in the upper section the inner pipe is mechanically decoupled from the other pipes allowing axial expansion between them. In

order to avoid a powder leakage, the annular region is closed in the upper section by a graphite stopper. In the outer pipe, an expansion joint is installed to mitigate the stresses due to different axial expansion between the middle and the outer pipe walls. An air cooler completes the secondary circuit to maintain water temperature under its boiling point.

The fuel bundle (Figure 100), consist of two high thermal performance electrical pins with a nominal thermal power of about 43 kW. The main characteristics of the bundle are summarized in Table 9.

Table 9: NACIE bundle main parameters

N° of active pins	2
O.D.	8.2 mm
Total length	1400 mm
Active length	890 mm
Heat flux	100 W/cm^2
Thermal power (each pin)	21.5 kW

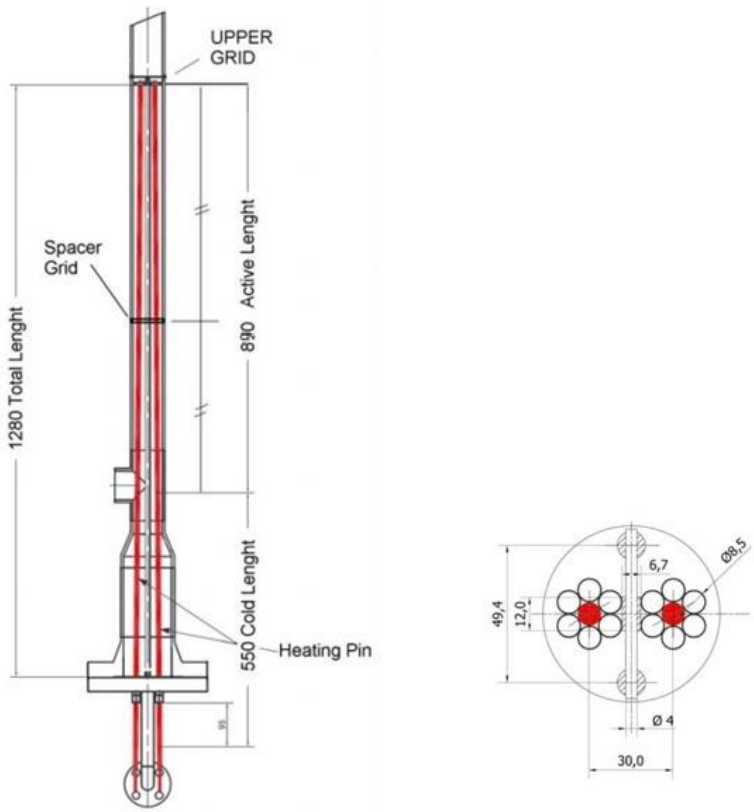

Figure 100: NACIE fuel bundle

The LBE mass flow rate is measured in the lower pipe section after the HX. The adopted mass flow meter is a prototypical contactless Phase-shift sensor developed at ENEA Brasimone R.C. jointly with the Helmholtz-Zentrum Dresden-Rossendorf (HZDR) and Systemanalyse & Automatisierungsservice GmbH (SAAS GmbH). It consists of two receiving coils and an emitting coil, placed on opposite sides of the duct containing the liquid metal (Figure 101). The emitting coil aligned perpendicularly with respect to the direction of the electrically conducting melt flow provides the alternating magnetic flux. The information about the averaged velocity v_0 or flow rate $\dot{m}$ is provided by a phase-shift $\Delta\varphi$ between the receiver coils.

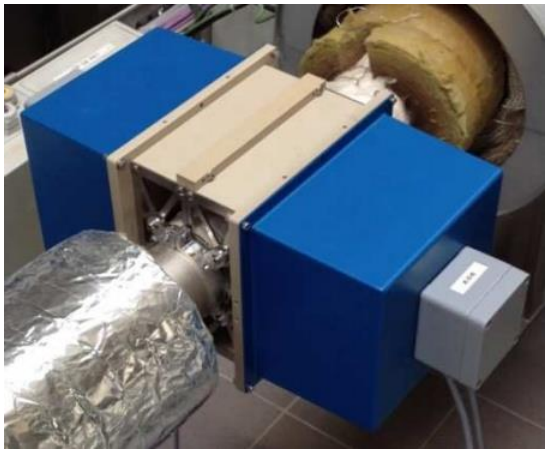

Figure 101: Prototypical induction flow meter

3.3. RELAP5 physical and geometrical computer model

A version of the RELAP5/mod.3.2 was modified in 1999 by ANSALDO Nucleare (Petrazzini M. et al., 1999) to account for liquid Lead and LBE alloy properties and behaviour, using "the soft sphere" model reported in the work of Young D.A. (1977). However, the thermodynamic properties used in this model are not well in agreement with the properties reported in the HLM Handbook, 2007 and in the most recent work of Sobolev (2011). As an example, the density is correlated according to Touloukian et al. (1970). Figure 102 shows the comparison of the density as a function of the temperature reported in Touloukian et al. and the trends predicted by the correlations proposed in the HLM Handbook and by Sobolev.

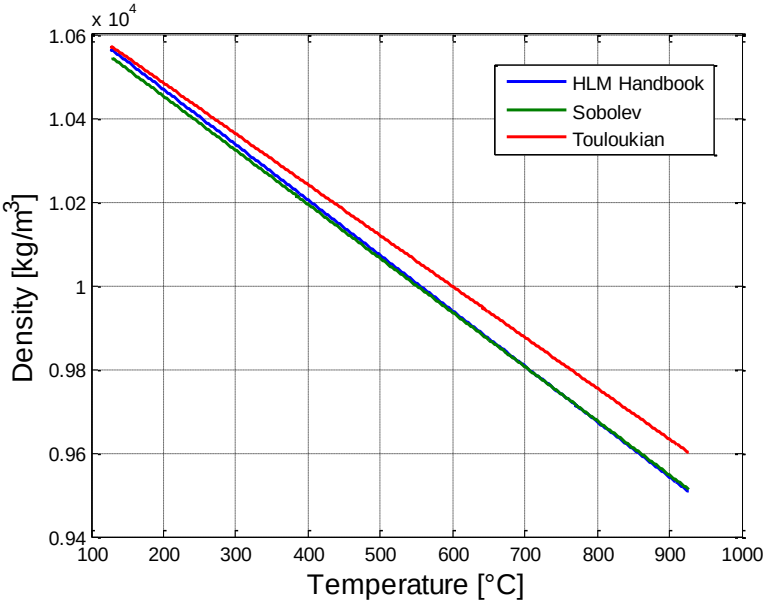

Figure 102: LBE density from different correlations

Appreciable differences between properties computed from the modified RELAP5/Mod.3.2 and from recent studies are evidenced.

In order to revise the thermodynamic properties employed to generate RELAP5 tables for LBE, Lead and Sodium, the RELAP5/mod3.3 has been recently modified at the University of Pisa in agreement with the last correlations available in the scientific literature (Martelli D. et al., 2013). In particular, equations needed to obtain temperature, pressure, specific volume, specific internal energy, thermal expansion coefficient, isothermal compressibility, specific heat at constant pressure and specific entropy both for saturation and single phase conditions are reviewed according to Sobolev (2011). By the way, it is essential that both RELAP5 and Fluent implement the same thermodynamic properties in order to avoid numerical instabilities during the execution of the coupled procedure. Convective heat transfer correlations for fuel bundle are also implemented according to Ushakov and Mikytiuk correlations (Ushakov et al., 1977; Mikytiuk, 2009). In particular, when a liquid metal (LBE or lead or sodium) is used as working fluid, a convective boundary condition must be set in the data for heat structures, in Word 3 of Cards 1CCCG501 and 1CCCG601, as reported in the following table (see Input Manual of RELAP5).

Table 10: Choice of Correlation in Word 3 of Cards 1CCCG501 and 1CCCG601 of RELAP5 code

RELAP5 option	Authors	Correlation
1, **100**, **101**	**Seban and Shimazaki** (uniform wall temperature)	$\mathrm{Nu} = 5 + 0.025\,\mathrm{Pe}^{0.8}$
102	**Cheng and Tak** (uniform heat flux)	$\mathrm{Nu} = A + 0.018\,\mathrm{Pe}^{0.8}$ with $A = \begin{cases} 4.5 & \text{if } \mathrm{Pe}<1000 \\ 5.4\text{-}9\cdot10^{-4}\mathrm{Pe} & \text{if } 1000 \le \mathrm{Pe} \le 2000 \\ 3.6 & \text{if } \mathrm{Pe}<2000 \end{cases}$
110 (set *P/D* on 801/901 card)	**Ushakov** (triangular lattice of fuel pins)	$\mathrm{Nu} = 7.55\frac{p}{D} - 20\left(\frac{p}{D}\right)^{-13} + 0.041\left(\frac{p}{D}\right)^{-2} \mathrm{Pe}^{(0.56+0.19\frac{p}{D})}$ $1 \le \mathrm{Pe} \le 4000;\quad 1.2 \le p/D \le 2.0$
111 (set *P/D* on 801/901 card)	**Mikityuk** (triangular and square lattice of fuel pins)	$\mathrm{Nu} = 0.047\left[1 - \exp\left(-3.8\left(\frac{p}{D} - 1\right)\right)\right]\left(\mathrm{Pe}^{0.77} + 250\right)$ $30 \le \mathrm{Pe} \le 5000;\quad 1.1 \le p/D \le 1.95$

This modified RELAP5 version is used to model the NACIE facility as shown in Figure 102. The amount of LBE inside the loop is about 835 kg in isothermal initial conditions (the numerical value of the temperature depends on the considered test) and fluid at rest. Argon upper plenum pressure in the Expansion Vessel is set to $1.2\cdot10^5$ Pa (*TmdpVol-320*). Referring to Figure 103, liquid metal follows an anticlockwise flow path through the loop components. LBE receives the supplied power flowing through *Pipe-110* (FPS, Fuel Pin Simulator) placed in the bottom section of the riser; the FPS active length is characterized by a height of 0.89 m and a single electrical pin supplying heating power is simulated (in accordance with the experiment). Gas lift circulation is modelled using time depending junction *TmdpJun-405* which connects time dependant volume *TmdpVol-400* (containing argon) to *Branch-125*, injecting the required argon flow into the riser (2.35 m from the bottom) and thereby promoting LBE circulation along the loop. Inside the Expansion Vessel argon is separated from the liquid metal and exits in *TmdpVol-320*; then, from the Expansion Vessel, LBE goes through the upper horizontal pipe (*Pipe-160* and *Pipe-170*) to the downcomer where it flows downwards through the Heat Exchanger (HX) primary side section (*Pipe-180*, located in the downcomer upper zone). Here the thermal power is removed by the secondary side water, flowing upwards, thermally coupled to the descending LBE.

The secondary side water system is modelled by means of *TmdpVol-500*, (where the inlet water properties are set) connected to *TmdpJun-505*, that defines the inlet water mass flow rate feeding the HX secondary side annular zone (*Annulus-510*); water flows upwards and exits in *TmdpVol-520*. Primary to secondary heat transfer involves the 1.5 m HX active length and simulates the tube in tube counter flow heat exchanger configuration, taking into account the presence of stainless steel powder filling the gap created by the internal and middle pipe (5.95 mm width) described above (see Table 8 and Figure 99). Thermal conductivity of the powder is chosen to be 12.5% of AISI 304 theoretical value (Coccoluto et al., 2011). External heat losses are considered as well. Taking into account the facility thermal insulation, an appropriate heat transfer coefficient with external environment is imposed.

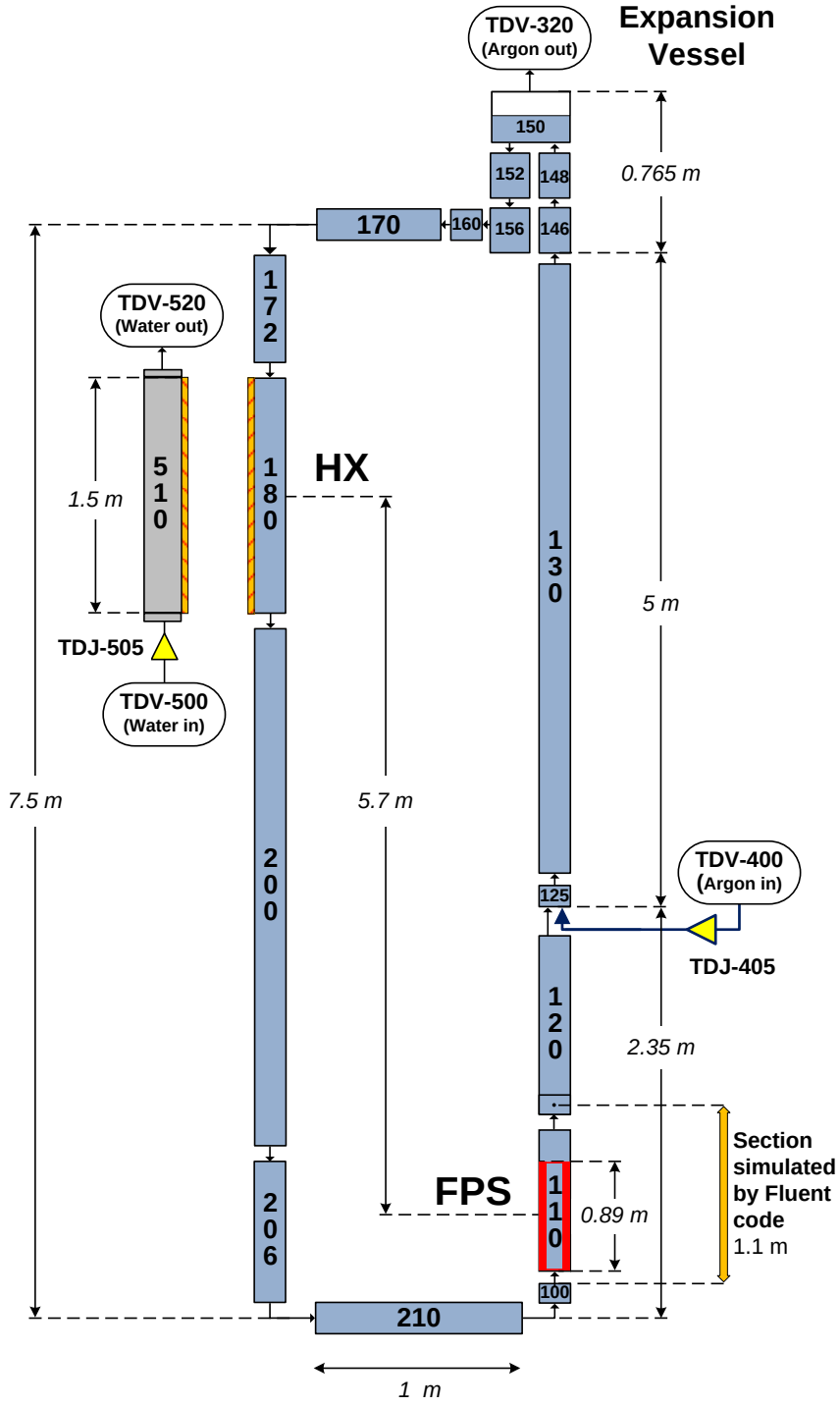

Figure 103: RELAP5 nodalization of the NACIE facility

3.4. Fluent geometrical domain

Starting from the RELAP5 "closed" nodalization (see Figure 103), the primary circuit is then re-arranged in such a way to split the overall domain into two regions, one to be simulated by RELAP5 system code and one to be simulated using the Fluent CFD code (non-overlapping domains technique). In particular, the portion of the loop to be simulated by the Fluent code is the Fuel Pin Simulator (FPS, active pin length 0.89 m) and a pipe of 0.21 m after it to reduce the possibility of occurrence of backflow conditions in the outlet section for the coupled code simulations. The overall length of the CFD domain is 1.1 m.

In Figure 104, the RELAP5 nodalization used for the coupled simulations is reported. In *TmdpJun-115* and in *TmdpVol-112*, respectively, boundary conditions of mass flow rate and temperature obtained from an inner reference section of the Fluent domain are applied (exit section of the CFD domain is at the same elevation of the cell centre of *pipe-120*). Pressure imposed in *TmdpVol-110* is obtained from the inlet section of the CFD domain in agreement with the scheme reported in Figure 105. To reduce the occurrence of the previously mentioned backflow conditions in the outlet section of the CFD domain, a very high value of reverse form loss coefficient is set for the junction that connects *Pipe-210* to *Branch-100* and for the junction that connects *Branc*h-125 with *Pip*e-130. Mass flow rate and LBE temperature needed as inlet boundary condition (b.c.) for the CFD geometrical domain, are evaluated at *Pipe-110* of the RELAP5 nodalization.

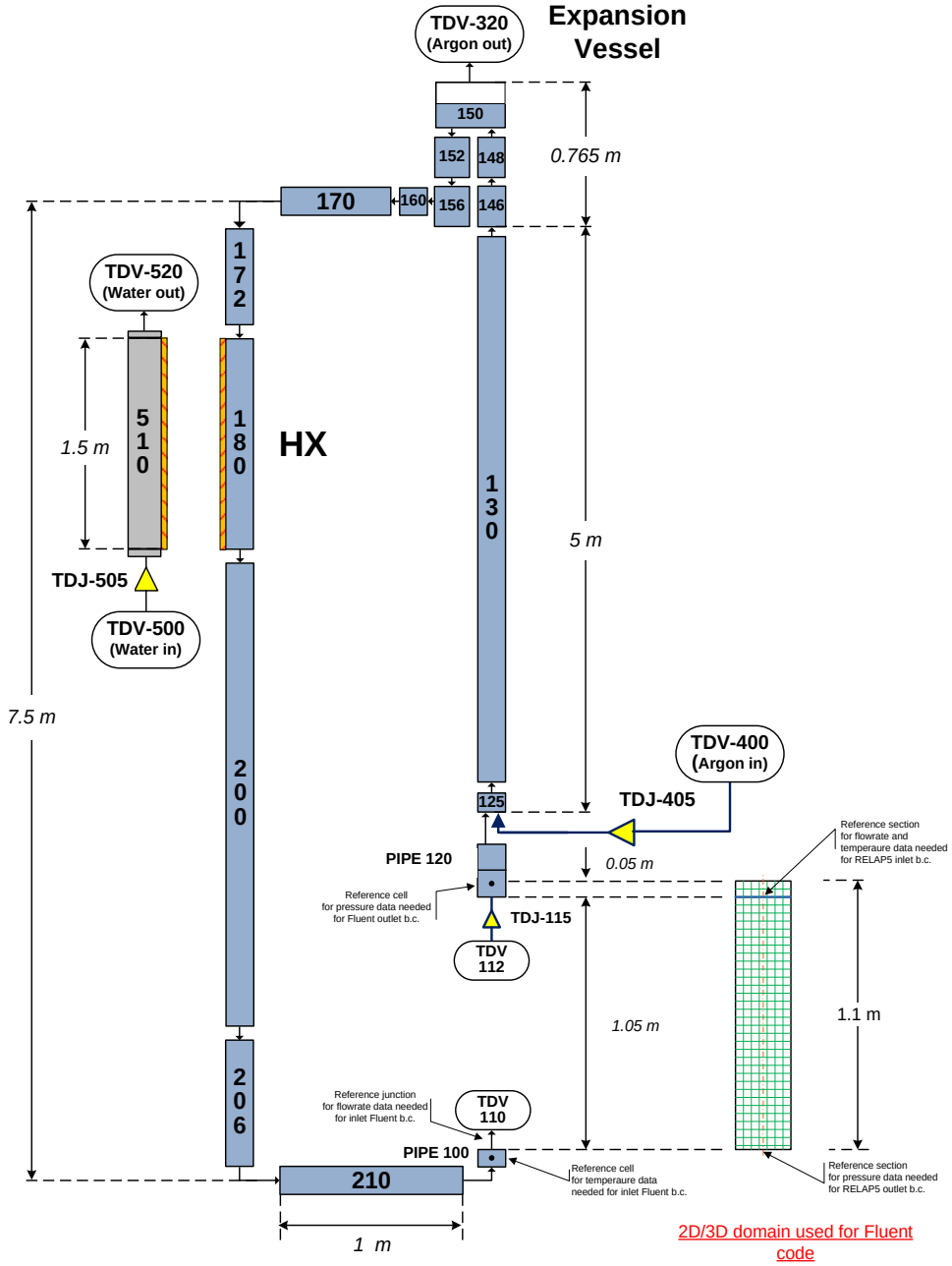

Figure 104: RELAP5 nodalization of NACIE loop for coupled simulations

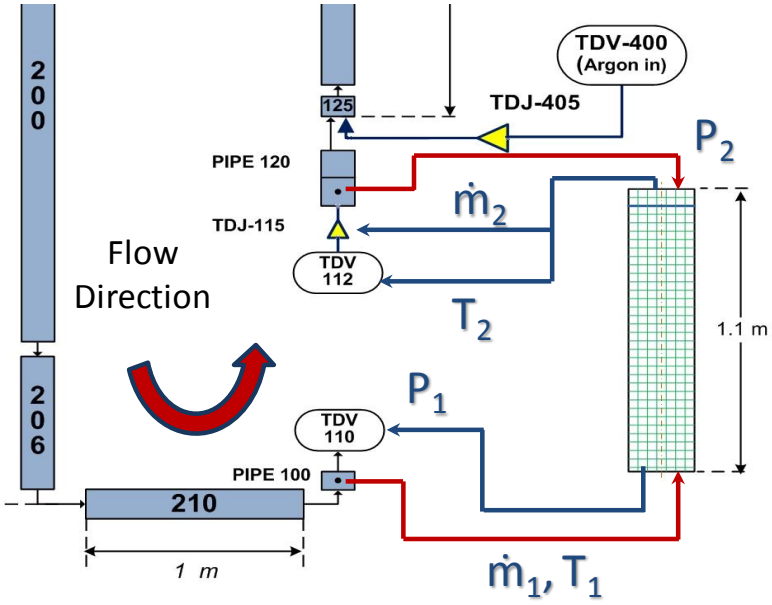

Figure 105: RELAP5-Fluent data exchange

The domain of the loop, simulated with the Fluent code, is firstly modelled as a simplified 2D axial-symmetric domain and then as a 3D symmetric domain. The 2D geometrical model is discretized by a structured mesh composed by 7668 rectangular cells, uniformly distributed both in the axial and radial coordinates (Figure 106).

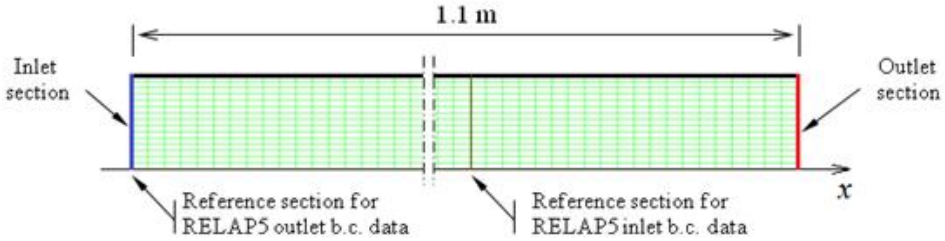

Figure 106: Axial-symmetric domain used in Fluent code for coupled simulations

To model the FPS form loss coefficient (spacer grids) a constant value of 3.5 is considered. For this purpose, five different interior faces are set as “porous-jump” in the 2D domain and an equivalent constant local pressure drop coefficient (0.7) is set in each of them. The 3D symmetric domain is modelled with the symmetry plane passing through the axis of the electric pins (not reproduced in the model), the pin bundle support rods are not reproduced in the model as well (Figure 107).

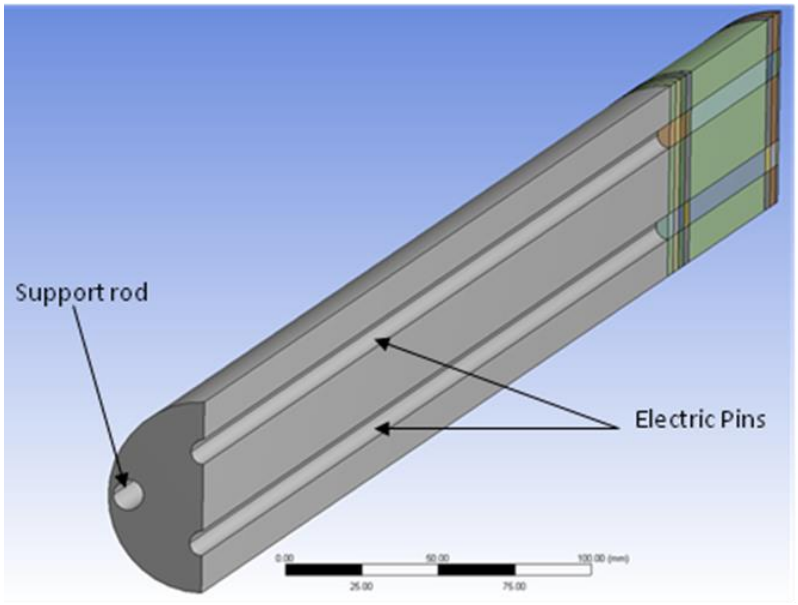

Figure 107: Domain used in Fluent code for coupled simulations

The 3D domain is discretized using 141045 hexahedral elements with refinements near the inlet and outlet sections in axial direction and near the electric pins wall along the radial direction (Figure 108). One interior face is set as a porous jump and an equivalent constant coefficient of concentrated pressure drop equal to 0.5 is set in order to introduce the pressure drop due to the spacer grid not simulated in the 3D geometrical domain.

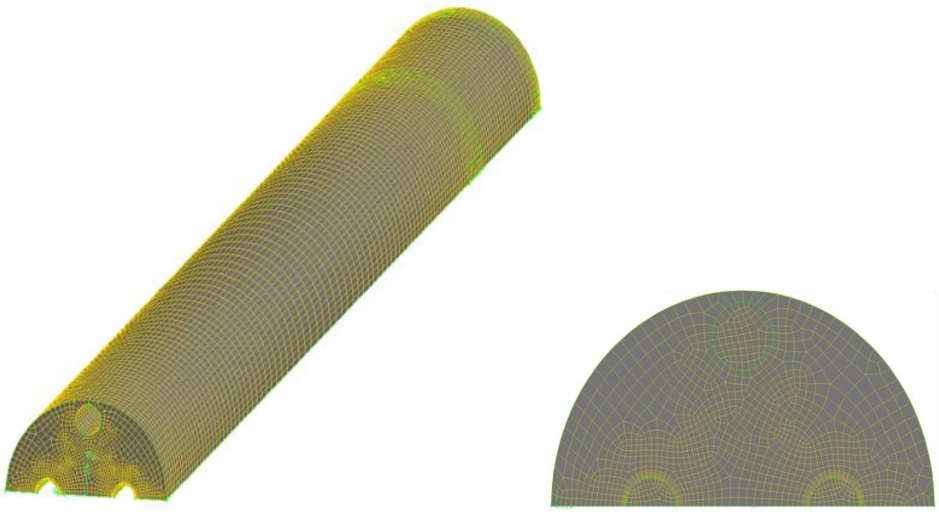

Figure 108: Spatial discretization of the 3D domain

3.5. Coupling procedure: explicit scheme

The developed coupled approach can be classified as "non-overlapping, two-way coupling scheme". The geometry or domain to be analysed is divided into regions that are modelled using CFD and regions that can be reasonably well simulated using the system code (non-overlapping). This partition identifies the interfaces where thermo-fluid-dynamics data are transferred from the system-code-portion to the CFD-code-portion fluid and vice versa (two-way coupling). The execution of the RELAP5 and Fluent codes is operated by an appropriate MATLAB script, where a processing algorithm is implemented allowing to receive boundary conditions (b.c.) data from Fluent, at the beginning of the RELAP5 time step, and to send b.c. data to the Fluent code, at the end of the RELAP5 time step. In addition, a special User Defined Function (UDF) is realized for Fluent code to receive b.c. data from RELAP5 and to send b.c. data to RELAP5 for each CFD time step. At the beginning of each time-step, the Fluent code receives from the RELAP5 code the mass flow rate ($\dot{m}_1$) and the temperature (T_1) to be set as inlet section boundary condition and the RELAP5 receives the pressure (P_1) from the Fluent code to be set in the Time dependent volume *TmdpVol-110*. Similarly, at the outlet section of the CFD model, the Fluent code receives from the RELAP5 the pressure (P_2), while it provides to RELAP5 the LBE mass flow rate ($\dot{m}_2$) and the outlet section average temperature according to the scheme shown in the previous Figure 105.

A special procedure is considered when the pressure data are exchanged between RELAP5 and Fluent codes, because the first code works with absolute pressure while the CFD code, to reduce the round-off error, works with a pressure field reduced by the gravitational pressure contribution and by the "operating pressure", representing the average absolute pressure in the domain. An initial RELAP5 transient of 1000 s is executed to reach steady state conditions with a uniform temperature (depending on the test simulated) and with fluid at rest. The end of this initial transient is then considered time zero from which the coupled simulation starts. After that, a sequential coupling calculation is activated where the Fluent code (master code) advances firstly by one time step and then the RELAP5 code (slave code) advances for the same time step period, using data received from the master code. After both the codes terminate the current time step, the RELAP5 data needed to Fluent b.c. are exchanged and the procedure for a new time step advancement is repeated (explicit coupling scheme).

In Figure 109, the explicit coupling scheme is described. The solution at time step i+1 is evaluated in terms of known quantities at the previous time step i. Nevertheless, explicit numerical methods are conditionally stable and, in order to guarantee the method convergence, the time step size is limited by the Courant-Friedrich-Levy (CFL) limit.

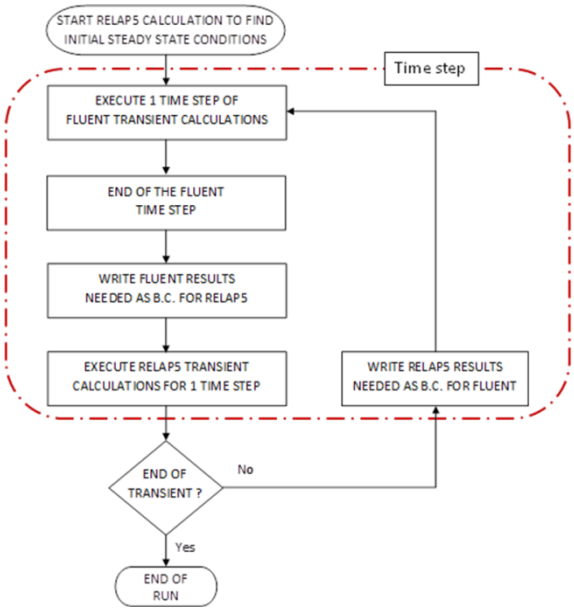

Figure 109: Explicit Coupling scheme

3.6. Sensitivity analyses

In order to verify the behaviour of the developed coupling tool, a sensitivity analysis is performed. It must be noted that these analyses were done before the modifications related to the LBE properties in the RELAP5/mod3.3 code. The basic simulations considered are two under natural circulation conditions (NC), with a heating power of 10 and 20 kW, and three under assisted circulation conditions (FC), with an injected gas flow rate of 5, 10 and 20 Nl/min respectively. The 2D-CFD computational domain is used for limiting the computational time. For NC-Tests the heating power is increased linearly in the first 30 s of the transient and then is maintained constant in the remaining transient, while for FC-Tests, the argon mass flow rate injected in the riser is increased linearly in the first 30 s of the transient and then is maintained constant in the remaining transient.

A first sensitivity analysis has shown that assisted circulation tests require a time step one order of magnitude lower than for natural circulation tests in order to guarantee the convergence of the simulation. This choice is essentially due to the higher velocity of the flow field for the FC-Tests. In particular, for the natural circulation tests a value of 0.1 s has been found sufficiently low to give results independent from the time step value itself, while a value of 0.01 s was found acceptable for the assisted circulation tests. Anyway, to verify the time step independence, three additional tests have been added in the matrix of simulations with higher and lower time step values compared to those used in the reference calculations. A further simulation regarding an Unprotected Loss Of Flow (ULOF) accident with the shut-down of the gas injection into the riser while the HS and HX are activated, is also performed. The test matrix of the performed coupled simulations is shown in Table 11.

Table 11: Test Matrix

Test name	Thermal power [kW]	Argon flow rate [Nl/min]	Time step [s]	Description	Monitoring variables
A	10	-	0.1	Natural circulation	• LBE flow rate • T_{in} and T_{out} in the HS • T_{in} and T_{out} in the HX primary side
B	20	-	0.1		
C	20	-	0.2		Check of the time step independence for the obtained results
D	-	5	0.01	Assisted circulation (gas injection)	• LBE flow rate
E	-	10	0.01		
F	-	20	0.01		
G	-	20	0.02		Check of the time step independence for the obtained results
H	-	20	0.005		
I	20	20	0.02	Unprotected loss of flow accident	• LBE flow rate • T_{in} and T_{out} in the HS • T_{in} and T_{out} in the HX primary side

3.6.1. Natural circulation

The LBE mass flow rate time trends obtained from the two natural circulation tests simulated by the coupled codes are reported in Figure 110, where results are compared with those obtained by RELAP5 stand-alone calculations. LBE mass flow rate steady state conditions are reached before 4000 s, obtaining an asymptotic value of about 1.5 kg/s for the Test *A* (thermal power of 10 kW) and 1.9 kg/s for the Test *B* (thermal power of 20 kW). Good agreement is found between RELAP5 stand-alone and coupled calculations, with differences of about 2-3%.

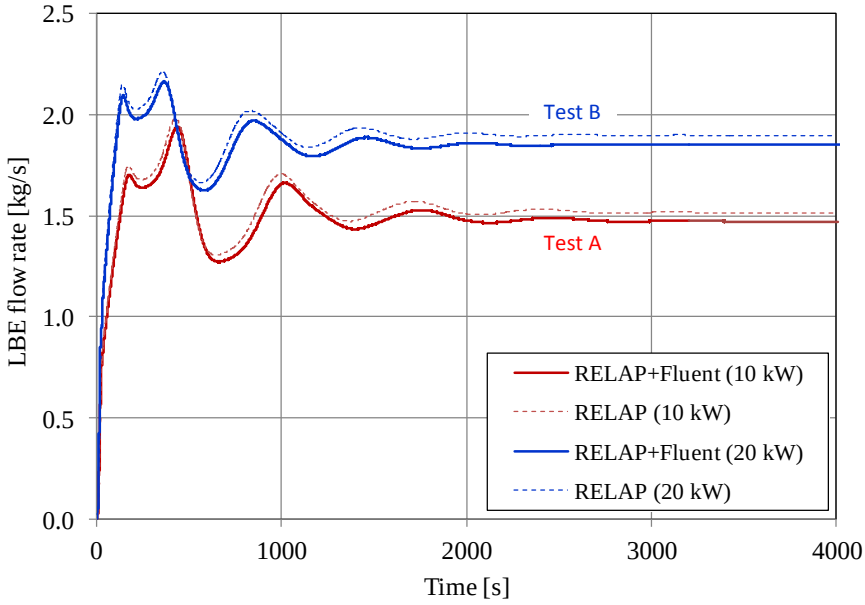

Figure 110: LBE mass flow rate time trend

Concerning temperature distribution along the loop after 4000 s, steady state conditions are not yet reached for Test *A* (Figure 111 and Figure 112). Nevertheless, good agreement is found between RELAP5 and coupled RELAP5-Fluent results for HS and HX temperature time trends. Concerning Test *B*, with higher thermal power, steady state conditions are achieved also for the temperature time trends (Figure 113and Figure 114). The first temperature peak of 370°C for Test *A* (Figure 111) and of 414°C for Test *B* (Figure 113) is due to the mechanical inertia of the liquid metal combined with the heat flux imposed in the HS. The fluid requires a sufficient driving force due to the buoyancy effect to start moving and this creates in the first instant of the transient a heating of LBE that remains at rest inside the HS section.

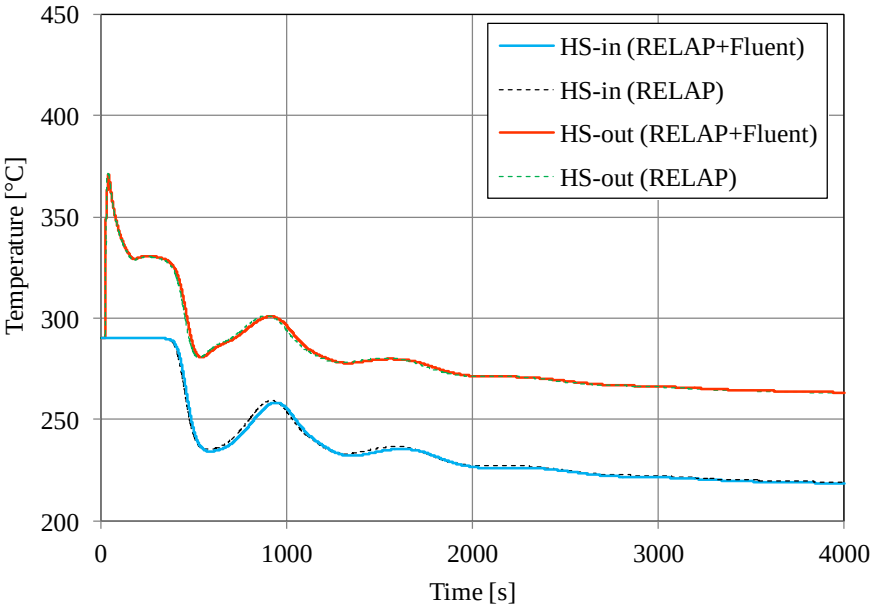

Figure 111: Inlet and outlet time temperature trend in the HS for Test *A* (10 kW)

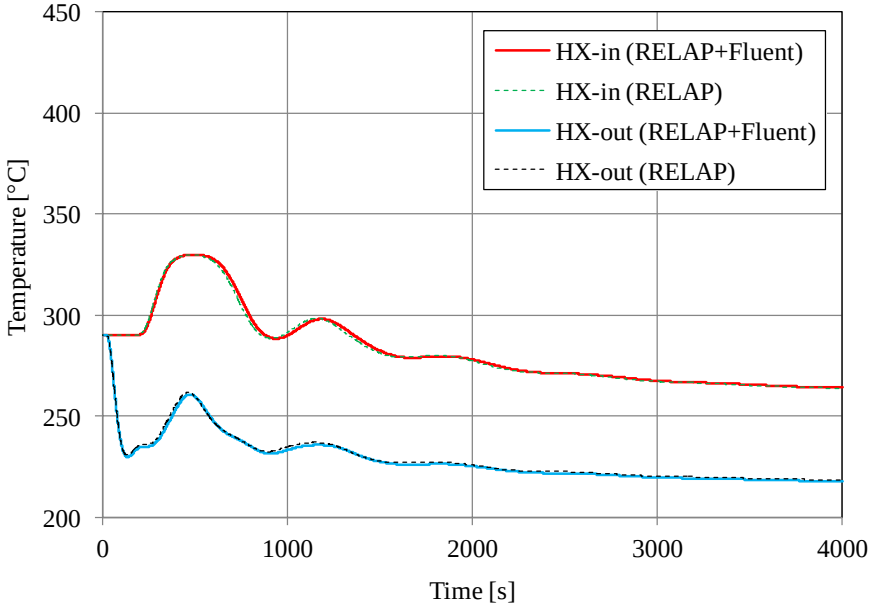

Figure 112: Inlet and outlet time temperature trend in the HX for Test *A* (10 kW)

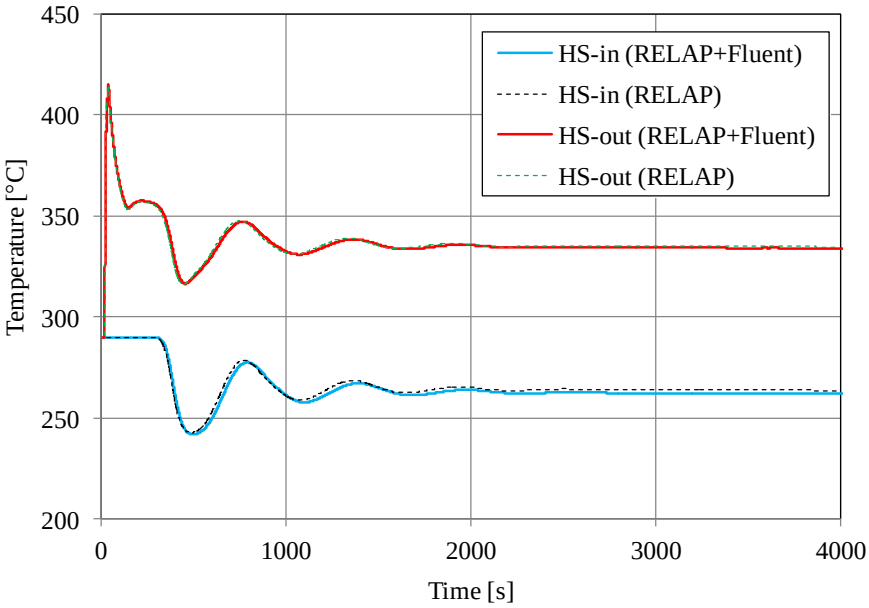

Figure 113: Inlet and outlet time temperature trend in the HS for Test *B* (20 kW)

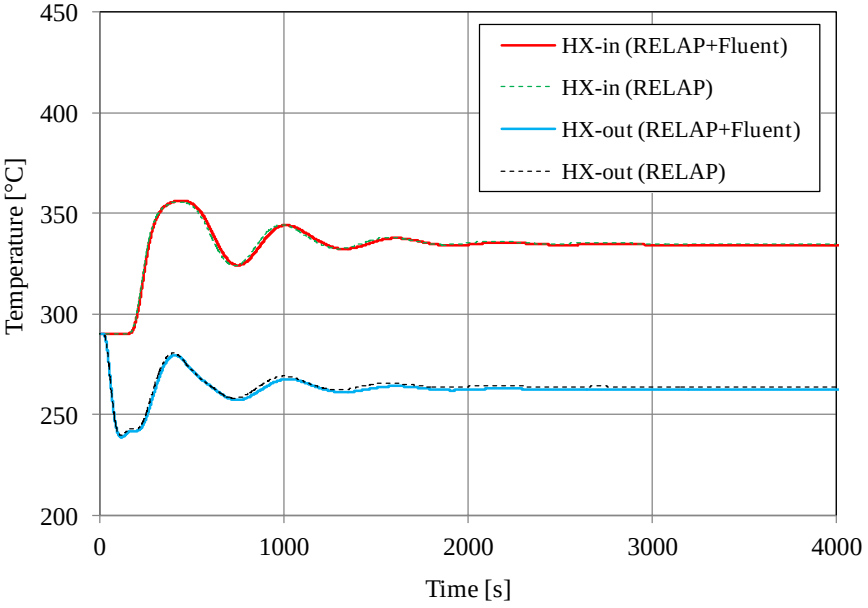

Figure 114: Inlet and outlet time temperature trend in the HX for Test *B* (20 kW)

Figure 115 shows the temperature distribution in the 2D CFD domain of the HS for Test *B* at 40 s (corresponding to the time of the peak in the temperature in the HS). The maximum temperature reached near the heated wall is in the order of 470°C.

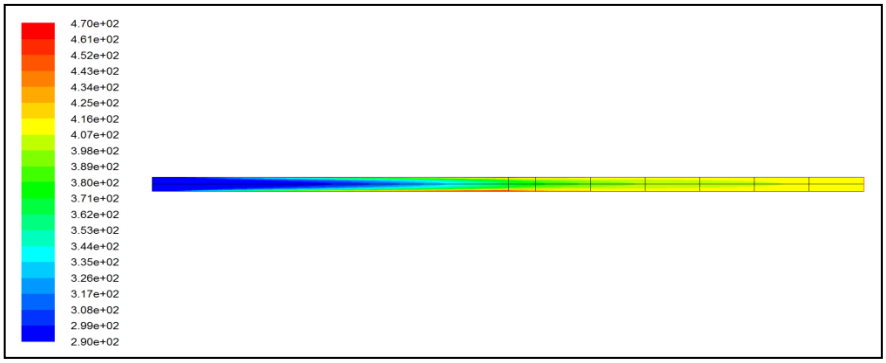

Figure 115: Temperature contour plot [°C] at 40 s of transient (Test *B*)

Figure 116 and Figure 117 show the LBE mass flow rate and the HS temperatures obtained for different time step values in order to verify the time step independence of the results obtained with the coupled codes (Test *B* and Test *C*). Perfect agreement between the corresponding time trends can be observed.

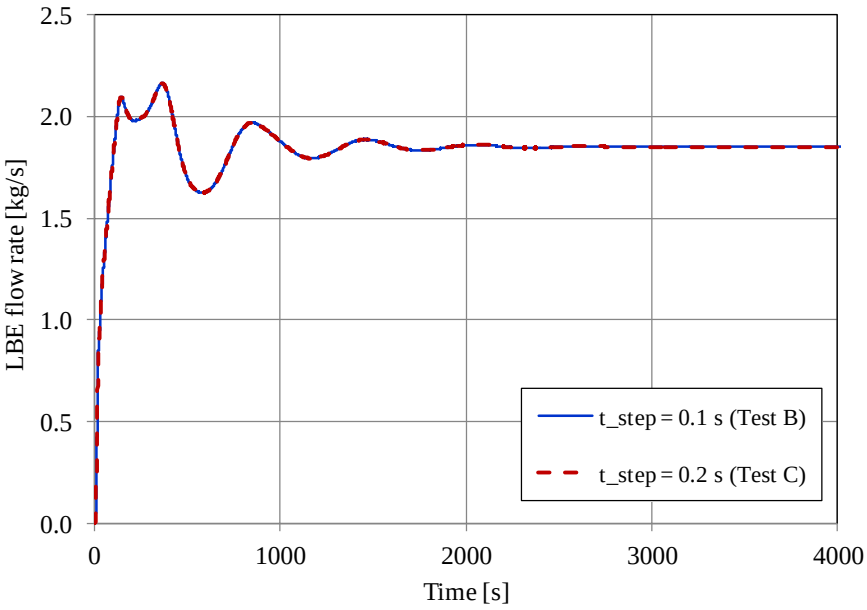

Figure 116: LBE mass flow rate time trend for two different time step values

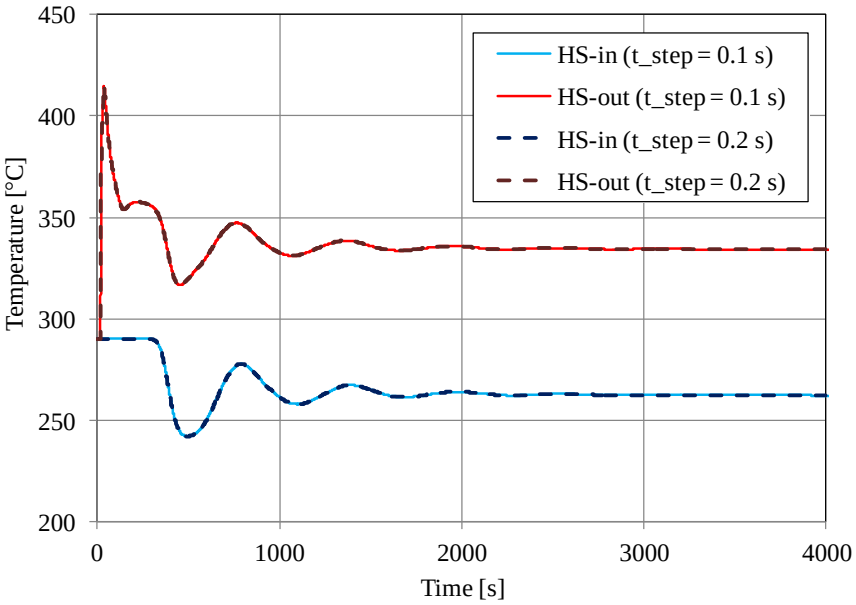

Figure 117: Inlet and outlet time temperature trend in the *HS* for two different time step values

3.6.2. Assisted circulation tests

The LBE mass flow rate time trends obtained from the three gas-injection circulation tests simulated by the coupled codes are reported in Figure 118, where the results are compared with those obtained from the corresponding simulations performed with the stand-alone RELAP5 code. Differences are essentially due to different ways to compute pressure losses in RELAP5 and in Ansys Fluent. The RELAP5 is developed based on one dimensional lumped parameter models and requires user input for singular losses, while uses the Darcy-Weisbach equation to take into account distributed losses. The Fluent code is instead a mechanistic computational fluid dynamics code. In particular, singular losses are directly computed by the code with the exception of those parts (e.g. the spacer grids) not geometrically simulated and whose effect is accounted by the use of porous jump model. Moreover, if the enhanced wall treatment option is used, as the Near-Wall Treatment, then the wall roughness parameters are not applicable and smooth walls are considered.

The average velocity reached inside the HS channel in steady state conditions for Test F is about 0.7 m/s. The velocity magnitude distribution inside the 2D domain at the end of the analysed transient is reported from Figure 119 to Figure 122. The maximum velocity predicted by the CFD code inside the channel is about 0.8 m/s and is reached at about half length of the domain. In Figure 122, the distribution of the turbulence kinetic energy is instead reported. From this figure, it can be seen as turbulence, considered as uniform at the inlet section, develops along the channel. The LBE mass flow rate obtained for two different time step (0.01 s (Test *F*), 0.02 s (Test *G*) and 0.005 s (Test *H*)) are compared in Figure 123 and Figure 124. The time step independence of the results obtained with the coupled codes is verified.

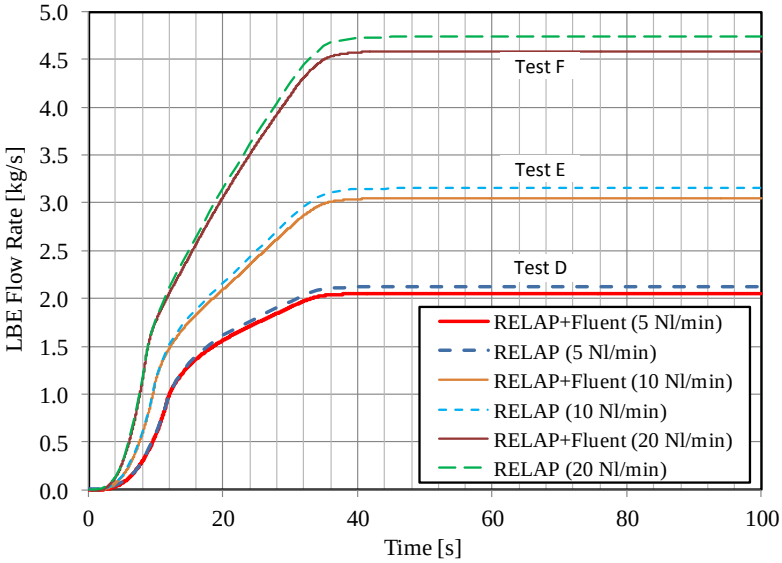

Figure 118: LBE mass flow rate time trend

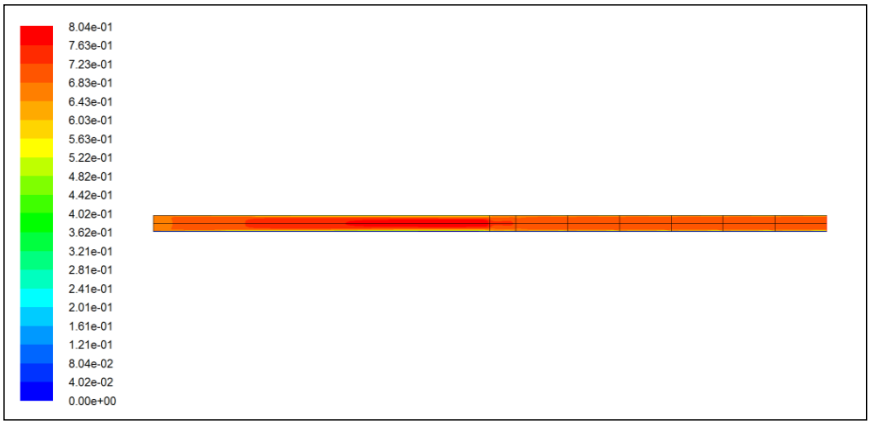

Figure 119: Velocity magnitude contour plot [m/s] at the end of the analysed transient (Test *F*)

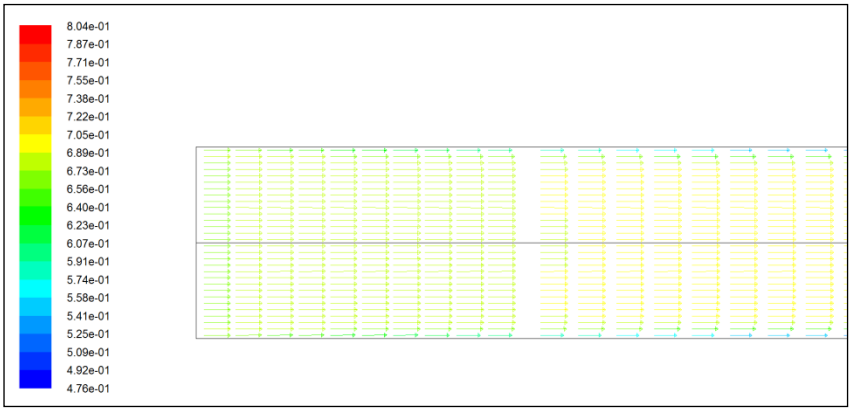

Figure 120: Velocity vector distribution near the inlet section, at the end of analysed transient (Test *F*)

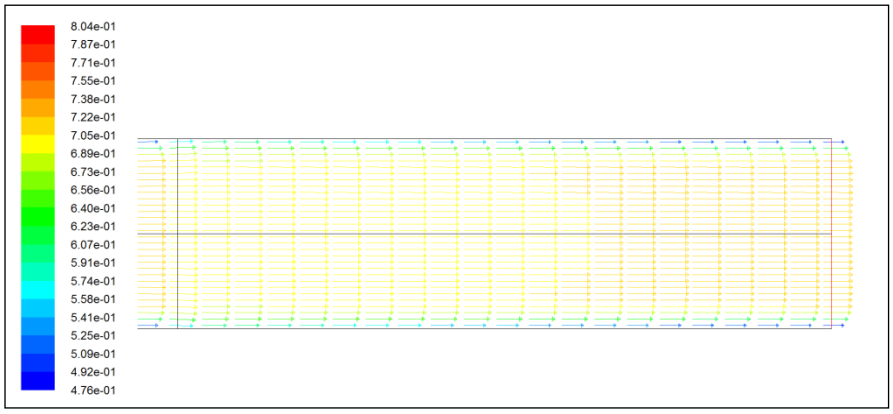

Figure 121: Velocity vector distribution near the outlet section, at the end of analysed transient (Test *F*)

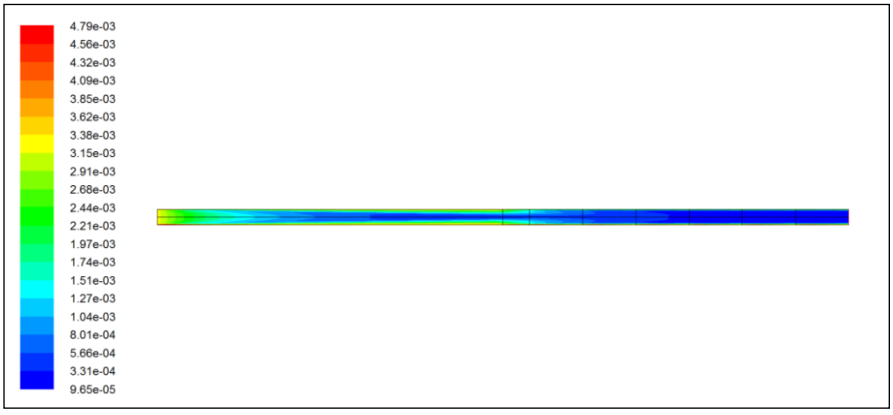

Figure 122: Turbulence kinetic energy [m^2/s^2] contour plot at the end of analysed transient (Test *F*)

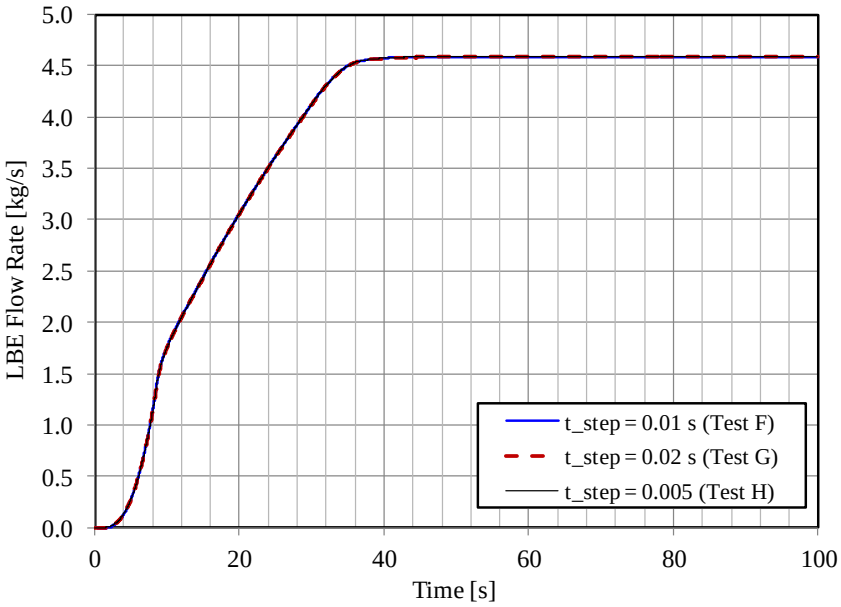

Figure 123: LBE mass flow rate time trend for three different time step values

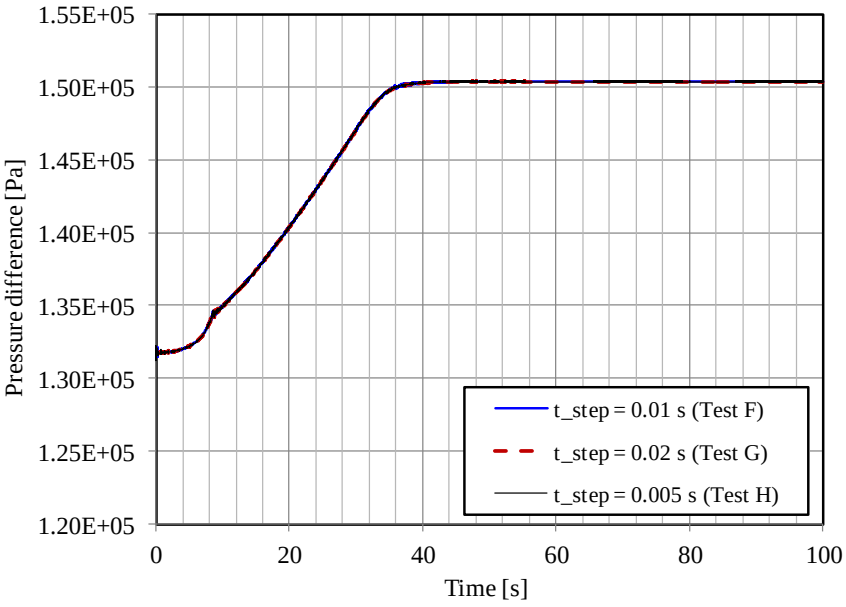

Figure 124: HS pressure drop for three different time step values

3.6.3. ULOF test

The ULOF accident transient (Test *I*) is of fundamental interest for the safety of HLM reactors. It represents the transition from forced to natural circulation conditions without the shutdown of the heater system. In Table 12, boundary conditions imposed in this test are

described with the related RELAP5 actions. The time step used to simulate this test with the coupled codes is 0.02 s.

Table 12: ULOF transient

Time [s]	Event	Description
0-30	Argon gas flow rate increase linearly from zero to 20 Nl/min; after 30 s its value remains constant up to ULOF event	***Starting phase**: achieving of the reference conditions*
50-80	Thermal power supplied through the HS increased linearly from zero to 20 kW; in the same interval, the water flow rate injected in the secondary side of the HX increases linearly. From 80 s to the end of the analysed transient, the value of the HS thermal power and of the HX water flow rate remains constant.	
200-210	Gas flow injection system switched off decreasing linearly its value in 10 s	***ULOF**: occurrence of initiating accidental event*
210-1000	The HS thermal power remains constant (20 kW), while HX is at operative set conditions.	***ULOF**: accident evolution*

As shown in Figure 125, the induced LBE mass flow reaches a value of about 4.6 kg/s for the asymptotic conditions with the only gas injection period and a value of about 5 kg/s in the phase of both gas injection and heating/cooling. After the argon injection shutdown the LBE mass flow rate reduces to a value of about 2 kg/s. This time trend agrees quite well with that obtained from the simulation performed by the RELAP5 stand-alone code. The LBE temperature results obtained with the coupled codes for both the heated section and the heat exchanger present an adequate agreement with those obtained by the RELAP5 stand-alone code (see Figure 126 and Figure 127), once again confirming the suitability of the set-up numerical scheme for coupled code calculations.

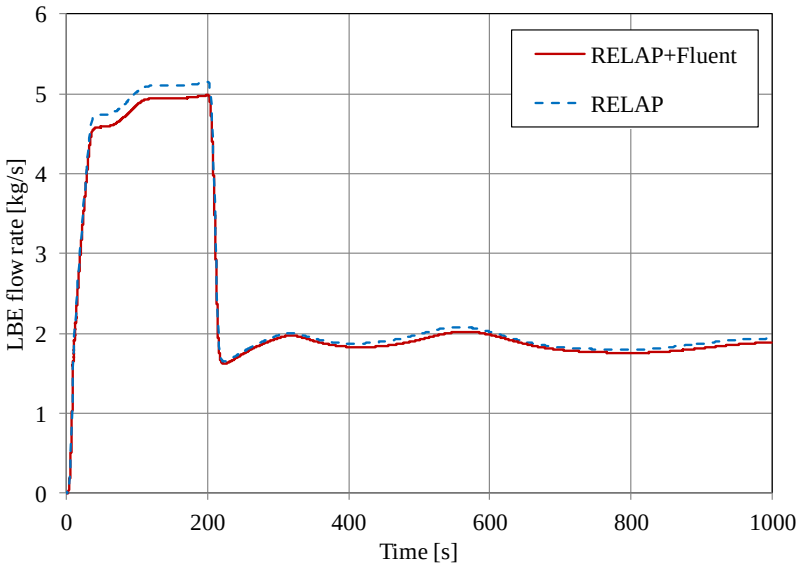

Figure 125: LBE mass flow rate time trend for Test I (ULOF)

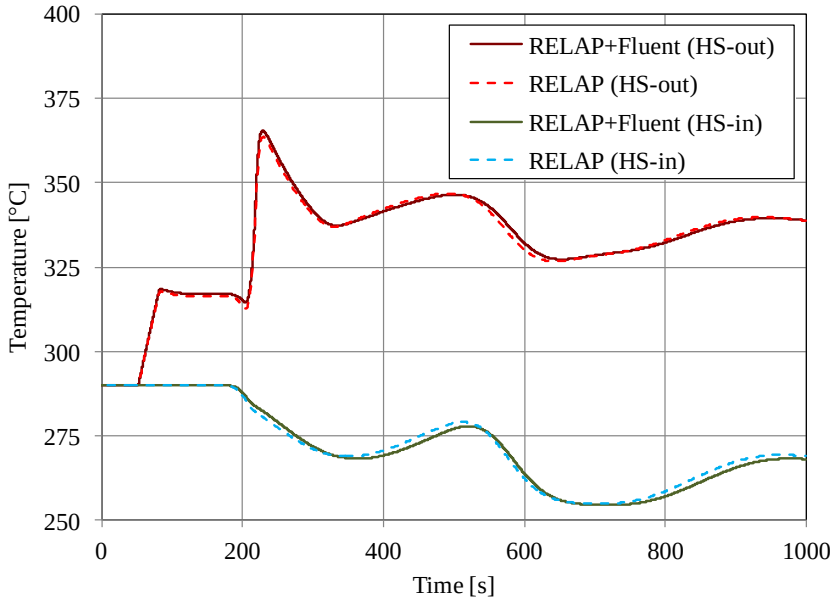

Figure 126: Inlet and outlet HS temperature time trends for Test *I* (ULOF)

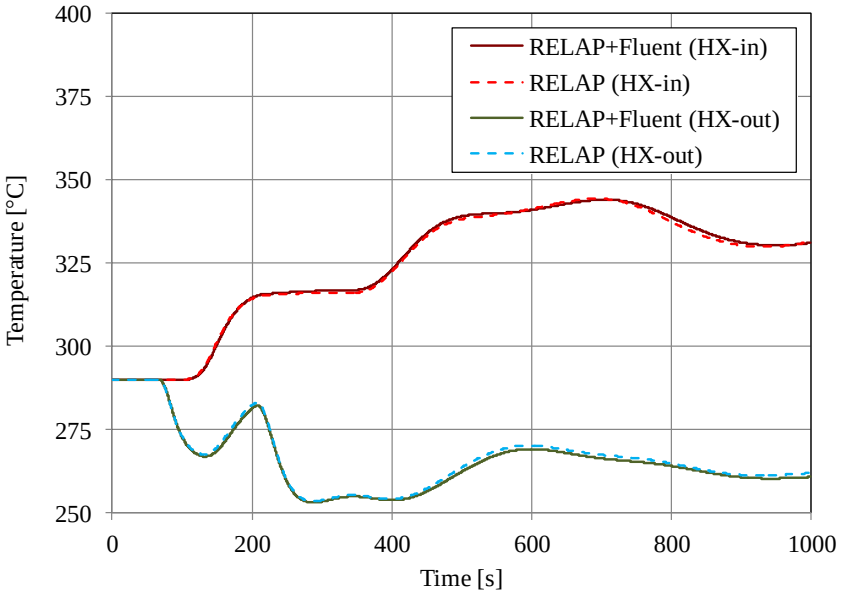

Figure 127: Inlet and outlet HX temperature time trends for Test *I* (ULOF)

3.7. Post-test analyses

3.7.1. Validation of RELAP5 stand-alone computer model

In the following, the developed RELAP5 computer model of the NACIE facility is validated through a post-test simulation of an experimental test named Test 303, designed to reproduce an Unprotected Loss of Flow (ULOF) like scenario. Table 13 summarizes the sequence of events characterizing the test.

Table 13: Test 303

	Time [h]	Action	Description
t_0	0.0	Test starts	*LBE* loop at rest. Initial temperature = 284°C
t_1	1.28	Argon on	Activation of argon injection. Set flow = 5 Nl/min.
t_2	1.78	*FPS* on	Heat power supplied to fuel pin simulator. Mean power = 21.5 kW
t_3	1.86	*HX* on	Activation of Heat Exchanger. Secondary water supply = 0.42 m^3/h
t_4	5.85	Argon off	***ULOF*** event. Argon injection Shut off
t_5	7.60	*FPS* and *HX* off	Deactivation of heat power supply to *FPS* and feedwater to *HX*

In Figure 128 and Figure 129, boundary condition time trends set in RELAP5 input deck are compared with experimental data. The electric power supplied during Test 301 to the pin simulator is plotted, as a function of time, in Figure 128 together with heating power set in RELAP5 input deck. Electrical heating starts at t=1.78 h, increasing linearly to the value of 21 kW in about 2 minutes. Afterwards, the power profile shows a non-constant trend especially in the first 2 h from FPS activation. Power supply stops at t=7.6 h. Figure 129 shows the HX water mass flow rate as a function of time (experimentally measured by flow meter MP201) and imposed as boundary condition for the secondary water loop, (see TmdpJun-505, Figure 103). The HX is activated at t=1.86 h and operates until t=7.6 h. The feed water is injected after the FPS activation and stops when the FPS power is shut off. Inlet water mass flow rate is approximately equal to 0.12 kg/s.

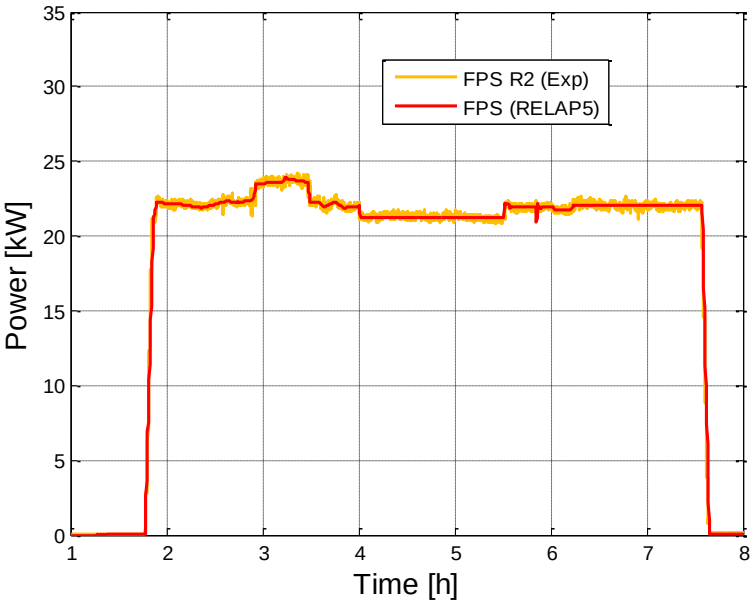

Figure 128: Electrical power supplied to FPS

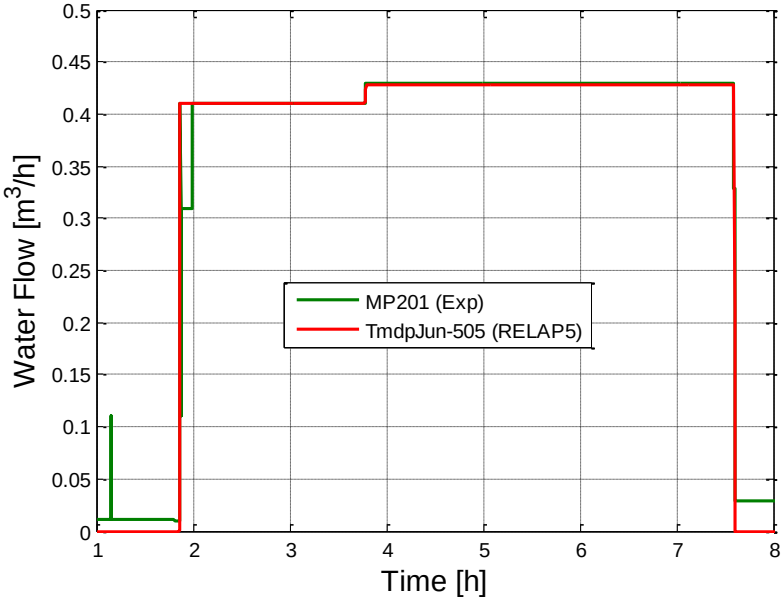

Figure 129: Water Flow imposed as b.c. in RELAP5

The argon flow rate is experimentally measured by a gas flow meter (F101) and adopted in RELAP5 simulation as reference for the gas mass flow rate provided by *TmdpJun-405* (constant value of 5 Nl/min). LBE starts to circulate as argon injection starts (enhanced circulation); then, to simulate an Unprotected Loss of Flow (ULOF) accident, argon injection is deactivated (t=5.85 h) and the flow is then solely driven by buoyancy phenomena (natural circulation).

During the enhanced circulation regime, the measured mass flow rate (Figure 130) reaches a mean value of about 13 kg/s characterized by oscillating behaviour mainly due to the argon injection compressor system, while a heat balance gives a slightly lower value of about 12 kg/s, very close to the value estimated by the RELAP5 code. Afterwards, in natural circulation regime, the mass flow rate drops to about 5 kg/s and good agreement can be observed between experimental data and RELAP5 results. After deactivation of FPS and HX at t=7.6 h, the flow slowly decreases to zero. LBE temperature trends related to FPS inlet and outlet sections are plotted in Figure 131; experimental values, provided by thermocouples *T109* (inlet) and *T105* (outlet), are compared to RELAP5 results showing good agreement. RELAP5 initial LBE temperature has been set to 284°C for the whole loop assumed adiabatic until the FPS activation, to account for the external wire heaters employed in the experimental setup, which maintain the required LBE temperature. Afterwards, a heat transfer coefficient towards the environment has been imposed setting the external air temperature and heat transfer coefficient (accounting for the loop thermal insulation), respectively equal to 20°C and 1 W/m^{2}K. Following FPS and HX activation, temperatures start to increase up to a mean temperature of about 335°C (t=3.5 h), then temperature decreases reaching a near stationary condition (mean temperature of 320°C). It can be observed that the temperature trend reflects the power supply variation (see Figure 128 and Figure 131); accuracy in reproducing FPS experimental power trend in RELAP5 model is mandatory to obtain adequate temperatures trend from the code.

The ULOF event takes then place deactivating gas injection (t=5.85 h) and natural circulation establishes inside the loop. Inlet/outlet temperatures undergo a sudden decrease/increase of about 10°C followed by an ascending trend up to a new equilibrium value (after less than 2 h) of 320°C and 348°C respectively, achieving a stationary state for this new regime. FPS and HX are then shut off (at t=7.6 h) producing a decrease of temperatures due to loop heat losses. RELAP5 data adequately reproduces the temperature profile characterizing the test and the transition from forced to natural circulation regimes although slight discrepancies are observed mainly during ULOF transient phase. Figure 132 plots measured and simulated water inlet and outlet temperatures in the secondary side of the HX. Experimental water inlet temperature, *T201*, has been reproduced as a boundary condition in RELAP5 (in *TmdpVol-500*) during HX activation, from t=1.86 h to t=7.6 h; the simulated outlet temperature profile, in this time span, is in good agreement with the experimental water outlet temperature (*T202*).

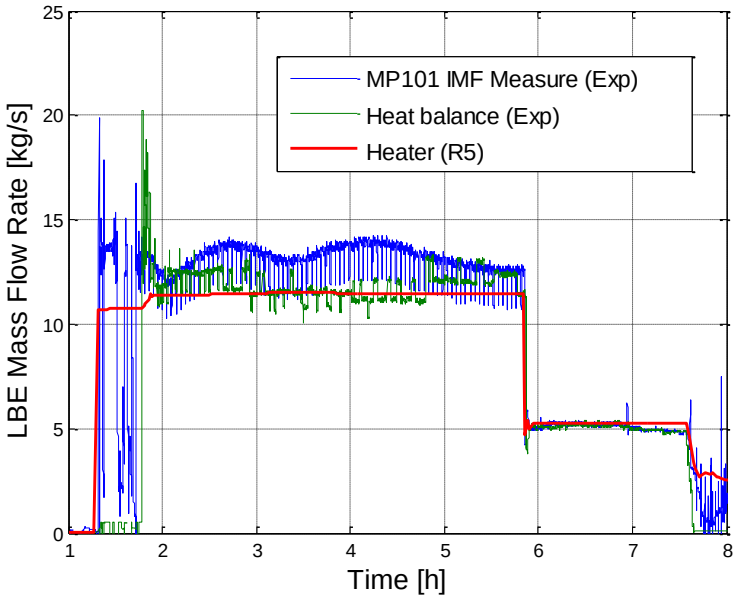

Figure 130: LBE mass flow rate measured by the Induction Magnetic Flow meter and derived by energy balance compared with RELAP5 results

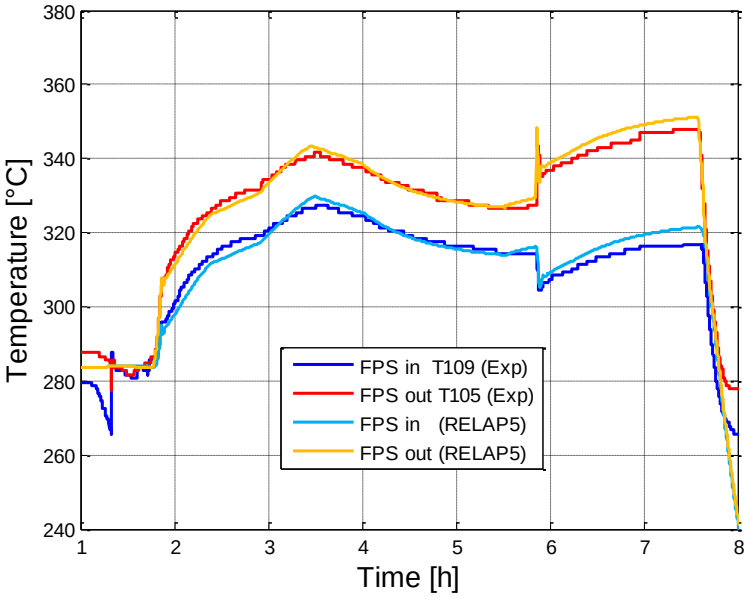

Figure 131: LBE temperatures at inlet/outlet sections of the FPS

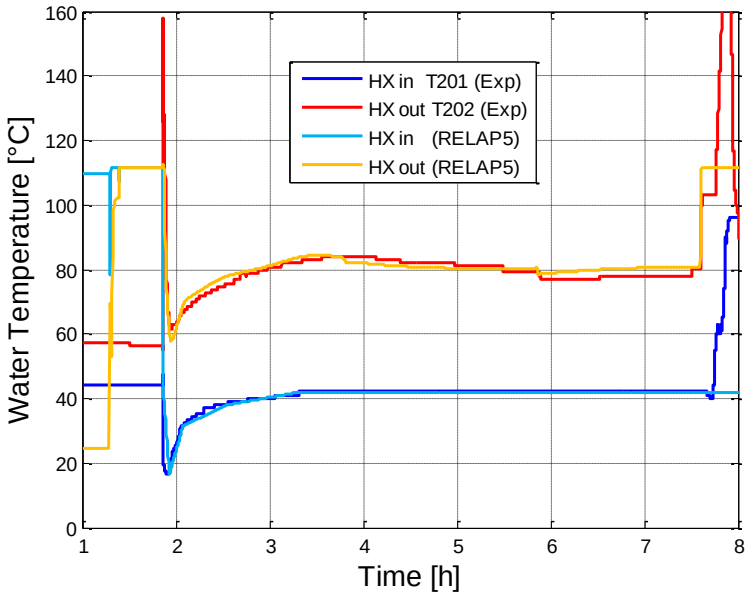

Figure 132: Water temperature at inlet/outlet sections of the HX

The convective heat transfer coefficients related to LBE flowing inside the FPS and the HX are evaluated from RELAP5 together with the value for the secondary water flowing in HX annular region. Results, plotted in Figure 133, report, for assisted circulation regime, values of about 5000 and 3700 W/(m^2 K) for FPS and HX respectively; these values reduce to 3400 and 2400 W/(m^2 K) for the natural circulation regime. For secondary water, a value of 1500 W/(m^2 K) is obtained; a peak is observed at the HX activation due to the initial rapid vaporization of injected feed water. The Heat Exchanger double wall (see Figure 99) separating the descending LBE from ascending water is modelled in RELAP5 by means of three consecutive cylindrical layers representing the inner tube wall (W_1), the powder gap (GAP) and middle tube wall (W_2), each subdivided in six mesh intervals. The two walls are made of AISI 304, while the gap consists of a stainless steel powder for which thermal conductivity is assumed 12.5% of AISI 304 (Coccoluto et al., 2011).

Figure 134 shows the temperature profile along the double wall structure (at HX mid-plane) together with the fluids bulk temperatures. A comparison between assisted and natural circulation shows an overlapping of temperature profiles except for the LBE side bulk temperature, which increases due to the lower heat transfer coefficient associated with the natural circulation regime. The powder gap (5.8 mm) represents the major contribution to the thermal resistance with a temperature drop of about 180°C versus 25°C for the two walls (W_1 and W_2), pointing out the importance of reliably defining the thermal properties of the stainless steel powder gap for the accuracy of model results.

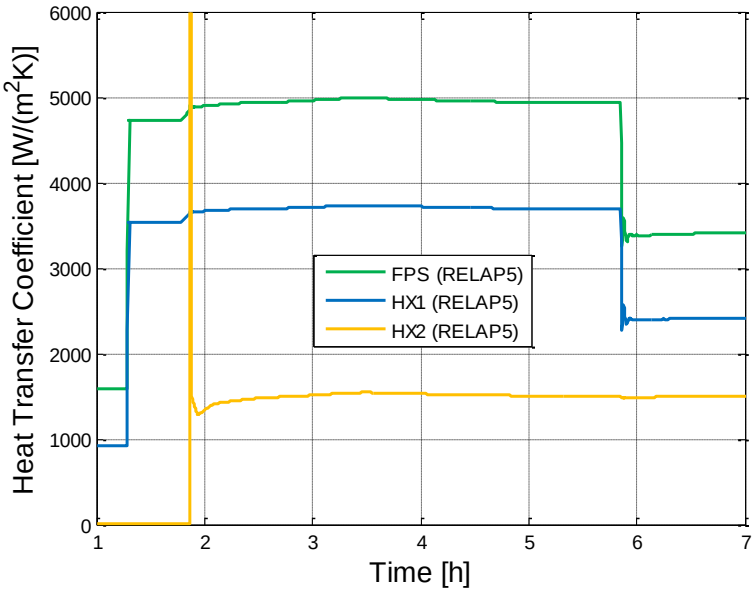

Figure 133: RELAP5 HTC for LBE in FPS, HX primary side and water in HX secondary side

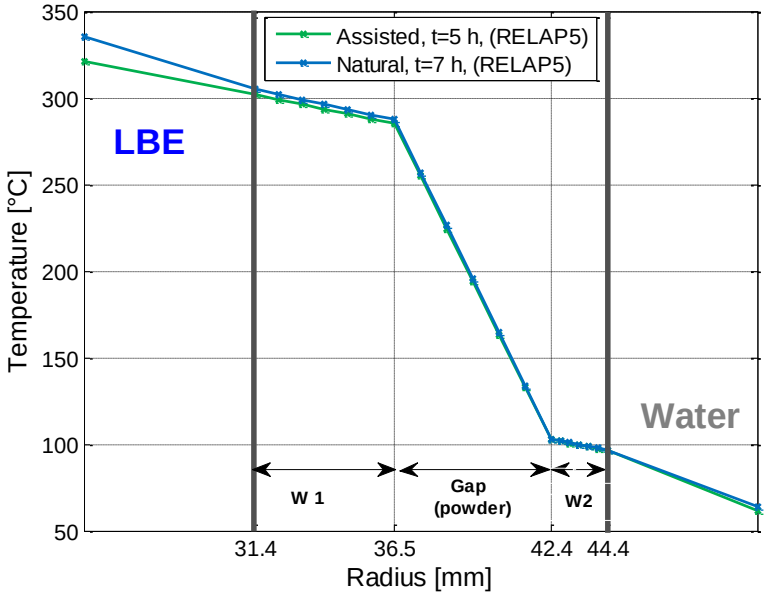

Figure 134: Temperature profile in HX double wall

The available driving force, during the assisted circulation phase, is calculated using RELAP5 data as follows:

$$\Delta P_{DF} = \Delta\rho \cdot g \cdot H_r \tag{6}$$

where H_r is the riser height, set to 5.4 m, g is the gravity acceleration and $\Delta\rho$ is defined as:

$$\Delta\rho = \bar{\rho}_{LBE} - \rho_{r,TP} \tag{7}$$

and where $\bar{\rho}_{LBE}$ and $\rho_{r,TP}$ are LBE mean density and two phase fluid mean density inside the riser respectively. The obtained driving force (ΔP_{DF}) for the assisted circulation phase, is plotted in Figure 135, together with the mean riser void fraction, showing respectively values around 90 mbar and 1.65%.

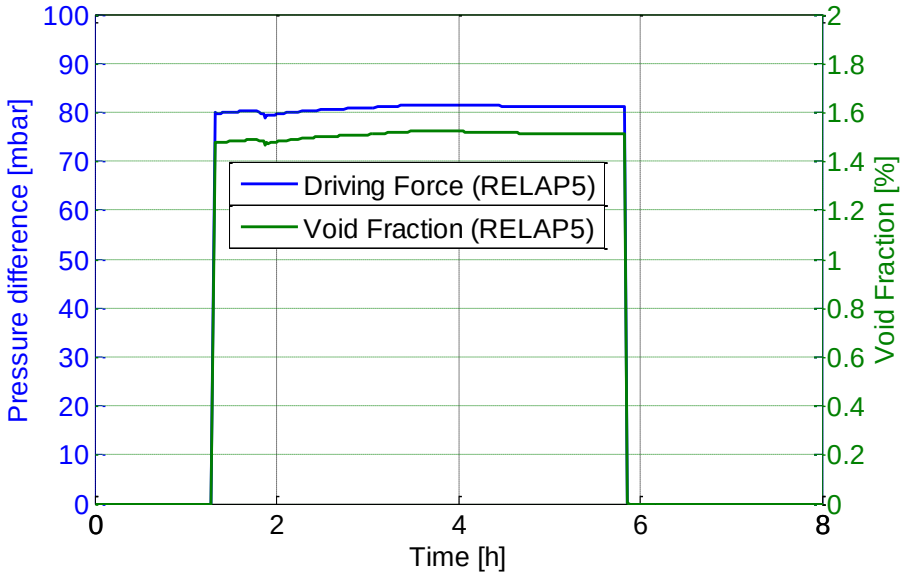

Figure 135: Driving force and void fraction in the riser

3.7.2. RELAP5-Fluent coupled simulations (explicit scheme)

The performed simulations are representative of two gas enhanced circulation tests and of a natural circulation test. The experiments carried out in the NACIE loop and chosen as a reference tests for numerical simulations are Test 206, Test 301 and Test 306. A total of seven simulations were performed, three for Test 206 three for Test 306 and two for Test 301. In particular, a RELAP5 stand-alone simulation, a coupled simulation using a Fluent 2D axis symmetric domain and a coupled simulation using a Fluent 3D symmetric domain were carried out for Test 206 and 306, while for Test 301 a RELAP5 stand-alone simulation and a coupled simulation using a Fluent 2D axis symmetric domain were performed. The test matrix of the experimental tests chosen as representative cases for the numerical simulations is shown in Table 14 reporting the adopted boundary conditions.

Table 14: Test matrix

Name	T_{av} [°C]	*FPS* Power %	G_lift [Nl/min]	Monitored variables
Test 206	200-250	0	2,4,5,6,8,10, 8,6,5,4,2	*LBE* flow rate and Temperature
Test 306	300-350	0	2,4,5,6,8,10, 8,6,5,4,2	
Test 301	250-300	100%	0	

In Test 206 and 306, the argon mass flow rate injected in the riser is increased linearly in the first 5 seconds of the transient for each step and then maintained constant according to the experimental time-tables for Test 206 (Table 15) and for Test 306 (Table 16).

Table 15: Argon flow rate time schedule (Test 206)

Time [h]	Argon flow rate [Nl/min]	Time [h]	Argon flow rate [Nl/min]
0-1.13	0	5.43-5.72	8
1.13-1.91	2	5.72-6.05	6
1.91-2.18	4	6.05-6.50	5
2.18-2.45	5	6.50-6.76	4
2.45-2.73	6	6.76-7.14	2
2.73-3.03	8	7.14-7.5	0
3.03-5.43	10		

Table 16: Argon flow rate time schedule (Test 306)

Time [h]	Argon flow rate [Nl/min]	Time [h]	Argon flow rate [Nl/min]
0-1.77	0	5.10-5.42	8
1.77-2.10	2	5.42-5.74	6
2.10-2.36	4	5.74-6.01	5
2.36-2.62	5	6.01-6.27	4
2.62-2.89	6	6.27-6.79	2
2.89-3.15	8	6.79-7.5	0
3.15-5.10	10		

The performed preliminary sensitivity analysis showed that the time step needed to assure the convergence and independency of the results from the adopted time step is in the order of 0.005 s. Transient simulations with fixed time step have been carried out for an overall simulated transient of 27000 s. The following section, describes the obtained results of coupled RELAP5-Fluent simulations for simulations carried out adopting the explicit coupling scheme (Figure 109).

Test 301, representative of a natural circulation test, is conducted with only one pin activated in the heating section, with a nominal power of 21.5 kW. At the beginning of the experiment the average temperature of the LBE in the loop is about 250-300 °C. The heating power increased linearly in the first 262 s of the transient and then it is maintained constant for the remaining of the transient. After the activation of the fuel bundle, the water secondary system was also activated.

3.7.2.1. Forced circulation tests

The LBE mass flow rate is evaluated in *TmdpJun-115* at the outlet section of the NACIE FPS (see Figure 104) and results are compared against experimental data, measured by the prototypical inductive flow meter (MP101, see Figure 101) and with RELAP5 stand-alone results.

After the argon gas injection activation, the LBE mass flow rate increases to a value of about 7.7 kg/s (argon flow rate equal to 2 Nl/min) and steady state conditions are reached in few minutes. The argon flow rate is maintained constant for about half an hour and then it is increased to 4 Nl/min; as a consequence, LBE mass flow rate increased to about 9.2 kg/s. Similarly, subsequent increases of argon flow rate have been considered (5-6-8-10 Nl/min) and in correspondence with a value of 10 Nl/min the obtained LBE mass flow rate is about 13-14 kg/s.

In the second part of the test, gas injection is decreased symmetrically with respect to the increasing ramp. Compared to the experimental data, the calculated LBE mass flow rate overestimates them by less than 12%. Good agreement is found between the coupled code simulations with a 2D and 3D CFD domain, while the results of the coupled code simulations overestimate results obtained from the stand-alone RELAP5 by less than 5%. This difference is essentially due to differences between RELAP5 and Ansys Fluent in evaluating pressure losses. As well known, RELAP5 is developed based on one dimensional lumped parameter models and requires user input for singular losses, while uses the Darcy-Weisbach equation to take into account distributed losses. The Fluent code is instead a mechanistic computational fluid dynamics code. In particular, singular losses are directly computed by the code with the exception of those parts (e.g. the spacer grids) not geometrically simulated and whose effect is accounted by the use of porous jump model. Moreover, if the enhanced wall treatment option is used, as the Near-Wall Treatment, then the wall roughness parameters are not applicable and smooth walls are considered.

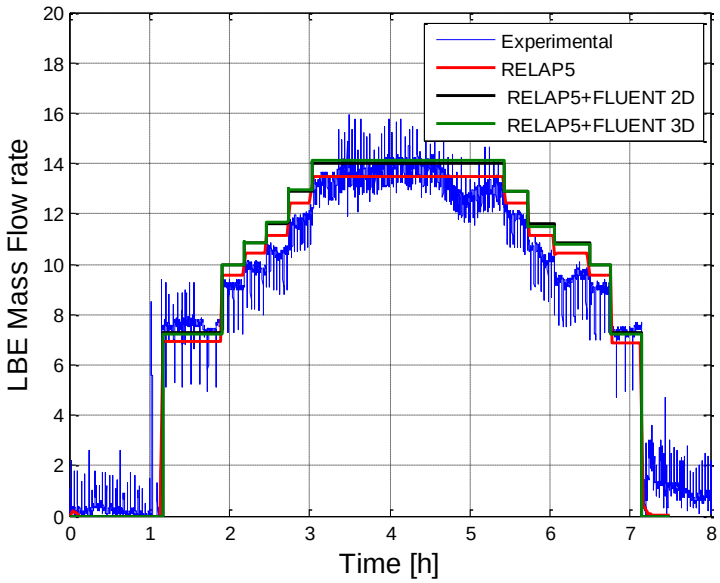

Figure 136: LBE mass flow rate (Test 206)

Oscillations in the mass flow rate measured by the inductive flow meter are generated by perturbations in the argon mass flow rate due to the specific design of the ancillary gas pumping system. Figure 137 shows a detail of such an oscillation. It can be observed that the inductive flow meter (MP101) follows correctly the periodic oscillation of the gas injection, which affects the pressure head of the riser column and the mass flow rate oscillations. The mass flow rate calculated from the energy balance equation (temperature balance mass flow rate TBMFR) cannot follow such phenomena.

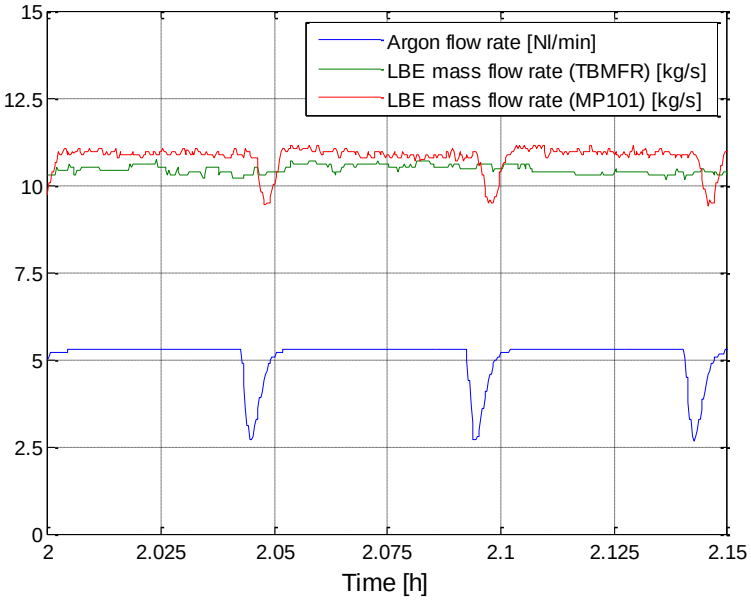

Figure 137: Detail of oscillations in gas flow rate
and subsequent LBE mass flow rate oscillation

Figure 138 shows the pressure difference between the FPS inlet and outlet sections evaluated from the numerical simulations. In particular, this value is obtained as difference between the volume pressure computed in the centroid of last element of *pipe-100* and the centroid of the first element of *pipe-120* (corresponding to the outlet section of the Fluent CFD domain). At the beginning of the simulated transient, with fluid at rest and isothermal conditions (constant temperature of 237°C), the pressure difference between the inlet and outlet sections of the FPS is about $1.12 \cdot 10^5$ Pa, which represents the pressure of the LBE fluid column that fills the FPS.

After the activation of the gas injection, the pressure difference between the FPS inlet and outlet sections increases (as the gas flow rate is increased) reaching a value of $1.16 \cdot 10^5$ Pa when the argon mass flow rate is 10 Nl/min. Discrepancies in the pressure difference (inlet/outlet section of the FPS) between stand-alone and coupled simulations are lower than 1%. Figure 139 shows the pressure time trend at the inlet and outlet sections of the FPS. Differences between pressures computed by coupled and RELAP5 stand-alone lower than 1%.

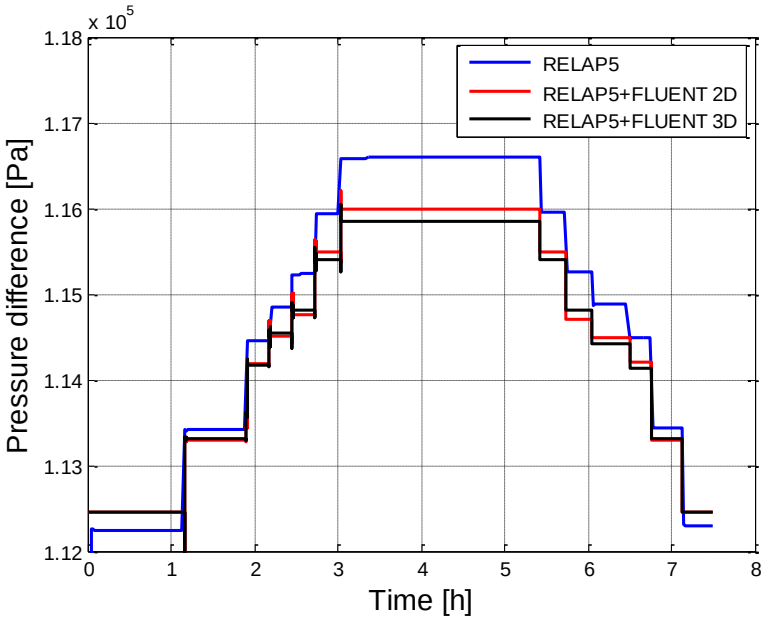

Figure 138: FPS inlet outlet pressure difference (Test 206)

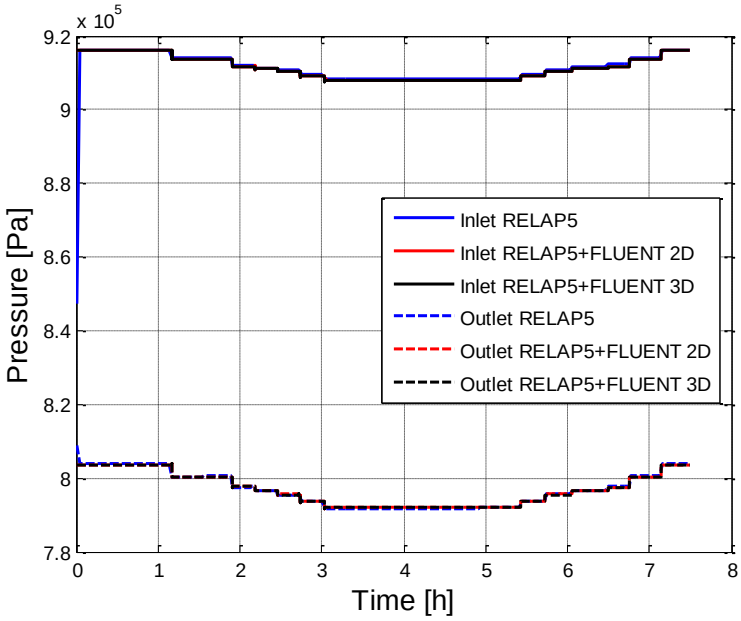

Figure 139: FPS inlet and outlet pressures (Test 206)

Figure 140 shows the vector velocity in the FPS region (*w*, along vertical (*z*) direction). The magnitude of *w* (area-weighted *z*-velocity) predicted by the *CFD* code at the outlet section of the 3D geometrical domain is about 0.88 m/s (t = 3.5 h argon flow rate 10 Nl/min). In Figure 141, the contour of the velocity field is shown. The Region between the exit of the pin bundle and the outlet section of the CFD domain is evidenced. It is important to set the outlet section of the CFD domain sufficiently far away from the outlet section of the active pin, not only in order to reduce the occurrence of reverse flow in the outlet section (the developed coupling procedure does not take into account reverse flow), but first of all in order to reduce the error introduced by averaging the outlet velocity given to the RELAP5 code as boundary condition.

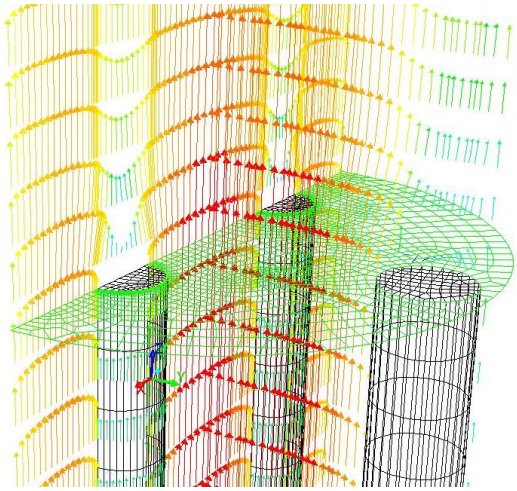

Figure 140: 3D CFD domain: vector velocity colored by z-velocity (Test 206)

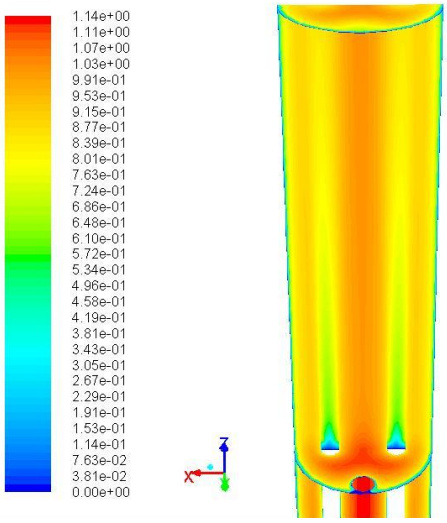

Figure 141: Velocity contour plot [m/s]

The experimental Test 306 is similar to Test 206, with differences in the initial temperature conditions and in the argon gas injection timing (see Table 14 and Table 16). Higher temperature implies lower LBE density, hence different pressure inside the loop. In particular, the decrease in LBE density implies appreciable changes in the LBE mass flow rate for the same amount of gas injection (gas-enhanced circulation).

Nevertheless, the simulation of Test 306 aimed at verifying the stability of the implemented coupled tool. In particular, main stability issues were found at the beginning of the coupled transient when the two codes start to exchange data and even small differences in the data exchanged produce oscillations of the main results (mainly in the pressure results). Figure 142 shows the LBE mass flow rate comparison between experimental and simulations results. Considerations similar to those for Test 206 also apply in this case. After the argon gas injection activation, the LBE mass flow rate increases according to the gas injection time-step trend reaching a value of about 14-15 kg/s in correspondence of an argon injection of 10 Nl/min.

In the second part of the test, the gas injection is again decreased symmetrically with respect to the forward ramp. The obtained numerical results (both RELA5 stand-alone and coupled results) generally overestimate experimental results by less than 12%. Good agreement is again found between the coupled code simulations (with a 2D and 3D CFD domain), while the results of the coupled code simulations overestimate results obtained from the stand-alone RELAP5 by less than 5%.

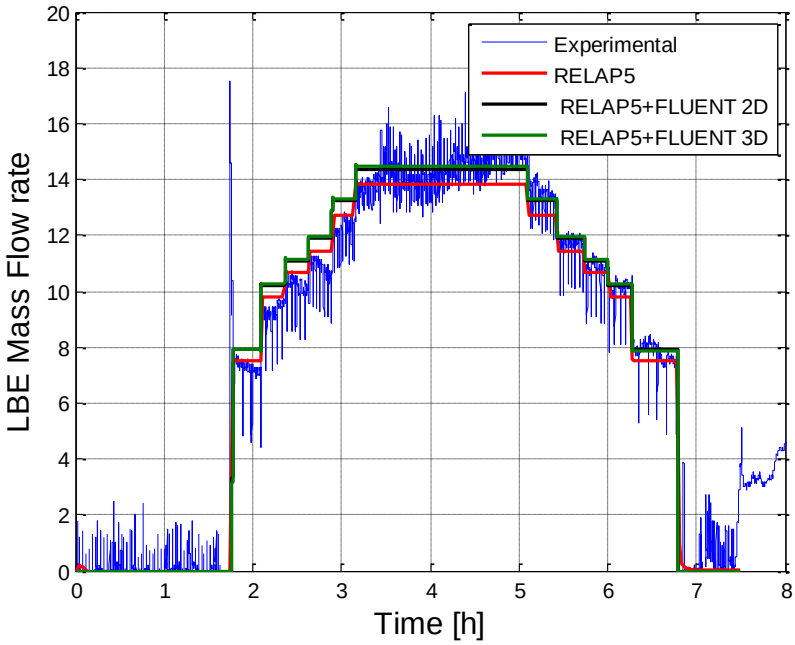

Figure 142: LBE mass flow rate (Test 306)

Differences between RELAP5 and RELAP5-Fluent coupled calculations, evidenced in the obtained mass flow rate time trends, are due to the higher pressure difference predicted between the inlet and outlet sections of the FPS, by the RELAP5 stand-alone calculation (Figure 143).

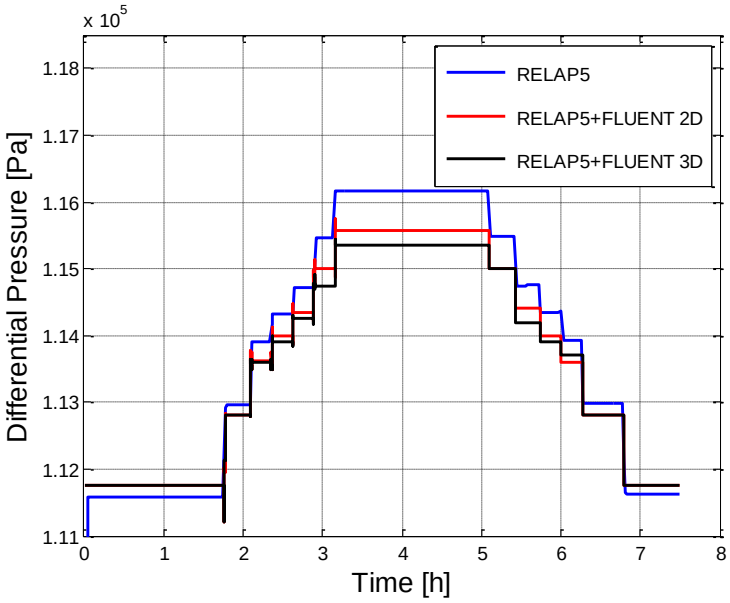

Figure 143: FPS inlet outlet pressure difference (Test 306)

3.7.2.2. Natural circulation test

The LBE mass flow rate time trend obtained from Test 301 simulated by the coupled methodology is reported in Figure 144, where the results are compared with those obtained by stand-alone RELAP5 simulation and with experimental data as well.

The inductive flow meter installed in the NACIE facility is accurate for high mass flow rate (8-20 kg/s) and the uncertainty of the measurements at low mass flow rates is due to the diameter of the pipe in which the inductive effect is measured, (i.e. 2.5″ diameter pipe). At low flow rate, the LBE velocity is not high enough to allow a good flow measurement; therefore, the experimental mass flow rate is evaluated by an energy balance equation. When the natural circulation starts the difference in temperature between the inlet and outlet section of the heater is small resulting in the high peak value obtained for the mass flow rate. The different behaviour observed at t=0.1 h can be related to the fact that the difference in temperature between the heater inlet and outlet sections has not reached a steady state condition, therefore the balance equation results, obtained for steady state, are not reliable for the first 0.1 h of the transient.

Results obtained from the RELAP5 stand-alone simulation and from the coupled simulation are practically overlapping. The mass flow rate predicted by the simulations at steady state condition is about 5.03 kg/s overestimating the mass flow rate obtained from the energy balance equation by less than 2%. Figure 145 shows the comparison between temperature measurements evaluated at the heater inlet and outlet section and experimental data. In particular, at the heater outlet section the peak temperature observed at t=0.09 h (324 s) is well predicted by RELAP5 and coupled simulations.

The temperature at the inlet of the heater, predicted by RELAP5 stand-alone and coupled simulations, starts to increase about 180 s earlier than the experimental data. This behaviour is due to the simplified temperature distribution imposed at the beginning of the simulation

as loop initial condition of the RELAP5 nodalization; in particular, the initial temperature trend in the REALP5 model is approximated according to the local experimental data along the loop. At the inlet section of the fuel pin bundle, numerical results tend generally to overestimate the experimental temperature by less than 2%.

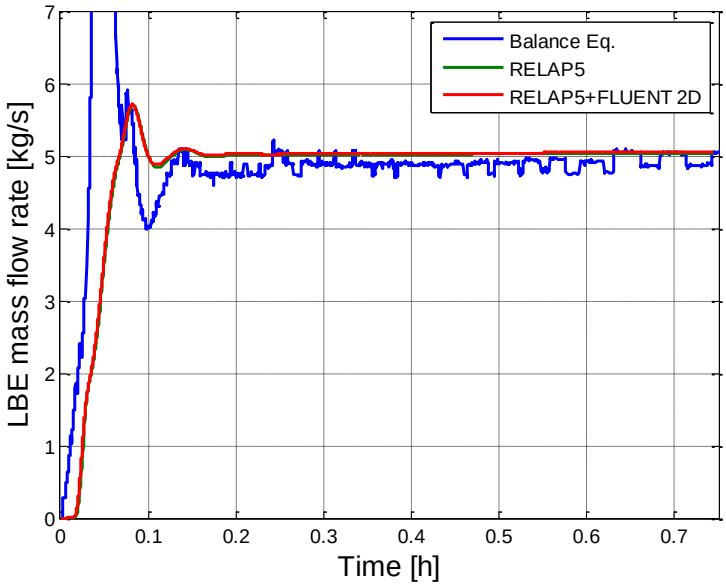

Figure 144: LBE mass flow rate (Test 301)

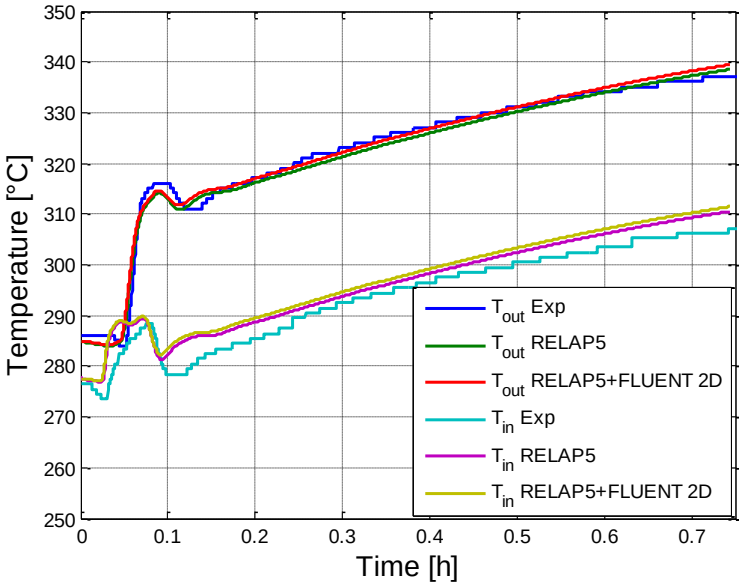

Figure 145: Temperature at the FPS inlet and outlet sections (Test 301)

Figure 146 shows temperature trends at the inlet and outlet sections of the heat exchanger for the primary LBE side. As already mentioned for the FPS inlet and outlet temperature, differences at the beginning of the transient are due to the simplified temperature distribution imposed at the beginning of the simulation as initial condition in the RELAP5 nodalization. The thermal power removed by the secondary water circuit is reported in Figure 147.

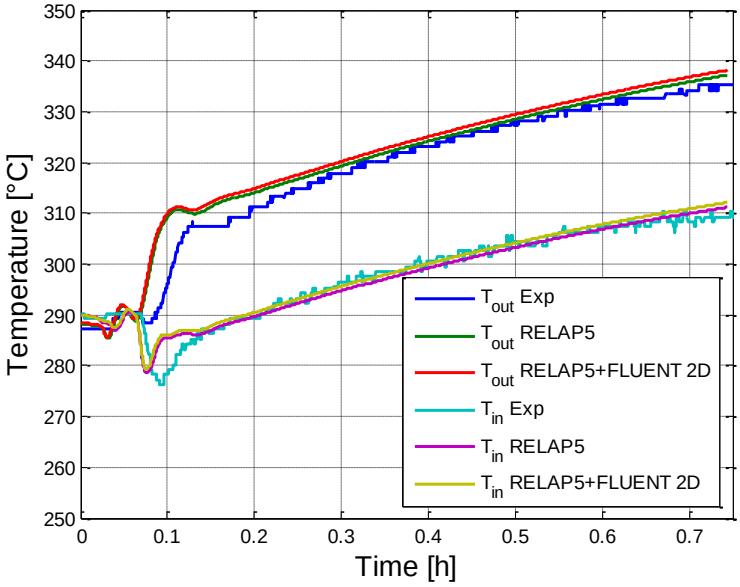

Figure 146: HX inlet and outlet section temperatures (Test 301)

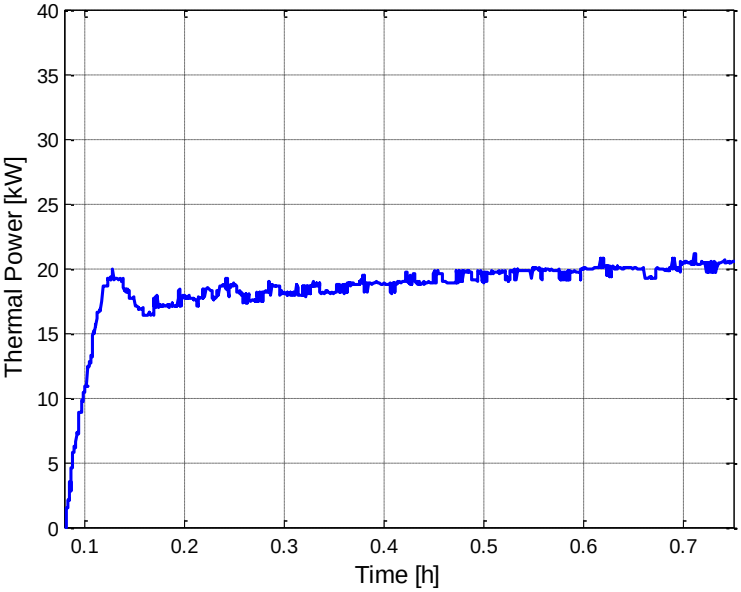

Figure 147: Thermal power removed by the secondary water system

In Figure 148, the temperature distribution inside the 2D domain (Fluent domain for the FPS section) is reported at t = 0.74 h (2680 s) from the beginning of the transient. This instant corresponds to the maximum average temperature time reached at the outlet section of the FPS domain. The maximum temperature reached near the heated wall is in the order of 384°C.

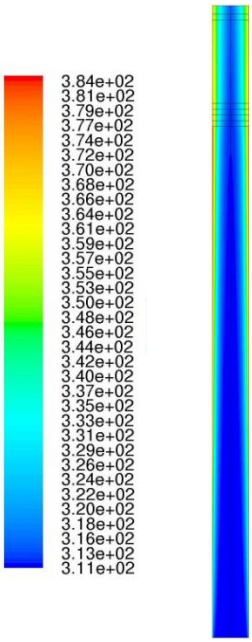

Figure 148: Temperature contour plot [°C]

3.8. Coupling procedure improvements

The performed simulations gave a positive feedback on the feasibility and capability of the developed coupling methodology. The advantage of the adopted explicit coupling scheme, lies in its simplicity of implementation on the other hand exchanging data only after the closure of the time step can be penalizing for the simulation stability hence, the need to use lower time step values. Improvements in the coupling procedure in order to enhance the stability of the method and to reduce computational efforts are described in the following section. In particular, an implicit coupling scheme is developed and, moreover, the UDF implemented for the Fluent CFD code to manage the data exchange at boundaries is parallelized giving in this way the possibility to work with multiple processor, with both the explicit and the implicit coupling scheme.

Another important improvement developed for both the explicit and the implicit schemes is the way that the MATLAB code obtains the data to be exchanged from the RELAP5 code. In the new versions of the coupling scheme, MATLAB can access directly the RELAP5 restart file (name.rst file) and save data to be passed to the Fluent code. In the previous version of the coupling scheme, the RELAP5 data to be passed to the Fluent code were read in the output file (name.o file).

3.8.1. Implicit coupling scheme

The basic idea behind the implicit scheme is to repeat each time step several times with updated b.c at each "inner-cycle", until specified convergence criteria are satisfied; after that, both codes proceed to compute b.c. for the next time step. The variables exchanged at each inner cycle and at each time step are pressure, temperature and mass flow rate according to the scheme shown in Figure 105. The implicit method described in Figure 149, raises greater difficulties in terms of implementation, but the effect of any disturbances is limited by the feedback at each sub cycle leading to a stronger numerical stability and allowing the use of relatively larger time step with respect to the explicit coupling scheme.

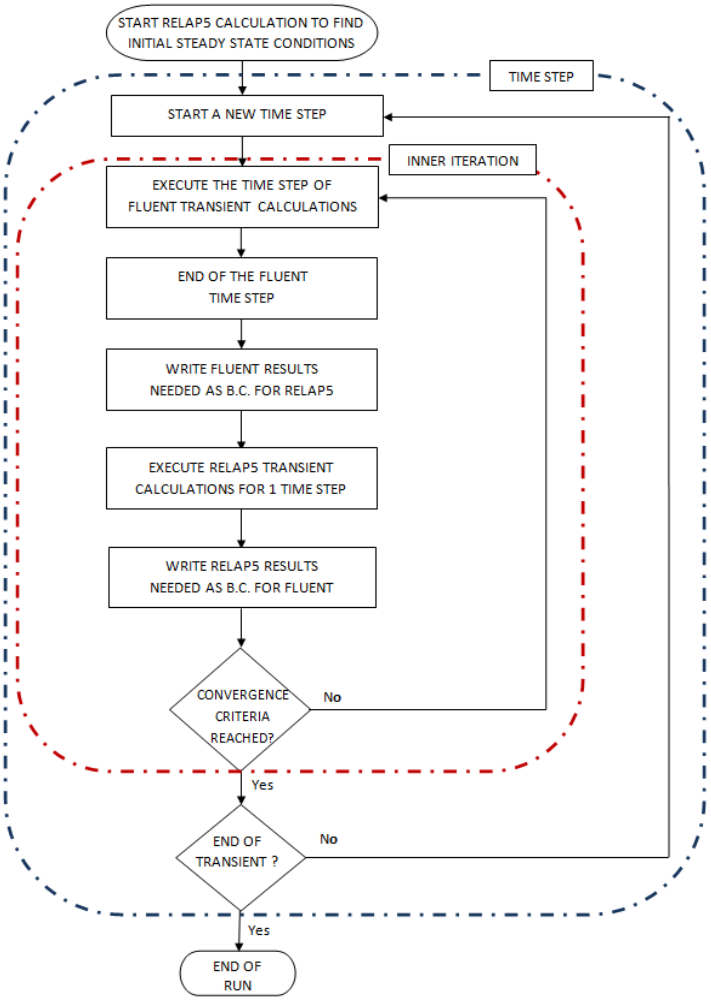

Figure 149: Implicit coupling scheme

Each inner iteration can be repeated until specified convergence criteria are satisfied or, for a simplified programming, setting a fixed number of inner iterations for each time step. For the performed simulations, a fixed number of inner iteration was imposed and from a first

sensitivity analysis, three inner iteration per each time step were chosen as a good compromise between CPU time and accuracy of results. The Fluent code (master code) advances firstly by one time step and then the RELAP5 code (slave code) advances for the same time step period, using data received from the master code.

The semi implicit numerical scheme is adopted for the RELAP5 calculations. For each of the three RELAP5 boundary condition data, a linear interpolation within the time step period between the initial value (final value of the previous time step) and the final value of the current time step (obtained by the Fluent code calculation) is considered for RELAP5. In the Fluent code, instead, b.c. are considered fixed in the time step, hence, for each inner iteration the b.c. imposed in the Fluent code are averaged between the previous and at the current iteration.

3.8.2. Parallelization of the UDF

The Fluent serial solver is essentially composed by a Cortex, and a single Fluent process (ANSYS® Academic Research, Release 14.5, Ansys Fluent UDF manual, 2012). The Cortex is the Ansys Fluent process responsible for user-interface and graphics related functions. The Fluent parallel solver instead computes the solution using simultaneously multiple processors splitting up the computational domain into multiple partitions and assigning each data partition to a different compute process (compute node). The Fluent parallel architecture is composed by the Cortex a Host a Compute node-0 and *n* Compute node-*n*. The Host primary purpose is to interpret commands from Cortex and to pass those commands to Compute node-0 which then distributes them to the other computer nodes (Figure 150). The Cortex and the Host do not have any numerical data.

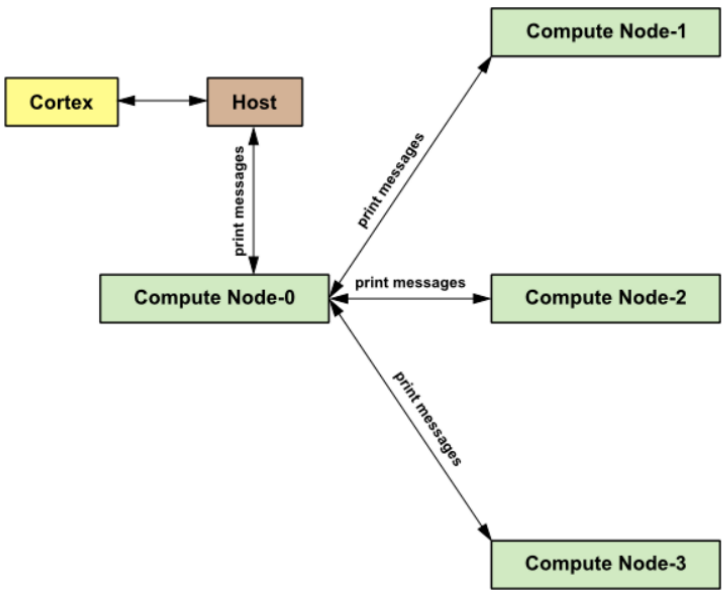

Figure 150: Example of Fluent parallel architecture

A UDF need to be parallelized when it performs operations that require information located on different compute nodes, such type of operations are operations involving summation or addition (integration) commonly performed in general purpose defined macros such as

DEFINE_ADJUST, DEFINE_EXECUTE_AT_THE_END, etc.. When a UDF is converted to run in parallel, some part of the script may need to be done by the host and some other by the compute nodes. As an example, since the host does not contain mesh data, it has to be not included in any calculation that otherwise will result in NaN value. At the same time when writing files in parallel, the file must be opened by the Host, then Compute nodes must send their data to Compute node-0 which collect the data and sends them to the host which write it to the file and then close the file.

3.8.3. RELAP5-Fluent coupled simulations (implicit scheme)

The implicit coupling scheme is adopted to simulate the experimental test named Test 206 representative of a gas enhanced circulation test (see Table 14). A total of five simulations are performed, involving both 2D and 3D geometrical CFD domains and adopting the implicit numerical scheme. The test matrix of the performed simulations is reported in Table 17. In particular, Test 206-0 is analysed adopting the serial solver and the same time step used for the explicit coupled simulation in order to evaluate the behaviour of the implicit coupling scheme. The other tests are performed in order to evaluate the modified UDF for the parallel solver and the use of the 3D domain with the implicit scheme.

Table 17: Matrix of simulations

Name	*Time Step*	CFD Geometrical Domain	Serial/Parallel
Test 206-0	0.005 s	2D	Serial
Test 206-1	0.025 s	2D	"
Test 206-2	0.025s	2D	Parallel
Test 206-3	0.025 s	3D	Serial
Test 206-4	0.025 s	3D	Parallel

In Figure 151 and Figure 152, coupled simulation results obtained adopting the explicit coupling scheme are compared with results achieved with the implicit coupling scheme. The simulations here presented, differ only for the numerical scheme: the same time step is used (0.005 s) and the same 2D-CFD geometrical domain is adopted. The LBE mass flow rate time trends and pressure differences between inlet and outlet section of the FPS are practically overlapping, with differences lower than 1%.

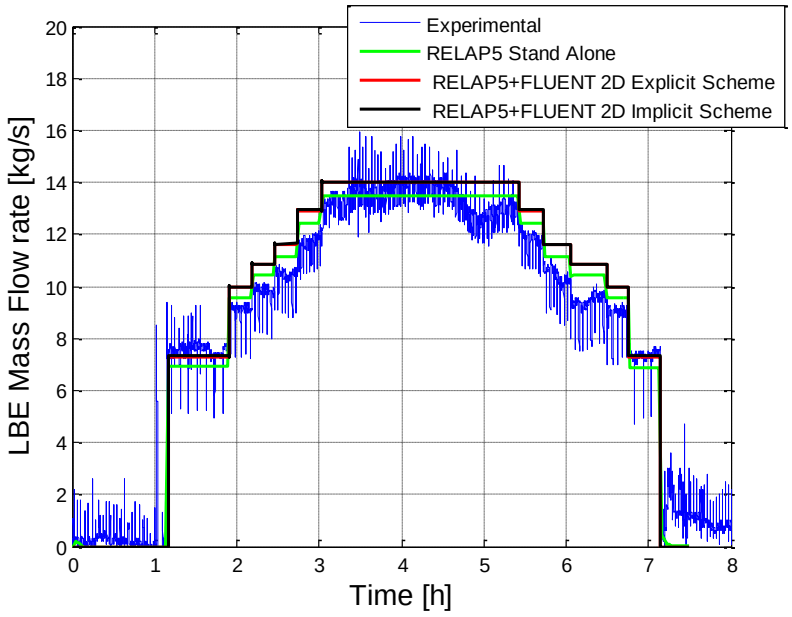

Figure 151: LBE mass flow rate, explicit vs. implicit coupling scheme

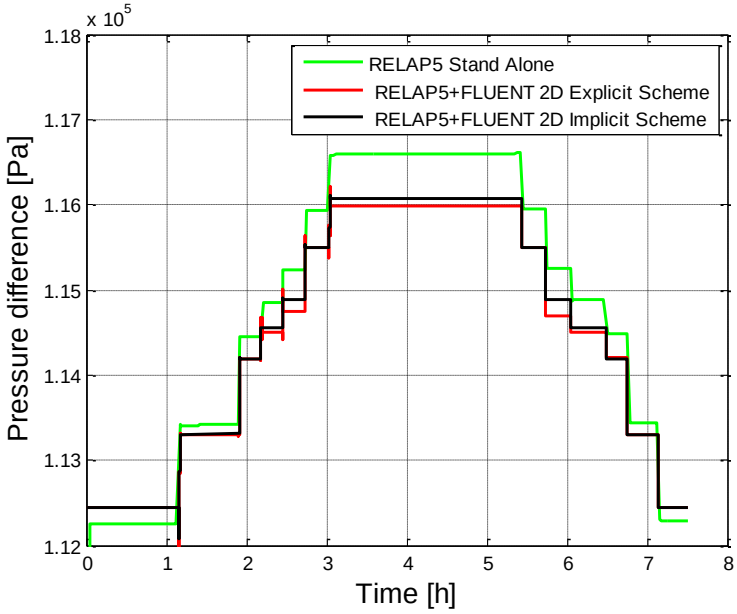

Figure 152: FPS pressure difference, explicit vs. implicit coupling scheme

As mentioned in § 3.8.1, implicit schemes allow larger time steps and tend to be more stable than explicit schemes. Anyway, in order to achieve an appropriate accuracy, the time step shall be chosen reasonably small. For this reason, a sensitivity analysis of the effect of the time step is carried out providing as a results that the implicit coupling scheme allows

the use of a time step of 0.025 s (five times greater than the one adopted for the explicit scheme) without losing in results accuracy. The implicit coupling scheme, together with the Ansys Fluent parallel solver, are adopted for the 2D and 3D simulations and obtained results are compared with those obtained from serial solver simulations and with experimental results. Figure 153 shows the results obtained for the forced circulation test. Good agreement is found among the performed simulations with 2D axial-symmetric and 3D symmetric CFD geometrical domains and with serial and parallel CFD solver. Obtained LBE mass flow rate time trends are overlapped for all the performed coupled simulations with differences that are 5% and 12% lower than the stand-alone RELAP5 and the experimental flow rate respectively. A significant reduction in the computational time is obtained both adopting the parallel solver and a greater time step value (implicit scheme). Performed simulations ran on different PC with different architectures, hence a precise estimate of the reduction of the computational time could not be performed.

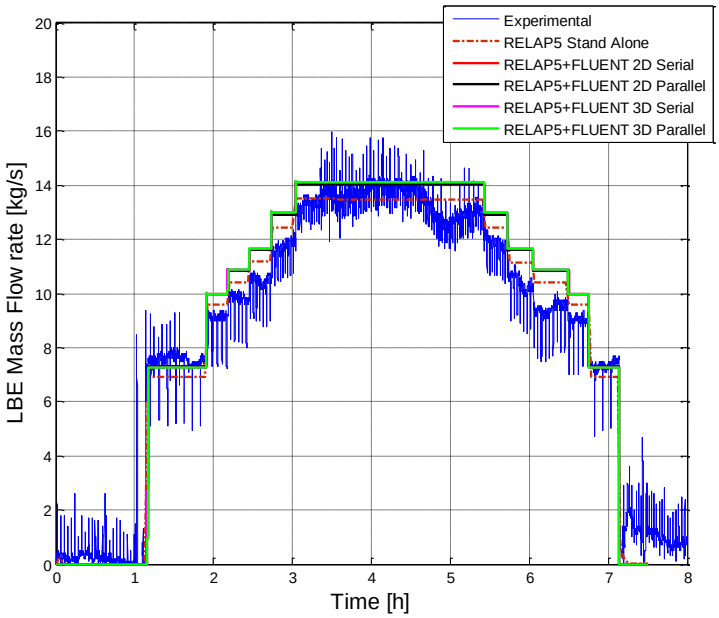

Figure 153: LBE mass flow rate, serial vs. parallel solver (2D and 3D CFD geometrical domains)

The use of a 3D geometrical domain for CFD simulations allows highlighting some thermal-hydraulic details that would otherwise not be visualized using STH codes. In particular, Figure 154 shows a 3D visualization of the velocity magnitude contours plot profile at the exit section of the electrical pins active length (*z*-coordinate 890 mm). The maximum velocity value for the maximum gas injection flow rate (10 Nl/min) is about 1.14 m/s reached in an "*X*" shape region near the centre of the bundle, while the average vertical velocity (area-weighted velocity) is about 0.88 m/s.

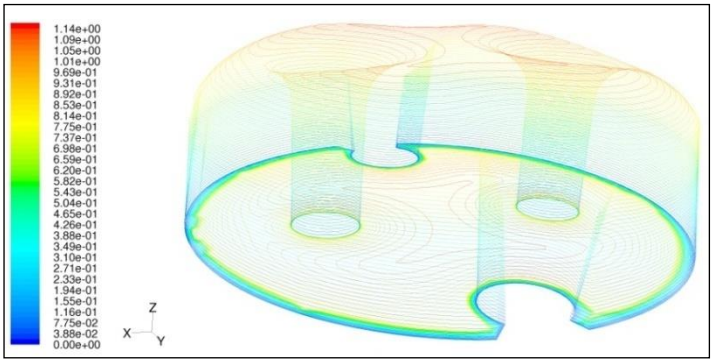

Figure 154: 3D contour plot of velocity magnitude at the exit section of the pins region

Figure 155 shows velocity magnitude vectors in the plane z = 890 mm, the support and heating rods (diameter 8.2 mm) are visualized in the background. Figure 156 shows the turbulent kinetic energy (ε) in the symmetry plane passing through the axis of the electric pins, in particular the contour highlights disturbances induced in the flow fields by the electric pins.

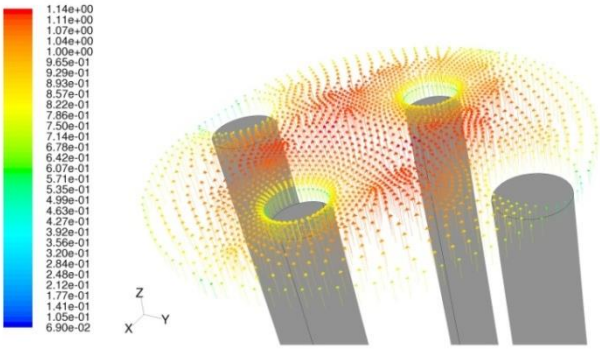

Figure 155: Velocity vectors [m/s] in the outlet section of the active length of the pins

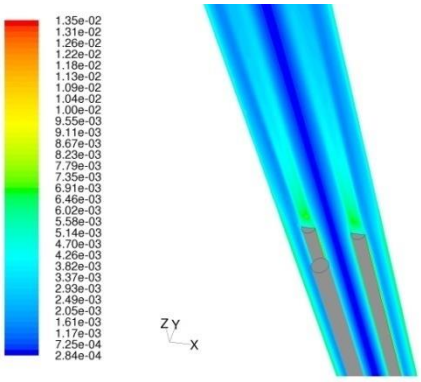

Figure 156: Turbulent kinetic energy contour [m^2/s^2]

Finally, in order to summarize the results of simulations (Tests 206, 301 and 306) the calculated LBE mass flow rate is plotted as a function of the experimental mass flow rate in Figure 157. Calculated results satisfactory predict the experimental data (most of the obtained results lie in a range between +10% and -10%) with a trend that generally tend to slightly overestimate the experimental LBE mass flow rate.

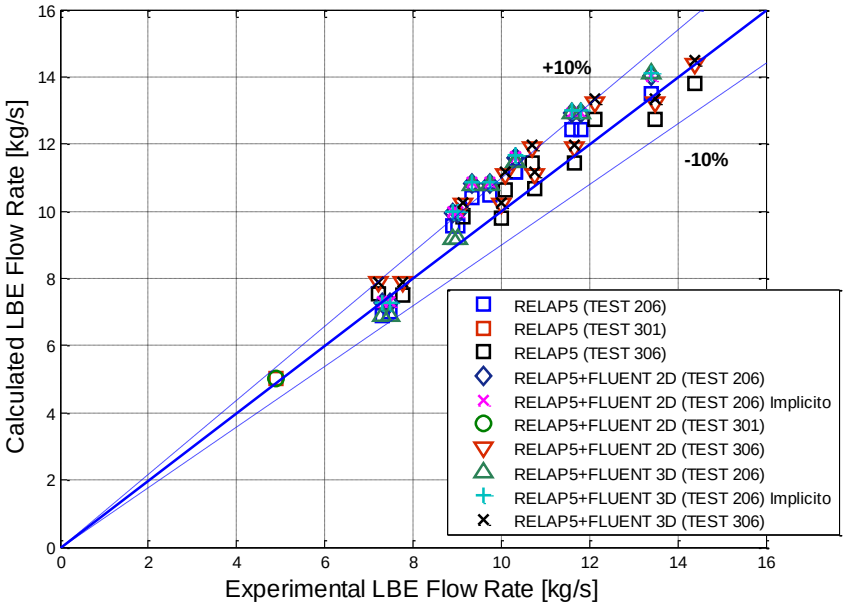

Figure 157: Experimental LBE mass flow rate vs. calculated LBE mass flow rate

4 HEAT TRANSFER INVESTIGATION IN FUEL PIN BUNDLE

4.1. Introduction

A series of experimental tests, performed in the CIRCE facility, refurbished with the ICE test section, were devoted to the characterization of heat transfer phenomena in the fuel bundle both in natural and forced circulation conditions. Heat transfer in HLM media significantly differs from the well-known heat transfer in water medium. The leading reason for this changed behaviour lies with the difference in the Prandtl number (Pr) between the two media (Mikityuk, 2009): liquid metals have a relatively low Pr with respect to water (10^{-2}-10^{-3}, much lower than for water). Most of the different experimental work available in HLM scientific literature deals with sodium-potassium alloy (NaK of different composition) or mercury (Hg) as reference fluid (Mikityuk, 2009). Therefore, specific experimental tests with Lead and Lead Bismuth Eutectic alloy (LBE) are mandatory in supporting the LFR core thermal-hydraulics design. The description of the FPS of the ICE test section and its instrumentation is reported in § 2.4.2.1.

4.2. Experimental procedure

4.2.1. Experimental tests

Tests performed under forced circulation regime are carried out fixing a temperature difference through the FPS of about 80°C and the electrical power to be supplied to the FPS is calculated by an energy balance equation imposing the desired LBE mass flow rate through the FPS.

During tests, subchannel temperatures are investigated at different Peclet numbers changing the LBE mass flow rate in the range of 40-70 kg in steps of about 5 kg/s. For each step, steady state temperature conditions in the FPS are reached and maintained at least for 15 min and the Nusselt number is evaluated. The adopted boundary conditions are summarized in Table 18. In particular, the imposed LBE mass flow rate, argon flow rate (gas-enhanced circulation) to reach the desired LBE mass flow rate and FPS electrical power to obtain the desired difference in temperature between the FPS inlet and outlet section are reported. Moreover, the difference between the pin clad temperature and the subchannel bulk temperature, foreseen using the Mikityuk and Ushakov correlations for the Nu evaluation, are listed (Mikityuk, 2009 and Ushakov et al., 1977). All data reported in this work refers to the central subchannel of the FPS and a reasonable approximation is to consider the central subchannel as representative of an infinite lattice.

For tests performed under natural circulation conditions, the power supplied to the FPS was changed from 100 to 600 kW with steps of 100 kW, obtaining LBE flow rate through the test section in the range of 12-25 kg/s. For each step, steady state temperature conditions in the FPS were reached and maintained for at least 15 min. In Table 19, a short description of natural circulation tests is reported; in particular, the electrical power supplied to the FPS, the obtained LBE flow rate and the temperature difference between the inlet and outlet section of the FPS are summarized.

Table 18: Boundary conditions adopted for FC tests

Name	LBE Mass flow rate [kg/s]	Argon Mass flow rate [Nl/s]	FPS Electrical Power [kW]	ΔT (outlet-inlet) FPS [°C]	ΔT (clad-bulk) Mikityuk [°C]	ΔT (clad-bulk) Ushakov [°C]
1-FC	70	5.00	800	80	35.0	36.0
2-FC	65	4.40	760	80	37.0	39.0
3-FC	60	3.00	700	80	39.5	41.0
4-FC	55	2.40	640	80	41.6	43.5
5-FC	50	1.60	580	80	43.5	45.7
6-FC	45	1.45	525	80	45.4	47.8
7-FC	40	1.41	465	80	47.0	49.5

Table 19: NC tests description

Name	LBE Mass flow rate [kg/s]	FPS Electrical Power [kW]	ΔT (outlet-inlet) FPS [°C]
1-NC	25	600	165
2-NC	23	500	151
3-NC	21	400	133
4-NC	19	300	109
5-NC	14	200	102
6-NC	12	100	58

4.2.2. Experimental results

For Test 1-FC the average temperature difference between the inlet and the outlet section of the FPS, obtained for setting an electrical power supplied to the bundle of 800 kW, is 73°C (Figure 158), about 7°C lower than the temperature set in the calculation of the required electrical power (see Table 18). The injection of Argon gas (5 Nl/s) ensured an averaged LBE mass flow rate through the FPS of about 70 kg/s (Figure 159).

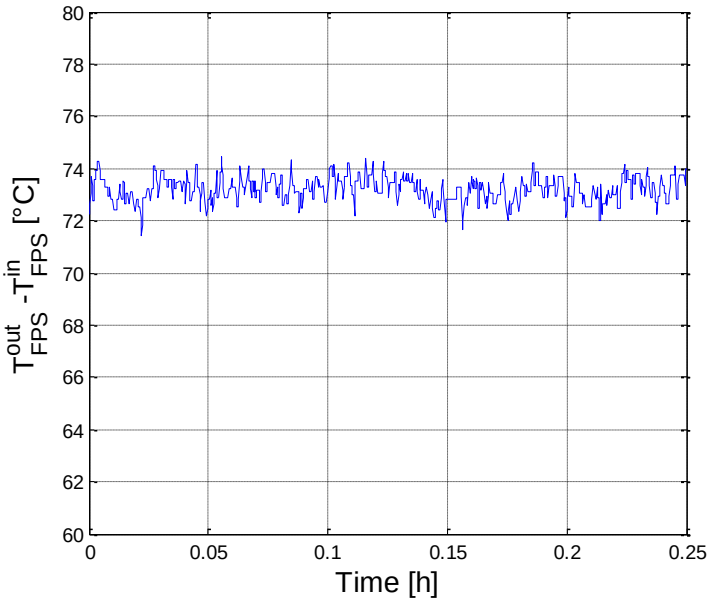

Figure 158: Test 1-FC, ΔT trough the FPS

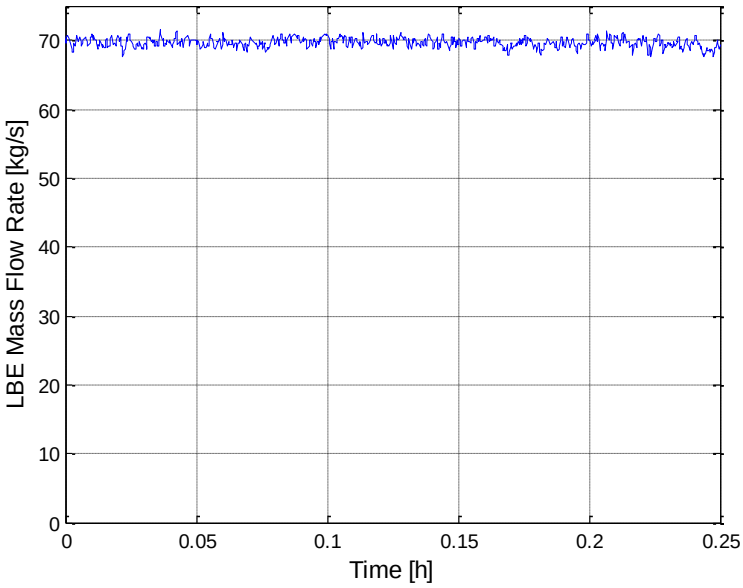

Figure 159: Test 1-FC, LBE mass flow rate through the FPS

Temperatures monitored in the central subchannel of Section 1 (see Figure 17) are plotted in Figure 160. The clad temperature measured on pins 1 and 7 is about 366°C while the bulk temperature is 312°C, i.e. about 54°C lower that the wall temperature and about 19°C higher than temperature foreseen using Mikityuk and Ushakov correlations (see Table 18). The average velocity in the FPS (both Section 1 and 3) is about 1.1 m/s and the Peclet number is about 2971 at Section 1. The Nusselt number calculated for the central subchannel of the same section is reported in Figure 161: its mean value is 27.3.

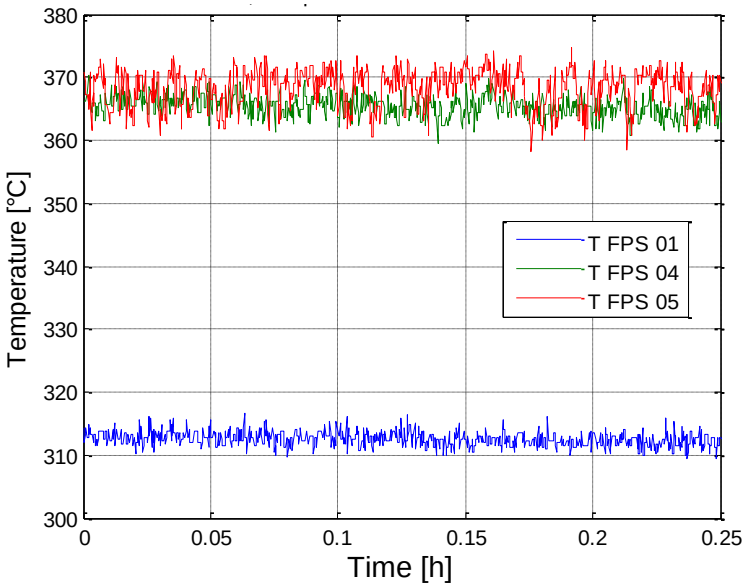

Figure 160: Section 1, central subchannel temperatures

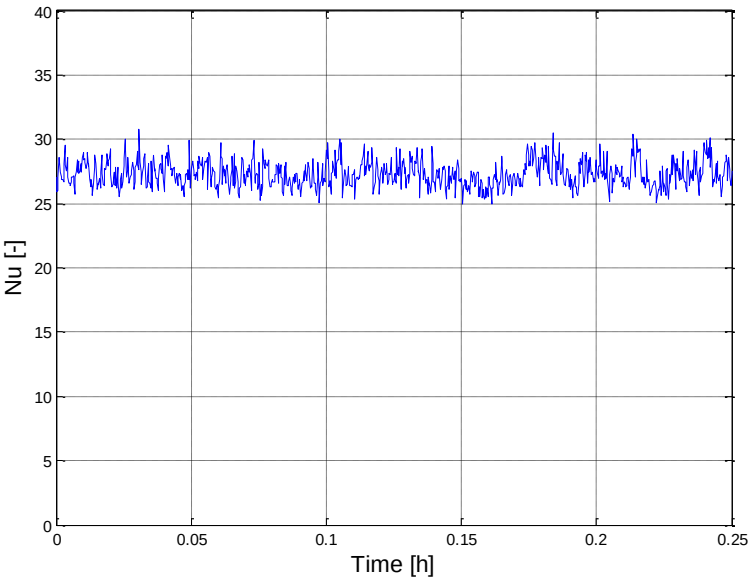

Figure 161: Section 1, Nusselt number

Considering the central subchannel of section 3 (see Figure 19), the average bulk temperature is about 355°C while the average wall temperature measured on pin 1 is about 412°C. The average temperature measured on pin 7 is 395°C, about 17°C lower than on Pin 1 (Figure 162). This difference in the wall temperature between Pins 1 and 7 is essentially caused by pin manufacturing as reported in § 2.6.3.1, Figure 62.

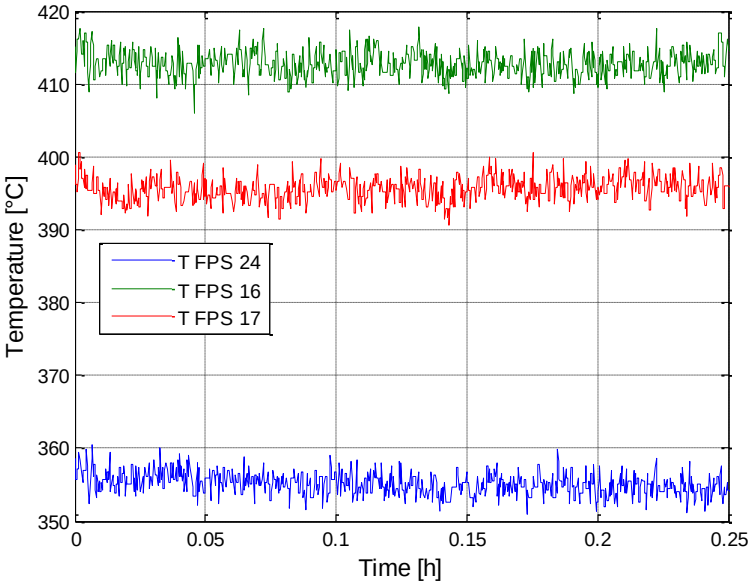

Figure 162: Section 3, central subchannel temperatures

The averaged Nusselt number calculated in the central subchannel of section 3 is 28.9 (Figure 163).

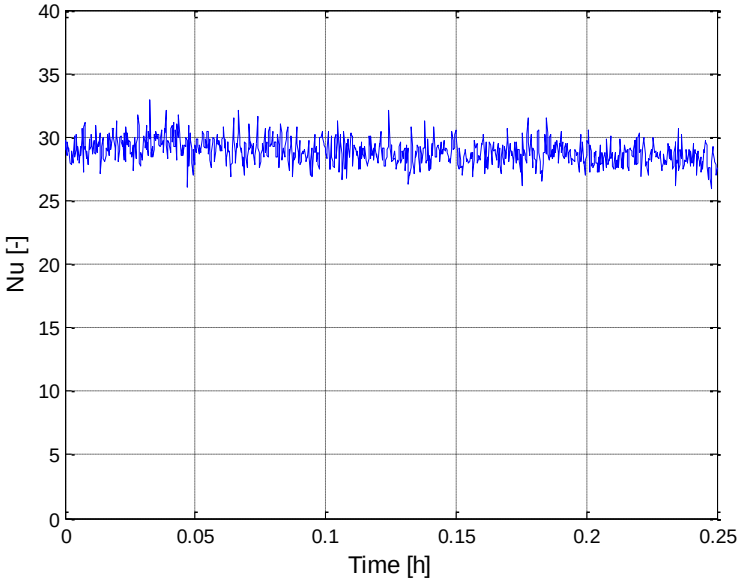

Figure 163: Section 3, Nusselt number

Considering Test 1-NC performed under natural circulation conditions the temperature difference between the inlet and outlet sections of the FPS obtained by setting the electrical power supplied to the bundle at 600 kW is about 113°C (Figure 164). Regarding the operation under natural circulation regime the difference in level (H) between the thermal centre of the heat source (FPS) and the one of the heat sink (Heat Exchanger, HX) provides the pressure head ($\Delta p \sim g\beta\Delta T\Delta H$) required to achieve the LBE mass flow rate, that for Test 1-NC is about 25 kg/s (Figure 165).

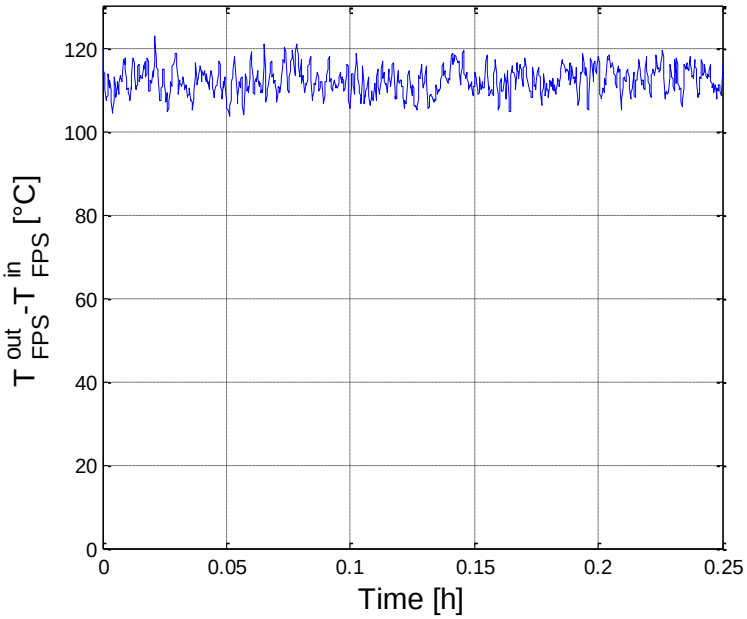

Figure 164: Test 1-NC, ΔT trough the FPS

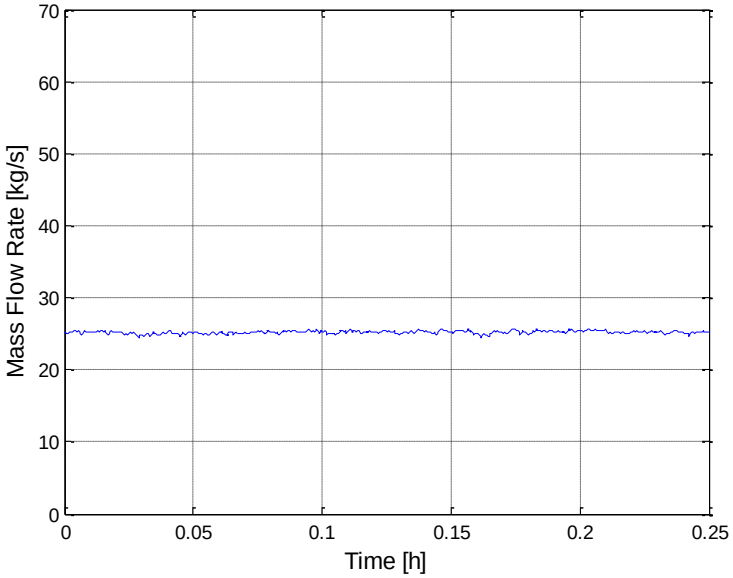

Figure 165: Test 1-NC, LBE mass flow rate

The average clad temperature measured on pin 1 and 7 at section 1 is about 434°C while the average bulk temperature is about 372°C and the temperature difference pin-bulk is about 62°C (Figure 166). The averaged velocity in the bundle is 0.41 m/s and the obtained Nusselt number is 16.9 (Figure 167). In the upper section (section 3) the average temperature measured on the wall of pin 1 is about 522°C (Figure 168) while on pin 7 it is about 11°C lower than on pin 1 due to the azimuthal variation of the thermal flux around the bifilar-type pin rods. The obtained Nu number for Test 1-NC shown in Figure 169, is 18.3.

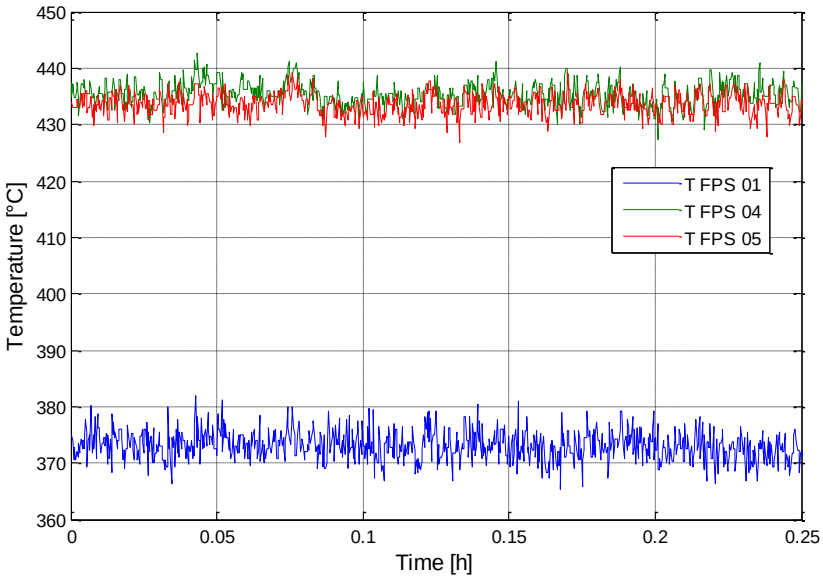

Figure 166: Section 1, central subchannel temperatures

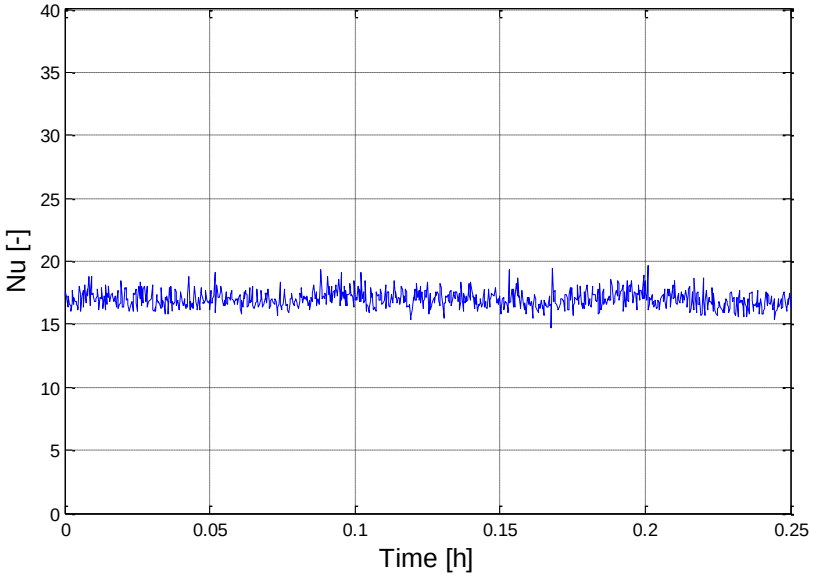

Figure 167: Section 1, Nusselt number

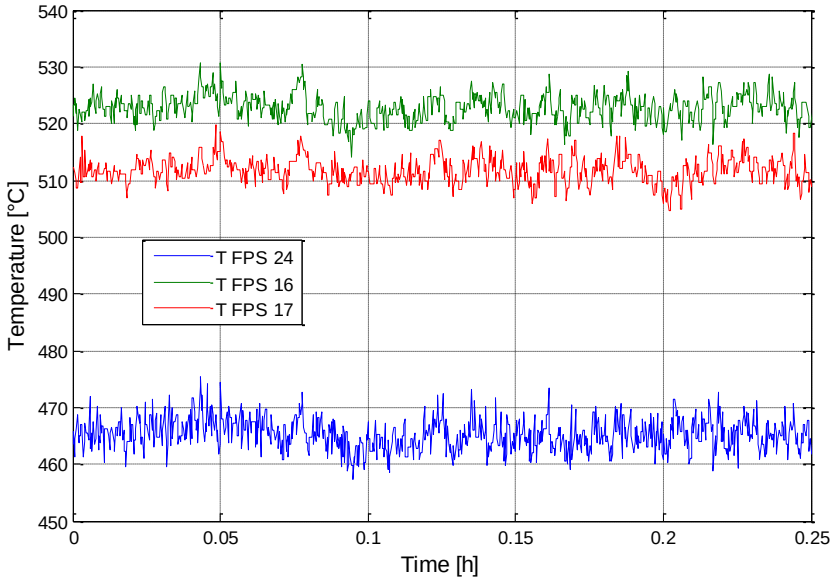

Figure 168: Section 3, central subchannel temperatures

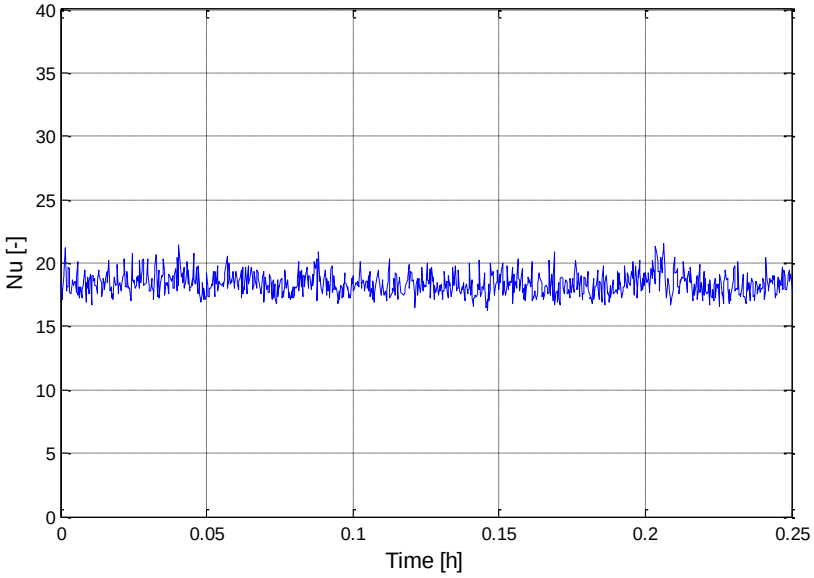

Figure 169: Section 3, Nusselt number

The primary variables measured for tests performed both under forced and natural circulation are summarized in Table 20 and Table 21. In particular, the LBE mass flow rate flowing through the bundle and the pin heat flux are reported together with temperatures in the centre of the channel and on the pin walls (Pin 1 and 7) for section 1 (Table 20) and section 3 (Table 21). Moreover, the standard deviation and the percentage error are reported for each variable in agreement with Appendix *A*.

Table 20: Primary variables measured at section 1 and their uncertainties

Name	$\overline{\dot{m}}$ [kg/s]	$\langle \sigma_X \rangle$ [kg/s]	$\left\langle \frac{\sigma_X}{X} \right\rangle$	$\overline{q''}$ [kW/m^2]	$\langle \sigma_X \rangle$ [kW]	$\left\langle \frac{\sigma_X}{X} \right\rangle$	$\overline{T}_{CC}$ [°C]	$\langle \sigma_X \rangle$ [°C]	$\overline{T}_{Pin1}$ [°C]	$\langle \sigma_X \rangle$ [°C]	$\overline{T}_{Pin7}$ [°C]	$\langle \sigma_X \rangle$ [°C]
1-FC	69.7	1.5	2.2%	839	126	15%	312.5	1.1	365.4	1.6	368.30	3.0
2-FC	65.7	1.5	2.3%	798	120	15%	311.1	1.1	362.6	1.5	363.70	2.8
3-FC	60.1	1.5	2.5%	735	110	15%	300.5	1.2	351.2	1.7	348.70	2.3
4-FC	55.4	1.4	2.5%	671	102	15%	304.2	1.3	351.9	1.9	351.70	2.0
5-FC	49.4	1.9	3.8%	608	92	15%	297.9	1.8	343.2	2.7	342.20	2.6
6-FC	43.8	2.6	5.9%	550	83	15%	291.1	2.6	335.8	3.7	335.00	3.8
7-FC	40.6	2.8	6.9%	487	73	15%	285.1	2.7	325.4	4.2	324.60	4.0
1-NC	25.2	0.5	2.0%	629	95	15%	372.4	2.5	435.0	2.1	433.10	2.0
2-NC	23.2	0.5	2.2%	524	79	15%	375.9	2.3	428.6	1.9	427.60	1.7
3-NC	21.1	0.5	2.4%	420	63	15%	409.3	1.7	452.3	1.3	450.40	1.4
4-NC	19.2	0.4	2.1%	315	47	15%	398.6	1.4	431.2	1.1	429.70	1.1
5-NC	14.1	0.3	2.1%	210	32	15%	341.0	1.5	364.2	1.2	364.40	1.2
6-NC	12.7	0.3	2.4%	105	16	15%	309.2	0.8	321.1	0.7	321.80	0.8

Table 21: Primary variables measured at section 3 and their uncertainties

Name	$\overline{\dot{m}}$ [kg/s]	$\langle \sigma_X \rangle$ [kg/s]	$\left\langle \frac{\sigma_X}{X} \right\rangle$	$\overline{q''}$ [kW/m^2]	$\langle \sigma_X \rangle$ [kW]	$\left\langle \frac{\sigma_X}{X} \right\rangle$	$\overline{T}_{CC}$ [°C]	$\langle \sigma_X \rangle$ [°C]	$\overline{T}_{Pin1}$ [°C]	$\langle \sigma_X \rangle$ [°C]	$\overline{T}_{Pin7}$ [°C]	$\langle \sigma_X \rangle$ [°C]
1-FC	69.7	1.5	2.2%	839	126	15%	355.1	1.4	412.8	1.7	395.6	1.6
2-FC	65.7	1.5	2.3%	798	120	15%	352.7	1.6	409.9	1.7	393.8	1.6
3-FC	60.1	1.5	2.5%	735	110	15%	342.9	1.9	397.8	2.0	383.0	2.0
4-FC	55.4	1.4	2.5%	671	102	15%	348.0	2.1	398.6	2.2	384.7	2.2
5-FC	49.4	1.9	3.8%	608	92	15%	339.8	3.3	387.3	3.9	378.2	4.1
6-FC	43.8	2.6	5.9%	550	83	15%	334.8	5.1	380.7	6.1	372.5	6.2
7-FC	40.6	2.8	6.9%	487	73	15%	325.9	5.5	368.9	7.0	361.4	6.6
1-NC	25.2	0.5	2.0%	629	95	15%	464.8	2.7	522.4	2.4	511.3	2.3
2-NC	23.2	0.5	2.2%	524	79	15%	460.5	2.4	509.6	2.0	498.8	1.7
3-NC	21.1	0.5	2.4%	420	63	15%	482.7	2.1	522.1	1.7	514.1	1.6
4-NC	19.2	0.4	2.1%	315	47	15%	459.4	1.7	490.3	1.4	486.8	1.4
5-NC	14.1	0.3	2.1%	210	32	15%	397.8	1.9	420.7	1.6	417.9	1.5
6-NC	12.7	0.3	2.4%	105	16	15%	341.8	1.2	353.6	0.9	352.7	0.9

Under forced circulation conditions, reducing the argon flow rate, the gas bubble flow was not uniform leading to an increase in mass flow rate oscillations and, therefore, to an increase of the spread in temperature data in the bundle. For this reason LBE mass flow rate values lower than about 40 kg/s could not be reached under forced circulation conditions. On the other hand, the maximum LBE mass flow rate reached under natural circulation conditions without an excessive increase of the pin wall temperature is about 25 kg/s. The Nu number was then calculated considering the equivalent diameter as the characteristic length, which is, for a triangular interior channel (assuming an infinite lattice), evaluated by:

$$d_{eq} = 4\frac{\left(\frac{\sqrt{3}}{4}\cdot p^2 - \pi\cdot d\right)}{\frac{\pi\cdot d}{2}} \tag{8}$$

In Table 21 and Table 22, the Nu numbers computed for all the performed experimental Tests are reported together with the Pe and Re numbers. The propagation of errors on secondary variables is calculated as discussed in Appendix *A*, taking the root-sum-of-squares of all partial error to get the total error (Moffat, 1988).

Table 21: Secondary variables at section 1 and their uncertainties

Name	Re	$\langle\sigma_X\rangle$	$\left\langle\frac{\sigma_X}{X}\right\rangle$	Pe	$\langle\sigma_X\rangle$	$\left\langle\frac{\sigma_X}{X}\right\rangle$	Nu	$\langle\sigma_X\rangle$	$\left\langle\frac{\sigma_X}{X}\right\rangle$
1-FC	$1.4\ 10^5$	$7.1\ 10^3$	5.3%	2971	260	9%	27.3	4.4	16.1%
2-FC	$1.3\ 10^5$	$6.7\ 10^3$	5.3%	2805	234	8%	27.1	4.3	15.9%
3-FC	$1.1\ 10^5$	$6.8\ 10^3$	5.9%	2603	219	8%	26.6	4.2	15.8%
4-FC	$1.1\ 10^5$	$5.7\ 10^3$	5.4%	2388	211	9%	25.2	4.1	16.3%
5-FC	$9.3\ 10^4$	$5.7\ 10^3$	6.1%	2144	200	9%	24.4	4.1	16.8%
6-FC	$8.1\ 10^4$	$6.2\ 10^3$	7.7%	1916	199	10%	22.7	4.0	17.6%
7-FC	$7.4\ 10^4$	$6.2\ 10^3$	8.3%	1794	194	11%	22.3	4.1	18.4%
1-NC	$5.5\ 10^4$	$2.9\ 10^3$	5.2%	1001	87	9%	16.9	2.8	16.5%
2-NC	$5.1\ 10^4$	$2.7\ 10^3$	5.3%	917	81	9%	16.6	2.7	16.4%
3-NC	$4.9\ 10^4$	$2.6\ 10^3$	5.2%	803	70	9%	15.9	2.6	16.3%
4-NC	$4.4\ 10^4$	$2.3\ 10^3$	5.3%	742	65	9%	15.9	2.6	16.4%
5-NC	$2.9\ 10^4$	$1.6\ 10^3$	5.3%	583	51	9%	15.5	2.6	17.0%
6-NC	$2.5\ 10^4$	$1.3\ 10^3$	5.3%	543	48	9%	15.2	2.6	17.3%

Table 22: Secondary variables at section 3 and their uncertainties

Name	Re	$\langle \sigma_X \rangle$	$\left\langle \frac{\sigma_X}{X} \right\rangle$	Pe	$\langle \sigma_X \rangle$	$\left\langle \frac{\sigma_X}{X} \right\rangle$	Nu	$\langle \sigma_X \rangle$	$\left\langle \frac{\sigma_X}{X} \right\rangle$
1-FC	$1.5\ 10^5$	$7.8\ 10^3$	5.3%	2823	247	9%	28.87	4.5	15.6%
2-FC	$1.4\ 10^5$	$7.3\ 10^3$	5.3%	2668	234	9%	27.46	4.3	15.7%
3-FC	$1.2\ 10^5$	$6.8\ 10^3$	5.4%	2472	219	9%	26.48	4.2	15.9%
4-FC	$1.2\ 10^5$	$6.3\ 10^3$	5.4%	2264	200	9%	26.17	4.1	15.7%
5-FC	$1.0\ 10^5$	$6.2\ 10^3$	6.1%	2037	189	9%	24.34	4.0	16.4%
6-FC	$8.9\ 10^4$	$6.9\ 10^3$	7.7%	1817	188	10%	22.76	4.2	18.5%
7-FC	$8.1\ 10^4$	$6.7\ 10^3$	8.3%	1706	184	11%	21.69	4.3	19.8%
1-NC	$6.4\ 10^4$	$3.3\ 10^3$	5.2%	906	79	9%	18.35	2.9	15.8%
2-NC	$5.9\ 10^4$	$3.1\ 10^3$	5.3%	836	73	9%	18.29	2.9	15.9%
3-NC	$5.5\ 10^4$	$2.9\ 10^3$	5.2%	743	65	9%	17.72	2.7	15.2%
4-NC	$4.9\ 10^4$	$2.6\ 10^3$	5.3%	695	61	9%	16.78	2.6	15.5%
5-NC	$3.2\ 10^4$	$1.7\ 10^3$	5.3%	546	48	9%	15.87	2.5	15.8%
6-NC	$2.6\ 10^4$	$1.4\ 10^3$	5.3%	543	46	8%	16.12	2.7	16.7%

Figure 170 shows the Nu number computed from the experimental data as a function of the Pe number and a comparison with empirical correlations available in the literature (Mikityuk, 2009, Pfrang and Struwe, 2007). In particular, among correlations for circular rods arranged in a triangular lattice, the Mikityuk and the Ushakov correlations (Mikityuk, 2009 and Ushakov et al., 1977) were selected, having a validity range containing the *p/d* ratio used for the CIRCE-ICE experimental campaign. The Mikityuk correlation is here reported:

$$Nu = 0.047 \cdot \left(1 - e^{-3.8 \cdot (p/d - 1)}\right)\left(Pe^{0.77} + 250\right) \qquad \text{valid for } 1.1 \le p/d \le 1.95 \text{ and for } 30 \le \mathrm{Pe} \le 5000 \tag{9}$$

It gives the best fit of four set of experimental data (658 data points). It is obtained from the review of experimental results obtained by Maresca and Dwyer (1964) Borishanskii et al. (1969) Gräber and Rieger (1972) and Zhukow et al. (2002) available in the literature. The Mikityuk correlation is recommended for square and triangular lattice of rods with *p/d* ratio of 1.1-1.95 and Peclet numbers up to 5000, it must be stressed, however, that correlations have an uncertainty due to the heterogeneity of the original data and they are derived for different heavy liquid metals.

The Ushakov correlation (Eq. (10)), is found by Mikityuk to have the highest quality in predicting the experimental data considered in the paper (no direct access to Ushakov' s reference was available, however the discussion of this correlation was found documented in A.V. Zhukov et al., 1992). The validity range is for Pe up to 4000 and *p/d* in the range 1.2-2.

$$Nu = 7.55 \cdot (p/d) - 20 \cdot (p/d) + 0.041 \cdot (p/d)^{-2} \cdot Pe^{(0.56 + 0.19 \cdot p/d)} \qquad \text{valid for } 1.2 \le p/d \le 2 \text{ and for } 1 \le \mathrm{Pe} \le 4000 \tag{10}$$

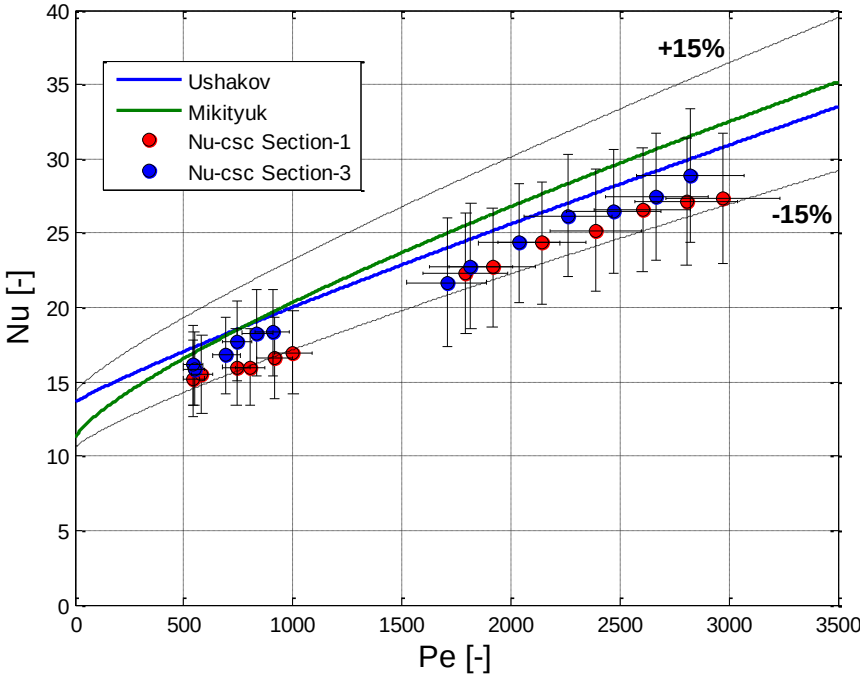

Figure 170: Nu vs. Pe number obtained from experimental data and comparison with Ushakov and Mikityuk correlations

5 CONCLUSIONS AND PERSPECTIVES

The aim of this thesis has been the experimental and numerical analysis of thermal-hydraulic phenomena of interest in support to LFR design. The research activity was performed at the Department of Civil and Industrial Engineering of the University of Pisa in cooperation with Brasimone R.C. in the international framework of the Thermal Hydraulic of Innovative Nuclear System (THINS) Seventh Framework Programme of EURATOM for nuclear research and training activities.

In the following, the main results obtained during this work, as well as future perspectives, are summarized.

Thermal stratification

The Fluent CFD code was used to simulate the experimental test of Uotani aimed to study heat transfer in a thermal stratified HLM system. The purpose was to investigate capabilities/limitations of the Fluent CFD code in simulating heat transfer under thermally stratified conditions and to provide a guideline for the study this phenomenon in the CIRculation Eutectic (CIRCE) large pool experimental facility.

Then a "one-way", off-line coupled simulation by the RELAP5 system code and the CFD Fluent code was firstly developed. A simplified 2D axial-symmetric domain was implemented in order to reproduce the test section, adopting the RNG (Renormalized group) k-ε model to take into account turbulence phenomena inside both air and LBE fluids and neglecting the heat losses through the external walls. The LBE mass flow rate through the FPS and the thermal power removed by the HX during the transition from forced to natural circulation conditions were supplied by a RELAP5 stand-alone simulation of the whole system and introduced in the CFD simulation as boundary conditions.

Obtained results, have predicted a well-defined and restricted region between the HX and the DHR exits where density variations are concentrated. The temperature difference between the upper "hot" region and the lower "cold" region is about 33°C. Experimental tests, carried out in the thermo-hydraulics laboratory of the ENEA Brasimone R.C and simulating the transition from forced to natural circulation in CIRCE large pool facility (PLOHS+LOF) are discussed. The vertical thermal gradient highlighted by the experiments is mainly localized in the region between the outlet sections of the HX and the DHR, with a temperature drop of about 20°C. Moreover, temperature variations in the pool are purely vertical with negligible changes in temperature on the horizontal planes, justifying in such way the use of a 2D CFD geometrical domain. After transition to natural circulation, the region where the thermal gradient is localized moves downwards at the exit section of the DHR-system. It is characterized by a temperature drop of about 10°C.

A post-test analysis was performed introducing the heat exchanged with the external environment and assuming initial boundary conditions in agreement with the experiment (Test I). The large temperature difference predicted in the pre-test calculations (33°C) decreases to 17°C, overestimating the experimental data of about 7°C and confirming therefore the importance of heat losses.

Development of a "two-way" coupling tool

In order to better reproduce the simulated accidental scenarios and improve the accuracy of numerical simulations, a new "two-way" RELAP5-Fluent coupling tool was developed. The coupling approach can be classified as "non-overlapping, two-way coupling scheme".

The analysed domain was divided into regions modelled using the CFD approach and regions that can be reasonably well simulated using the system code (non-overlapping). This partition identifies the interfaces where thermo-fluid-dynamics data (pressure, temperature and LBE mass flow rate) are transferred from the system-code-portion to the CFD-code-portion and vice versa (two-way coupling).

A preliminary application of the developed coupling tool to the Natural Circulation Experiment (NACIE) loop type facility was described. In particular, explicit and implicit numerical schemes were implemented and serial and parallel calculations were carried out (both 2D and 3D CFD domain were used). Obtained results were compared with RELAP5 stand-alone calculations and data obtained from the experimental campaigns performed in the NACIE facility. Three experiments were chosen as reference tests for the numerical simulations. Two of them are representative of a gas enhanced circulation tests and one of a natural circulation test with a thermal power supplied by the Fuel Pin Simulator (FPS, simulated by the CFD code) of 21.5 kW. LBE mass flow rate time trends obtained from coupled simulations were found in good agreement with RELAP5 stand-alone simulations and experimental results, with differences lower than 5% and 12% respectively. The comparison of pressure differences (between inlet and outlet section of the FPS), calculated by the coupled codes simulations and by the RELAP5 code, showed discrepancies lower than 1% pointing out the reliability of the developed tool.

The modelling approach proposed to perform thermal-hydraulic analyses in pool-type HLM-cooled reactors is then based on a coupling tool involving both a STH code, as RELAP5, and a CFD code, as Fluent, with the possibility to use two-way explicit or implicit schemes. The proposed tool has to be obviously accurately validated and verified (V&V) and the activity performed in the frame of the present work, consisting in the simulation of the experimental data available from the NACIE facility, represents just a preliminary work for the V&V process.

Heat transfer investigation in fuel pin bundle

The last part of this work, deals with the experimental campaign performed to investigate heat transfer in the CIRCE fuel bundle under typically large pool reactor conditions. The results shown in the present work and related to the CIRCE-ICE experimental data represent the first set of experimental data obtained concerning fuel pin bundle behaviour in a heavy liquid metal pool, both under forced and natural circulation. Future and innovative nuclear systems based on the HLM technologies (ADSs, LFRs) will be supported by these experiments in their design, safety analysis and licensing phases.

In particular, after a detailed description of the ICE Test section and of its instrumentation, an extended characterization of the performed experiments is introduced and differences between the operation of natural and forced circulation tests are shown.

In order to obtain a standard deviation representative of the dispersion and neglecting the effects due to an imperfect steadiness of acquired experimental variables, a linear regression for each thermocouple signal was evaluated and subtracted from the original one.

For each of the performed experiments (seven tests operated under forced circulation and six under natural circulation conditions) Nusselt numbers were evaluated within a Peclet range of 500-3000 assuming the hypothesis of infinite lattice.

The uncertainty of the obtained Nu is within ±20%, while the uncertainty of the Pe is within ±12%.

The major contributor to the Nu uncertainty was due to the uncertainty of azimuthal thermal flux of the adopted bifilar type pin rod. The central copper pin rod solution was not adopted because of manufacture problems related to the required length to reach the downcomer of the CIRCE pool main vessel (about 8 m).

Then, Nu obtained from experimental data were compared with values obtained from empirical correlations available in literature for heat transfer convection in heavy liquid metals. In particular, a comparison with data obtained from Mikityuk and Ushakov correlations is presented.

Experimental data point out a trend in agreement with the above-cited correlations; in particular, the experimental Nu values are lower than the empirical correlation data by less than 15%.

Future developments

This research activity has great potential for further development and validation activities. In fact, in the frame of the European funding programme for research and innovation (HORIZON 2020) two European projects have been recently approved: thermal hydraulics Simulations and Experiments for the Safety Assessment of MEtal cooled reactors (SESAME) and MYRRHA Research and Transmutation Endeavour (MYRTHE).

Each project has an expected duration of 48 month and the DICI of the University of Pisa (UniPi) is involved in both projects with tasks directly linked to future developments of this research activity. In particular, in the SESAME project, focused on safety assessment on HLM reactors, UniPi is involved in the WP5 “Integral System Simulation”, for the development and validation of system\CFD coupled approach to improve modelling of complex 3D effects and improve the code’s prediction. In this frame, a blind benchmark is foreseen for system-alone and coupled simulations on the basis of NACIE-UP (NACIE loop refurbished with a nineteen wired spaced fuel bundle deeply instrumented) under the lead of UniPi, in order to contribute to the validation of these methodologies for HLM reactors.

The MYRTHE project, aims to perform the necessary research in order to demonstrate the feasibility of transmutation of high-level waste at industrial scale through the development of the MYRRHA, research facility. In this frame, UniPi is involved in the WP3 “Integral Systems and pool thermal hydraulics” for the definition of STH\CFD performances and in the establishments of best practice guidelines for STH\CFD coupled simulations.

REFERENCES

[1] Abderrahim H. A., Baeten P., De Bruyn D., Fernandez R. "MYRRHA – A multi-purpose fast spectrum research reactor",Energy Conversion and Management 63, 4-10, 2012.

[2] Alemberti et al., 2013, "The lead fast reactor – demonstrator (ALFRED) and ELFR design" International Conference on Fast Reactor and Nuclear Fuel Cycle (FR13), Paris, France (2013) www.iaea.org/NuclearPower/Meetings /2013/2013-03-04-03-07-CF-NPTD.html.

[3] Ambrosini W., Azzati M., Benamati G., Bertacci G., Cinotti L., Forgione N., Oriolo F., Scadozzo G., Tarantino M., "Testing and qualification of CIRCE instrumentation based on bubble tubes", Journal of Nuclear Materials, pp. 293-298, 2004.

[4] Austregesilo H., Bals B., Hora A., Lerchl G., Romstedt P., "ATHLET Mod 2.1 Cycle A Models and Methods", code documentation, July 2006

[5] ANSYS® Academic Research, Release 14.0, Help System, Ansys Fluent 14.0 User's Guide, ANSYS, Inc.

[6] ANSYS® Academic Research, Release 14.0, Help System, Ansys Fluent 14.0 UDF manual, ANSYS, Inc.

[7] Artioli C.,"Specification for the EFIT Core and Fuel Element Design", Deliverable D. 1.6, DM1 DESIGN, IP-EUROTRANS, 2006.

[8] Bandini G., Di Piazza I., Gaggini P., Del Nevo A., Tarantino M., "CIRCE experimental set-up design and test matrix definition", ENEA UTIS-TIC Technical Report, IT-F-S-001, 28/02/2011.

[9] Barbensi A., Corsini G., "Specification for the EFIT primary system", Deliverable D. 1.4, DM1 DESIGN, IP-EUROTRANS, 2006.

[10] Bavière R., Tauveron N., Perdu F., Garré E., "System-CFD Coupled Simulation of the PHENIX Reactor Natural Circulation Test", proceedings of NURETH 15, Pisa, Italy, May 12-17,2013.

[11] Benamati G., Bertacci G., Elmi N., Scaddozzo G., "Report on Gas Enhanced Circulation Experiments and Final Analysis (TECLA D41)", Report ENEA HS-A-R-016, 2005.

[12] Bertolotto D., Manera A., Frey S., Prasser H.M., Chawla R., "Single-phase mixing studies by means of a directly coupled CFD/system-code tool", Annals of Nuclear Energy, 36 pp. 310-316, 2009.

[13] Bestion D., "Extension of CFD codes application of two-phase flow safety problems", Nucl. Eng. Tech., Vol.42 pp 365-376, 2010.

[14] Borishanski, V.M., Gotovski, M.A., Firsova, E.V., "Heat transfer to liquid metals in longitudinally wetted bundles of rods", Atomnaya Energiya 27 (6), 549–552, 1969.

[15] Buksha Yu. K., Bagdassarova Yu. E., Kiryushinb A. I., Kuzavkovb N. G., Kamaninb Yu. L., Oshkanovc N. N., Vylomovc V. V., "Operation experience of the BN-600 fast reactor", Nucl. Eng. Des. 173, 67-69, 1997

[16] Cheng X., Tak N., "Investigation on turbulent heat transfer to lead-bismuth eutectic flows in circular tubes for nuclear applications", Nuclear Engineering and Design, Vol. 236, 2005, 385-393,.

[17] Coccoluto G., Gaggini P., Labanti V., Tarantino, M., Ambrosini W., Forgione N., Napoli A., Oriolo F., "Heavy liquid metal natural circulation in a one-dimensional loop", Nuclear Engineering and Design 24, 1301-1309, 2011.

[18] Davis C.B., Shieh A.S., "Overview of the use of ATHENA for Thermal-Hidraulic Analysis of System with Lead-Bismuth Coolant", proceedings of ICONE 8, Baltimore MD USA April 2-6, 2000.
[19] ESNI, www.snetp.eu/esnii/, (last access 16/03/2015).
[20] European commission, ec.europa.eu/clima/policies/roadmap/index_en.htm, (last access 16/03/2015).
[21] European commission, http://ec.europa.eu/programmes/horizon2020/, (last access 16/03/2015).
[22] European Nuclear Society, www.euronuclear.org/info/encyclopedia/n/ nuclear-power-plant-world-wide.htm, (last access 16/03/2015).
[23] FALCON, www.euronuclear.org/e-news/e-news-43/ansaldo.htm, (last access 16/03/2015).
[24] Geffraye G., Antoni O., Farvacque M., Kadri D., Lavialle G., Rameau B., Ruby A., "CATHARE 2 V2.5_2: A single version for various applications", Nucl. Eng. and Des. 241, 4456-4463, 2011.
[25] Generation IV International Forum, "A Technology Roadmap for Generation IV Nuclear Energy Systems", Report GIF-002-00, 2002.
[26] Generation IV International Forum, "Technology Roadmap Update for Generation IV Nuclear Energy Systems", Report GIF-002-00, 2014.
[27] Giraud B., "Review and justification of the main design options of XT-ADS", Deliverable D. 1.5, DM1 DESIGN, IP-EUROTRANS, 2006.
[28] Gräber, V.H., Rieger, M., "Experimentelle Untersuchung des Wärmeübergangs an Flüssigmetalle (NaK) in parallel durchströmten", Rohrbündeln bei konstanter und exponentieller Wärmeflussdichteverteilung. Atomkernenergie (ATKE) Bd. 19, 23–40, 1972.
[29] Hannink M.H.C., Kuczaj A.K., Blom F.J., Church J.M., Komen E.M.J., "A coupled CFD-FEM strategy to predict thermal fatigue in mixing tees of nuclear reactors" EUROSAFE Forum, 2008.
[30] IAEA-TECDOC-1539, "Use and Development of Coupled Computer Codes for the Analysis of Accidents at Nuclear Power Plants", proceedings of a technical meeting held in Vienna 26-28 November 2003.
[31] IAEA, www.iaea.org/PRIS/WorldStatistics/OperationalReactorsByType.aspx, PRIS database (last access 16/03/2015).
[32] INFN, trasco.lnl.infn.it/basic.htm, (last access 16/03/2015).
[33] INL, Idaho National Laboratory, 2525 Fremont Ave. Idaho Falls, www4vip.inl.gov/ebr/, (last access 16/03/2015).
[34] Ishitori T., Ogura K., Sato K., Oshima I., Nei H., Uotani M., Fukada T., Akimoto T. "Experimental study of sodium natural convection heat transfer in the intermediate plenum for pool-type LMFBRs", Nuclear Engineering and Design, Vol 99, pp. 431-440, 1987.
[35] Knebel J. U. et al., "European research programme for the transmutation of high-level nuclear waste in an accelerator-driven system: EUROTRANS", ninth International Exchange Meeting on Actinides and Fission Products Partitioning and Transmutation (IEM9), Nimes, France, 2006
[36] Leipunskii A. I. et al., "The BN-350and the BOR fast reactors", Translated from Atomnaya Énergiya, Vol. 21, No.6, pp. 450-462, December, 1966.
[37] Li W., Wu X., Zhang D., Su G. Tian W., Qiu S., "Preliminary study og coupling CFD code FLUENT and system code RELAP5", Annals of Nuclear Energy, 73 pp. 96-107, 2014.

[38] Jeltsov M., Kööp K., Villanueva W., Kudinov P., "Multi-scale Coupling of STH and CFD Codes for Pre-Test Analysis of TALL-3D Experiments", THINS International Workshop, Modena Italy,January 20-22, 2014.
[39] LEADER project, www.leader-fp7.eu/default.aspx, (last access 16/03/2015).
[40] Mansani L., "Candidates Materials for XT-ADS and EFIT, Operating Conditions and Testing Requirements", Deliverable D. 4.1, DM4 DEMETRA, IP-EUROTRANS, 2005.
[41] Martelli D., Barone G., Forgione N., W. Ambrosini, "System codes and CFD codes applied to loop- pool-type experimental facilities", CIRTEN technical report CERSE-UNIPI RL 1530/2013, Pisa (Italy),September 2013.
[42] Mareska, M.V., Dwyer, O.E., "Heat transfer in a mercury flow along bundles of cylindrical rods", Journal of Heat Transfer, Transactions ASME, Series C 2, 180–186, 1964.
[43] Mikityuk K., "Heat Transfer to Liquid Metal: Data and Correlation for Tube Bundles", Nuclear Engineering and Design, Vol. 239, pp 680-687, 2009.
[44] Moffat, R.J., "Describing the uncertainties in experimental results", Exp. Therm. Fluid Sci. 1 (1), 3–17, 1988.
[45] Mohamad A.A., Viskanta R. "Modeling of turbulent buoyant flow and heat transfer in liquid metals", International Journal of Heat and Mass Transfer. 1993.
[46] Mochizuki H., "Analysis of thermal stratification in the upper plenum of the "Monju" reactor", Nucl. Eng. Des. 270,48-59, 2014.
[47] Papukchiev A., Lerchl G., "Extension of the Simulation Capabilities of the 1D System Code ATHLET by Coupling with the 3D Software Package ANSYS CFX", proceedings of NURETH13, Kanazawa City, Ishikawa Prefecture, Japan September 27 - October 2, 2009.
[48] Pfrang, W., Struwe, D., "Assessment of correlations for heat transfer to the coolant for heavy liquid metal cooled core designs", Technical Report FZKA 7352, Forschunszentrum Karlsruhe GmbH, 2007.
[49] Petrazzini M., De Angelis F., Alamberti A., "Lead and Lead bismuth eutectic liquid-vapor thermodynamictables and physical properties", Ansaldo Tecnical Report EAFG.L30003, Genoa (Italy), 1999.
[50] Poette C., Brun-Magaud V., Morin F., Pignatel J.-F., Stainsby R., Mikityuk K. "ALLEGRO: The European gas fast reactor demonstrator", Project Proceedings of the 17th International Conference on Nuclear Engineering, (Brussels, Belgium, July 12–16) (2009)
[51] RELAP5-3D code development Team, "RELAP5-3D© Code Manual", INEEL-EXT-98-00834, Revision 4.1, September 2013.
[52] RELAP5/Mod.3.3 Code Manual, Volume II. Appendix *A*: Input Requirements, Nuclear Safety Analysis Division, January 2003.
[53] Schultz R., Weaver W.L., Schowalter D., Basu N., "Evaluating Fluid Behaviour in Advanced Reactor Systems using Coupled Computational Fluid Dynamics and Systems Analysis Tools", proceedings of ICONE 13, Beijing China, 2005.
[54] Sobolev V., "Database of thermophysical properties of liquid metal coolants for GEN-IV", SCK-CEN, Belgium, November 2010 (rev. Dec. 2011).
[55] Tarantino M., Scaddozzo G., "Test specifications of the Integral Circulation Experiments", Report ENEA ET-F-S-001, Deliverable D. 4.15, DM4 DEMETRA, IP-EUROTRANS, 2006.
[56] Tarantino M., Benardi D., Coccoluto G., Gaggini P., Labanti V., Forgione N., Napoli A. "Natural and gas Enhanced circulation test in the NACIE Heavy Liquid

Metal Loop", proceedings of ICONE, 18th International Conference on Nuclear Engineering, May 17-21, Xi'an, China, 2010.

[57] Theodoridis G., Papukchiev A. Scholz D., Lerchl G., "A new data-driven ATHLET-ANSYS CFD coupling method for efficient simulation of nuclear power plant circuits", Proceedings of the 2014 22nd International Conference on Nuclear Engineering ICONE22 July 7-11 Prague, Czech Republic, 2014.

[58] Touloukian,V. I., et al., "Thermophysical Properties ofMatter: Thermal Conductivity of Metallic Liquids" IFI/Plenum, New York, 1970.

[59] Turroni P., Cinotti L., Corsini G., Mansani L., "The CIRCE Facility", AccApp'01&ADTTA'01, Nuclear Application in the new Millennium, Reno (Nevada- USA), November 11-15, 2001.

[60] Uotani, M. "Natural convection heat transfer in thermally stratified liquid metaL", Journal of Nuclear Science and Technology. June 1987, p. 442 - 451.

[61] Ushakov P. A., Zhukov A. V., Matyukhin N. M., "Heat transfer to liquid metals in regular arrays of fuel elements", High temperature, Vol.15, pp. 868-873, 1977.

[62] Van den Eynde G.,"Specification for the XT-ADS Core and Fuel Element Design", Deliverable D. 1.7, DM1 DESIGN, IP-EUROTRANS, 2007.

[63] Vendryes G. A., "Superphénix: A Full-Scale Breeder Reactor" Scientific American 236, No. 3, 26 (1977).

[64] Waata Ch. L., Frank Th., "Coupling of ANSYS CFX with 1D System Code ATHLET", Final Report, German Federal Ministry for Economy and Technology, Reactor Safety Research Project 1501328, Germany, 2008.

[65] Watanabe O., Motomiya Y., Takeda H., Koga T. "An application of higher order finite difference method to a natural convection experiment in the hot plenum of an LMFBR", Nuclear Engineering and Design, Vol 146, pp. 25-34, 1994.

[66] Watanabe T., Anoda Y., Takano M., " System-CFD coupled simulations of flow instability in steam generator U tubes", Annals of Nuclear Energy 70, 2014, 141-146.

[67] Weaver W. L., Tomlinson E. T., Aumiller D. L., "A generic Semi-Implicit Coupling Methodology for use in RELAP5-3D©", Nucl. Eng. Des., 211 pp. 13-16, 2002.

[68] World Nuclear Association, www.world-nuclear.org/info/Current-and-Future-Generation/Nuclear-Power-in-the-World-Today/, (last access 16/03/2015).

[69] Yan Y., Uddin R., "Coupled CFD-System-code Simulation of a Gas Cooled Reactor", International conference on Mathematics and Computational Methods Applied to Nuclear Science and Engineering, Rio de Janeiro, Brazil, May 8-12, 2011.

[70] Young D. A., "A Soft Sphere Model for Liquid Metals", Lawrence Livermore Laboratory, UCRL 52352, 1977.

[71] Zhukov, A.V., Sorokin A. P., Titov P. A., Ushakov P.A., "Thermohydraulic problems in lead-cooled reactors", Power-Physics Institute. Translated from Atomnaya Énergiya, Vol. 72 No. 2, pp. 142-151, 1992.

[72] Zhukov, A.V., Kuzina, Yu.A., Sorokin, A.P., Leonov, V.N., Smirnov, V.P., Sila-Novitskii, A.G., "An experimental study of heat transfer in the core of a BREST-OD-300 reactor with lead cooling on models", Thermal Engineering 49 (3), 175–184, 2002.

APPENDIX *A*. ERROR DATA ANALYSIS

A.1.

In this Appendix, sources of error in the performed measurements are considered and the effect of the uncertainty in single measurements on the calculated results is investigated (Lichten, 1999, Moffat, 1988). In particular, assuming a quantity *Z* (secondary variable) computed using a set of independent experimental measurements *Xi* (primary variables) can be represented as $Z=Z(X_1, X_2.. Xn)$. The uncertainty in the calculated results can be estimated with good accuracy using a root-sum square combination of the effect of uncertainties of each individual input Xi as reported in Eq. (*A*.1):

$$\sigma_Z = \sqrt{\left(\frac{\partial Z}{\partial X_1}\right)^2 \sigma_{x_1}^2 + .. + \left(\frac{\partial Z}{\partial X_n}\right)^2 \sigma_{x_n}^2} \qquad (A\text{-}1)$$

where σ_{X_i} is the standard deviation given by:

$$\hat{\sigma}_{X_i} = \sqrt{\frac{\sum_1^t (X_i(t) - \overline{X_i})^2}{t-1}} \qquad (A\text{-}2)$$

For each of the primary variables, global uncertainty is considered composed by the instrument uncertainty and the standard deviation of the considered variable *Xi* according to:

$$\sigma_{X_i}^2 = \hat{\sigma}_{X_i}^2 + \sigma_{X_i, Instr.}^2 \qquad (A\text{-}3)$$

The primary variables experimentally measured in this work are temperatures, LBE mass flow rates and heat fluxes on the walls of the electrical rods. Regarding the coolant properties, all the empirical correlations used in this work, are in agreement with the correlation for Lead-bismuth Eutectic available in the Handbook on Lead-bismuth Eutectic alloy, 2007 and their own accuracy is considered.

In order to obtain a standard deviation representative of the dispersion and neglecting effects due to an imperfect stationary of acquired experimental variables, a linear regression for each of gained thermocouple signals was evaluated and subtracted from the original one. In particular, linear regression was computed using the Ordinary Least Squares method (OLS). The statistical standard deviation was finally calculated using the modified data. Figure 171 shows temperature data in the centre of the channel and its linear regression for Test 1-FC; after 15 min the temperature decreases by about 1°C. Figure 172 shows the modified temperature values obtained reducing the modified source signal by its linear regression.

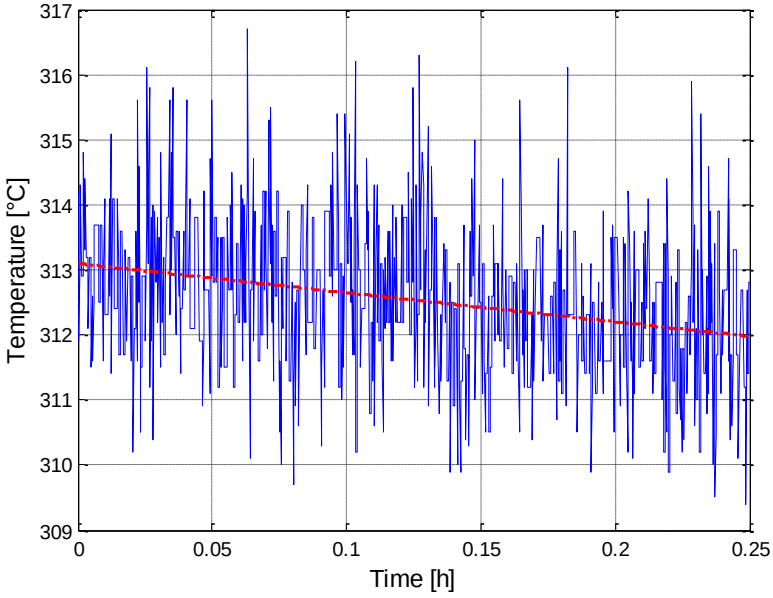

Figure 171: Test 1-FC, temperature in the centre of the channel

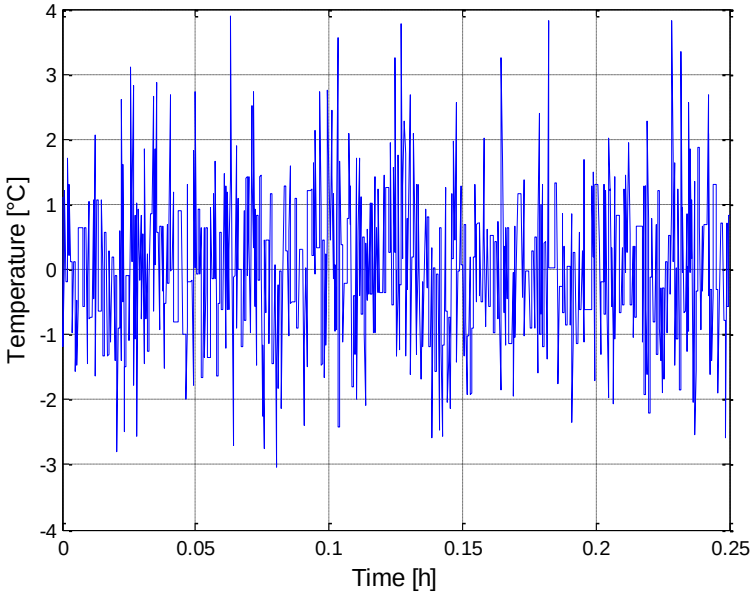

Figure 172: Test 1-FC, modified signal for statistical calculations

It must be noticed that for the purpose of Nu calculations, stationary conditions must be guaranteed for the temperature difference between the wall and the bulk.